Performance Analysis of Future Wireless Communication Systems under Residual Hardware Impairments

By

Mohd Hamza Naim Shaikh

under the guidance of

Dr. Vivek Ashok Bohara

Professor, IIIT-Delhi

&

Dr. Anand Srivastava

Professor, IIIT-Delhi

Indraprastha Institute of Information Technology, Delhi

September, 2022

Performance Analysis of Future Wireless Communication Systems under Residual Hardware Impairments

By

Mohd Hamza Naim Shaikh

PhD-16107

under the guidance of

Dr. Vivek Ashok Bohara

Professor, IIIT-Delhi

&

Dr. Anand Srivastava

Professor, IIIT-Delhi

submitted

in partial fulfillment of the requirements for the degree of

Doctor of Philosophy

to

Indraprastha Institute of Information Technology, Delhi

September, 2022

To the fond memories of all my teachers, the ones who changed the way I saw the world, gave me self-confidence, and whose influence I will never forget . . .

Certificate

This is to certify that the thesis titled **Performance Analysis of Future Wireless Communication Systems under Residual Hardware Impairments** is being submitted by **Mohd Hamza Naim Shaikh** to the Indraprastha Institute of Information Technology-Delhi, for the award of the degree of **Doctor of Philosophy**, is an original research work carried out by him under my supervision. In my opinion, the thesis has reached the standards fulfilling the requirements of the regulations relating to the degree.

The results contained in this thesis have not been submitted in part or full to any other university or institute for the award of any degree/diploma.

Prof. Vivek Ashok Bohara

Prof. Anand Srivastava

Indraprastha Institute of Information Technology Delhi
New Delhi-110020
January 2023

Acknowledgements

"*It is good to have an end to journey toward; but it is the journey that matters in the end.*"
– Ernest Hemingway

To begin, I would like to praise and thank the Almighty Allah, the Most Gracious and Merciful, for the countless blessings bestowed upon me. May Allah's blessing goes to His final Prophet Muhammad (peace be upon him), his family and his companions.

In addition to my efforts, my thesis's success relies heavily on others' help and direction. I want to take this opportunity to thank everyone who helped me finish this thesis.

I express my sincere gratitude to my advisor Prof. Vivek Ashok Bohara, for his invaluable guidance and support. This research would have been impossible without his zeal, understanding and suggestions. I admire his energy, insights, and constructive research suggestions. In terms of intensity, he is the best in the business. I was frequently unable to keep up with him. I owe him a debt of gratitude for his encouragement during my research work. To this day, I am grateful to him for all of his help and advice in furthering my career.

I also want to convey my gratitude to Prof. Anand Srivastava, who served as my PhD co-advisor, for his constant encouragement and support. The journey without both of them, viz. Prof. Anand & Prof. Vivek would have been an entirely different experience. In addition, I would like to express my appreciation to Professor Mohammad S. Hashmi, Dr. Gourab Ghatak and Dr. Abhijit Mitra for their participation as members of my committee and for taking the time out of their busy schedules to provide me with insightful feedback and helpful suggestions regarding my work.

The Wirocomm research group, in particular Gurinder, Anand, Rizwana and Dilnashin, deserve special recognition. Thanks to the Wirocomm group's former members, in particular Dr. Naveen Gupta, Dr. Parag Aggarwal and Dr. Mansi Peer, who helped guide and encourage me through my PhD work. The friendships I have built with each of them will be with me for the rest of my life.

The support and encouragement of my parents were crucial to my success. Thank you for all of the sacrifices you have made for me throughout the years. I cannot thank them enough, and I pray to God to preserve them. The Visvesvaraya PhD Scheme of MIETY India made my research feasible, to which I am grateful. Special thanks go to IIITD's admin office; I was free to devote all of my time and energy toward research rather than dealing with mundane administrative tasks.

Mohd Hamza Naim Shaikh

M. Hamza

Abstract

The widespread proliferation of wireless services in daily life has boosted the demand for very high data rates. This plunge in data rate leads to an increase in energy consumption. As a result, in order to meet the enormous demand, next-generation wireless networks must be spectrally and energy-efficient. Full-Duplex (FD) systems have the potential to double the spectral efficiency (SE) of current half-duplex (HD) communication systems. The FD system utilizes the same time-frequency resource for both transmission and reception. Likewise, intelligent reflecting surfaces (IRSs) have recently been proposed as a passive FD technique that could achieve the aforementioned sustainable growth goals of high energy efficiency (EE) and high SE. Inherently, IRS is a large surface comprising of tiny low-cost reflective elements (REs) that can modify the phase and amplitude of the reflected wave. The multiple reflected paths get coherently added to enhance the received signal power. Since the IRS passively reflects the incident signal, there is no RF chain, resulting in a considerable reduction in energy consumption. Thus, with its low cost and low energy usage, IRS is expected to play a crucial role in the beyond 5G wireless networks. Commercially, low-grade transceiver hardware is frequently used in modern communication systems to reduce the cost of prospective networks. It is critical to take into account the impact of hardware impairments (HIs) caused by low-quality transceiver hardware while designing and developing reliable communication systems. These transceiver HIs cause residual self-interference (SI) in the FD systems. Likewise, these transceiver HIs saturate the SE for the IRS-assisted systems. In addition, the HIs in IRS-assisted systems also arise due to the inability of infinite precision of the IRS phase shifts. Consequently, the impact of HIs should be considered while analyzing the performance of FD/IRS-enabled wireless communication systems, and this motivates the work done in this dissertation.

The first part of this dissertation analyzes the impact of residual SI on the performance of FD-based wireless systems. Further, the SI has also been utilized for recycling energy, commonly referred to as self-energy recycling (S-ER). S-ER improves the overall EE of the FD system. The proposed work also provides valuable insights on the impact of the antenna

allocation for S-ER. The analytical formulation derives closed-form expressions for the EE, SE and outage probability (OP). In addition, we have also proposed an adaptive antenna allocation scheme based on transmit antenna selection (TAS), which compensates for the reduction in antenna array gain and consequently improves the SE and OP while enhancing the EE.

In the second part, the performance of IRS-assisted wireless systems is analyzed under the impact of transceiver HIs. Specifically, in the presence of non-ideal hardware at the base station (BS), IRS and users, the performance is evaluated by deriving the closed-form expressions for the OP, SE and EE. The results show the importance of modeling and compensating for hardware impairment as they significantly restrict the performance of such systems. Further, the results show that although the IRS phase error degrades the performance, the transceiver HIs severely limit the system performance. Moreover, regardless of the number of reflecting elements (REs), transmit power, phase error and fading parameter, the transceiver HI imposes a finite limit on the SE, which cannot be further enhanced.

In the end, this dissertation presents the performance comparison of an IRS-assisted wireless communication system with the FD relay-assisted system in the presence of a transceiver HIs. Specifically, the performance is compared in terms of SE and EE. The results show that the IRS can never achieve more SE than the ideal FD relaying in the presence of a non-ideal transceiver, irrespective of the placement of the IRS and FD relay.

The frameworks proposed in this dissertation can be efficiently utilized in various wireless standards. They will be helpful for a communication engineer to design a link budget for FD/IRS-based wireless systems without performing extensive simulations or tedious experiments.

Table of contents

List of figures

List of tables

Nomenclature

Notations

$(\cdot)^*$	Conjugate Operator
$\mathscr{CN}(\mu, \sigma^2)$	Complex Gaussian Distribution with μ mean and σ^2 variance.
$F_{\mathscr{Z}}(z)$	CDF of RV $\mathscr{Z}$
$\Psi(\cdot)$	Digamma Function
$\mathrm{E}[\cdot]$	Expectation Operator
$\mathrm{E}_i(\cdot)$	Exponential Integral
$(\cdot)!$	Factorial Operator
${}_p\mathrm{F}_q(\cdot,\cdot;\cdot;\cdot)$	Gauss Hyper-Geometric Function
$\Gamma(\cdot)$	Gamma Function
$(\cdot)^H$	Hermitian Operator
$(\cdot)^{-1}$	Inverse Operator
$\gamma(\cdot,\cdot)$	Lower Incomplete Gamma Function
$\mathrm{L}_{\vartheta}(\cdot)$	Laguerre Polynomial (degree ϑ)
$I_p(\cdot)$	Modified Bessel Function of First Kind
$f_{\mathscr{Z}}(z)$	PDF of RV $\mathscr{Z}$
$(\cdot)^T$	Transpose Operator

$\mathrm{tr}[\cdot]$	Trace Operator
$\Gamma(\cdot,\cdot)$	Upper Incomplete Gamma Function

Abbreviations

5G	Fifth Generation
6G	Sixth Generation
AA	Antenna Allocation
ADC	Analog-to-Digital Converter
AF	Amplify-and-Forward
AWGN	Additive White Gaussian Noise
B5G	Beyond 5G
BER	Bit Error Rate
BS	Base Station
CDF	Cumulative Distribution Function
CLT	Central Limit Theorem
CSI	Channel State Information
DAC	Digital-to-Analog Converter
DF	Decode-and-Forward
e2e	End-to-End
EE	Energy Efficiency
FDD	Frequency-Division Duplexing
FD	Full-Duplex
FDR	Full-Duplex Relaying
HD	Half-Duplex
HIs	Hardware Impairments

HPA	High Power Amplifier
IBO	Input Backoff
IFBD	In-band Full-Duplex
IM	Index Modulation
IRS	Intelligent Reflecting Surface
KPIs	Key Performance Indicators
LIS	Large Intelligent Surface
LNA	Low Noise Amplifier
LoS	Line-of-Sight
MEMS	Micro-Electrical-Mechanical Systems
MIMO	Multiple-Input Multiple-Output
mmWave	Millimeter Wave
MU-MIMO	Multi User MIMO
NLoS	Nonline-of-Sight
NOMA	Non-Orthogonal Multiple Access
OP	Outage Probability
PDF	Probability Distribution Function
PLS	Physical Layer Security
QoS	Quality-of-Service
RE	Reflecting Element
RIS	Reconfigurable Intelligent Surface
RSI	Residual Self-Interference
RV	Random Variable
S-ER	Self-Energy Recycling

SDNR	Signal-to-Distortion-plus-Noise Ratio
SER	Symbol Error Rate
SE	Spectral Efficiency
SINR	Signal-to-Interference and Noise Ratio
SI	Self-Interference
SM	Spatial Modulation
SNR	Signal-to-Noise Ratio
SSK	Space Shift Keying
SWIFT	Simultaneous Wireless Information and Power Transfer
T-HIs	Transceiver Hardware Impairments
TDD	Time-Division Duplexing
THz	TeraHertz
TWC	Two-way Communication
UE	User Equipment
uHDD	Ultra-High Data Density
uHSLLC	Ultra-High Speed with Low Latency Communication
uMUB	Ubiquitous Mobile Ultra-Broadband
V2I	Vehicle-to-Infrastructure
V2V	Vehicle-to-Vehicle
WPCN	Wireless Powered Communication Network

Chapter 1

Introduction

This chapter discusses the motivation and objectives for this work. Further, it also summarizes the dissertation's significant contributions and related publications.

1.1 Motivation

Over the last decade, there has been a widespread proliferation of wireless services to cater to diversified applications with varying quality of service (QoS) requirements. The tremendous growth and ubiquitous access to wireless services have led to a manifold increase in the mobile broadband data traffic volume [1, 2]. Further, innovative applications such as augmented and virtual reality, unmanned mobility, big data analytics, three-dimensional media, digital twin, etc., are highly data-intensive. A major characteristic of the futuristic wireless network is the propensity to support such massive traffic. Thus, it requires a very large area spectral efficiency (SE) (hundreds of bits/s/Hz/sq. km) and ultra-high throughput per user equipment (UE) (multiple Gbps) [3].

This explosion of wireless data has continuously driven the advancement in wireless technologies such as millimeter-wave (mmWave) communication, large-scale multiple-input multiple-output (MIMO), capacity-achieving turbo and polar codes. The combination of mmWave with massive MIMO has also been proposed to enhance the data rate further. However, the deployment of large-scale MIMO usually results in a high cost of implementation and increased power consumption. Further, the combination of mmWave and massive MIMO needs sophisticated signal processing techniques, which require expensive and energy-consuming hardware [4].

The growing data traffic has heightened the energy requirements of wireless networks. The deployment of next-generation wireless networks may also lead to severe environmental and

economic concerns. Environmental concerns are mainly related to the harmful impact of the gaseous discharge in the atmosphere due to the consumption of fossil-fuel-based energy sources. The economic concerns are also fueled by the escalating costs of operating the wireless network due to the enormous energy consumption. Moreover, these devices will also raise significant environmental and economic concerns, such as radiation hazards and escalation of fuel costs due to the increase in the consumption of electricity. Hence, energy efficiency (EE) is one of the crucial performance metrics while designing the next-generation wireless network. The goal is to shift the paradigm towards a green and sustainable wireless standard that supports an increase in capacity without adversely impacting the environment and energy consumption.

Due to the scarcity of wireless spectrum, increasing spectrum efficiency has been viewed as a more efficient way to fully exploit the limited spectrum resources that we currently have, rather than seeking more spectrum resources in high-frequency bands such as millimeter waves and terahertz (THz) bands. Further, the excessive charges associated with the radio spectrum increase the significance of higher SE. Full-duplex (FD) transmission can be exploited to increase the SE without expanding the bandwidth of the system. Theoretically, FD systems can double the SE of the half-duplex (HD) systems, as they transmit and receive simultaneously over the same temporal and spectral resources. FD also gives the flexibility to point-to-point handshaking and multiple access techniques and reduces latency caused by HD operation delays [5].

Further, with the advent of metasurfaces, an intelligent reflecting surface (IRS) has also emerged as a cost-effective promising solution for the next-generation futuristic wireless systems. In contrast to FD relaying, the beamforming gain in the IRS is achieved through intelligent reflection without consuming any additional energy for re-transmission. Using the phase-adjusted reflections from each reflecting element (RE), IRS is capable of creating a constructive combination at the desired receiver. Since IRS does not employ a power amplifier, the circuit power consumption is much less than that of the FD relay. Thus, in terms of energy usage, the IRS is significantly more energy-efficient than FD relaying [6, 7].

Motivated by the above, in this research, we aim to investigate the performance of recently emerging beyond fifth-generation (5G) technologies viz. FD and IRS-based wireless communication systems under practical non-ideal hardware scenarios. In wireless communications systems, hardware impairments (HIs) are always present, yet, they are frequently neglected in the study of modern communication systems. However, the performance analysis and characterization under practical non-ideal hardware scenarios are vital in designing and executing modern reliable communication systems.

1.2 Objectives

The main aim of this dissertation is to create an analytical framework for evaluating the end-to-end performance of FD/IRS-based systems in the presence of residual HIs. Specifically, the objectives of this dissertation are as follows:

- To analytically evaluate the performance of FD systems under non-ideal transceiver hardware and residual self-interference (RSI). Further, to enhance the performance of FD systems through self-energy recycling (S-ER).
- To investigate the impact of transceiver HIs and IRS HIs on the performance of IRS-aided systems. Further, to characterize the performance of cascaded dual IRS-based systems with non-ideal hardware.
- To compare and analyze the performance of FD and IRS-based systems under non-ideal transceiver hardware.

1.3 Contributions

The major contributions of this work are summarized below, along with the relevant publications.

- The performance of a FD-relay system is investigated under the impact of RSI and transceiver HIs. Further, the performance of the FD-relay system is enhanced through S-ER. In particular, two S-ER schemes, the fixed S-ER scheme and the adaptive S-ER scheme, are proposed. The closed-form expressions for outage probability (OP), SE and EE are derived for the FD-relay-based system with proposed S-ER schemes. The analytical framework is further extended for FD multiuser MIMO (FD-MU-MIMO) scenario. Moreover, the trade-off between SE and EE is studied, and useful design insights have also been provided.
  - **M. H. N. Shaikh**, V. A. Bohara and A. Srivastava, "Performance Analysis of a Full-Duplex MIMO Decode-and-Forward Relay System With Self-Energy Recycling," *IEEE Access*, vol. 8, pp. 226248-226266, 2020.
  - **M. H. N. Shaikh**, V. A. Bohara, P. Aggarwal and A. Srivastava, "Energy Efficiency Evaluation for Downlink Full-Duplex Nonlinear MU-MIMO-OFDM System With Self-Energy Recycling," *IEEE Systems Journal*, vol. 14, no. 3, pp. 3313-3324, 2020.

- **M. H. N. Shaikh**, V. A. Bohara and A. Srivastava, "Performance Enhancement in Full-Duplex AF Relay System through Smart Antenna Allocation," *2020 IEEE 3rd 5G World Forum (5GWF)*, Bangalore, India, 2020, pp. 303-308.
- **M. H. N. Shaikh**, V. A. Bohara, A. Srivastava and G. Ghatak, "EE Enhancement in FD MIMO Relay System through Adaptive Antenna Allocation and Self-Energy Recycling," *2020 IEEE International Conference on Communications Workshops (ICC Workshops)*, Dublin, Ireland, 2020, pp. 1-6.
- **M. H. N. Shaikh**, V. A. Bohara, and A. Srivastava, "Energy Efficiency Enhancement in Full-Duplex Relay System through Adaptive Antenna Allocation," *2019 IEEE International Conference on Advanced Networks and Telecommunications Systems (ANTS)*, BITS-Goa, India, 2019, pp. 1-5.
- **M. H. N. Shaikh**, V. A. Bohara, P. Aggarwal and A. Srivastava, "On EE-SE Trade-Off for Downlink Full-Duplex MISO Systems with Self-Energy Recycling," *2019 IEEE 89th Vehicular Technology Conference (VTC2019-Spring)*, Kuala Lumpur, Malaysia, 2019, pp. 1-5.

- The performance of an IRS-assisted wireless system is investigated under practical and non-ideal hardware. We present a model to jointly characterize the impact of transceiver HIs and IRS HIs on the performance of IRS-assisted wireless systems, taking into account the effect of channel fading as well as the size of the IRS. The number of REs in the IRS characterizes its size. Next, we derive the closed-form expressions for the OP, SE and EE of the IRS-assisted wireless systems by first obtaining the instantaneous signal-to-distortion-plus-noise ratio (SDNR) and then utilizing it to derive the above performance metrics. Further, the analytical framework is extended for a dual IRS-based communication system.

  - **M. H. N. Shaikh**, V. A. Bohara and A. Srivastava, "On the Performance of Dual RIS-Aided Communication System under Non-Ideal Transceiver over Nakagami-*m* Fading Channels," *Internet Technology Letters*, vol. 5, no. 6, 2022.
  - **M. H. N. Shaikh**, V. A. Bohara, A. Srivastava and G. Ghatak, "A Downlink RIS-aided NOMA System with Hardware Impairments: Performance Characterization and Analysis," *IEEE Open Journal of Signal Processing*, vol. 3, pp. 288-305, 2022.
  - **M. H. N. Shaikh**, V. A. Bohara and A. Srivastava, "IRS-Aided Communication System with Phase Noise and Hardware Impairments: Performance Analysis and Characterization," accepted in *COMSNETS 2023*.

  - **M. H. N. Shaikh**, V. A. Bohara, A. Srivastava and G. Ghatak, "On the SE and EE of RIS-Aided NOMA System with Non-ideal Transceiver," *2022 IEEE Wireless Communications and Networking Conference (WCNC)*, 2022, pp. 1737-1742.
  - **M. H. N. Shaikh**, V. A. Bohara, A. Srivastava and G. Ghatak, "Performance Analysis of Intelligent Reflecting Surface-Assisted Wireless System with Non-Ideal Transceiver," *IEEE Open Journal of the Communications Society*, vol. 2, pp. 671-686, 2021.

- We compare the performance of IRS-supported transmission and FD relaying in the presence of transceiver HIs. Further, this work also analyzed the impact of the placement of IRS and compared it with HD and FD relaying.

  - **M. H. N. Shaikh**, V. A. Bohara, A. Srivastava and G. Ghatak, "Intelligent Reflecting Surfaces Versus Full-Duplex Relaying: Performance Comparison for Non-Ideal Transmitter Case," *2021 IEEE 32nd Annual International Symposium on Personal, Indoor and Mobile Radio Communications (PIMRC)*, Helsinki, Finland, 2021, pp. 513-518.

1.4 Other Contributions

Apart from the main contributions mentioned above, the author of this thesis has also contributed to the following publications.

- **M. H. N. Shaikh**, V. A. Bohara, A. Srivastava and G. Ghatak, "An Energy Efficient Dual IRS-aided Outdoor-to-Indoor Communication System," submitted in *IEEE Systems Journal*.

- K. Lata, V. A. Bohara, A. Srivastava and **M. H. N. Shaikh**, “Intelligent Reflecting Surfaces Versus Optical Mirrors: Performance Comparison for Indoor Physical Layer Security Environments,” *IEEE International Conference on Advanced Networks and Telecommunications Systems (ANTS)*, IIT-Gandhinagar, India, 2022, pp. 1-6.

- K. Joshi, **M. H. N. Shaikh**, S. A. Naqvi, and V. A. Bohara, "On the performance of IRS-assisted OFDM system with non-ideal oscillator and amplifier," *Internet Technology Letters*, vol. 5, no. 4, 2022.

- **M. H. N. Shaikh**, V. A. Bohara, and A. Srivastava, "Spectral Analysis of WOLA-OFDM in the Presence of DPD and HPA," *2020 Twenty-sixth National Conference on Communications (NCC)*, Kharagpur, India, 2020, pp. 1-6.

- **M. H. N. Shaikh**, A. Agarwal, P. Aggarwal and V. A. Bohara, "On the Spectral Content of Nonlinear Carrier Aggregated Windowed OFDM Systems," *2018 IEEE International Conference on Advanced Networks and Telecommunications Systems (ANTS)*, Indore, India, 2018, pp. 1-5.

These works are not discussed in this dissertation; however, they are relevant because the first two works investigate a practical use case scenario of IRS, while the third work analyzes the performance of an OFDM-based IRS-assisted communication system in the presence of non-ideal transceiver and oscillator. Likewise, the later two works evaluate the performance of a novel 5G waveform, i.e., WOLA-OFDM, in the presence of a non-ideal transceiver.

1.5 Organization

The rest of the thesis is organized as follows:

- Chapter 2 presents the background and related work of this dissertation. Initially, the basics of FD communication are briefly discussed, along with its potential benefits and limitations. This chapter also provides the concept of S-ER. It is followed by a discussion of literature related to the performance of a FD-based communication system. Further, the fundamentals of the IRS are discussed, along with the motivation for the IRS and its architecture. Likewise, the related literature on the performance of IRS-assisted communication is also reviewed.

- Chapter 3 investigates the performance of a FD-based communication system in the presence of RSI and S-ER. It also presents the proposed antenna allocation techniques for S-ER in a FD-MIMO relay. Further, in the latter part of this chapter, the analytical framework is extended to evaluate the performance of a FD MU-MIMO system with S-ER under RSI and transceiver HIs.

- Chapter 4 presents an analytical framework to investigate the performance of IRS-assisted communication systems in the presence of practical and non-ideal hardware. Further, comparisons are drawn between the performance of an ideal IRS-based system and non-ideal hardware-based IRS-assisted communication systems. In addition, a dual IRS-based communication system is also proposed for specific use cases. Further, the performance of a dual-IRS-based system is compared with that of a single-IRS-based system under practical, non-ideal hardware scenarios.

- In Chapter 5, the performance of FD relay-assisted and IRS-assisted communication systems under transceiver HIs is compared. It also discusses the relative placement scenario of IRS and FD relay and how it affects performance.
- Chapter 6 concludes the dissertation and discusses possible future research directions.

Chapter 2

Background and Related Work

This chapter, the first part, provides a brief overview of FD communication. The second part of this chapter reviews the IRS-assisted communication systems.

2.1 Full-Duplex Communication

2.1.1 Motivation for FD Communication

The wireless revolution has led to ever-increasing demands on our limited wireless spectrum, necessitating the search for solutions with greater SE. With the advent of the 5G wireless standard, data traffic volume is expected to increase further. Further, the 5G standard has to support massive connectivity, i.e., serving a huge number of devices with seamless connectivity. Thus, future wireless communication systems must operate in highly congested regions of the frequency spectrum, particularly the sub-6-GHz bands, where the channel has favorable propagation characteristics. Among the various ways to increase SE, in-band full-duplex (IBFD) operation has recently gained attention. Known as simultaneous transmit and receive, this method allows users to simultaneously transmit and receive on the same or different bands at the same time.

2.1.2 System Architecture for FD Communication

The basic concept of IBFD is as follows: Most modern communication systems include terminals such as base stations (BSs) or relays that serve as transmitters and receivers. Most of the time, these terminals work in HD mode or out-of-band FD mode, which means that they send and receive at different times or on different frequency bands. Allowing these wireless terminals to transmit and receive over the same frequency band simultaneously (i.e.,

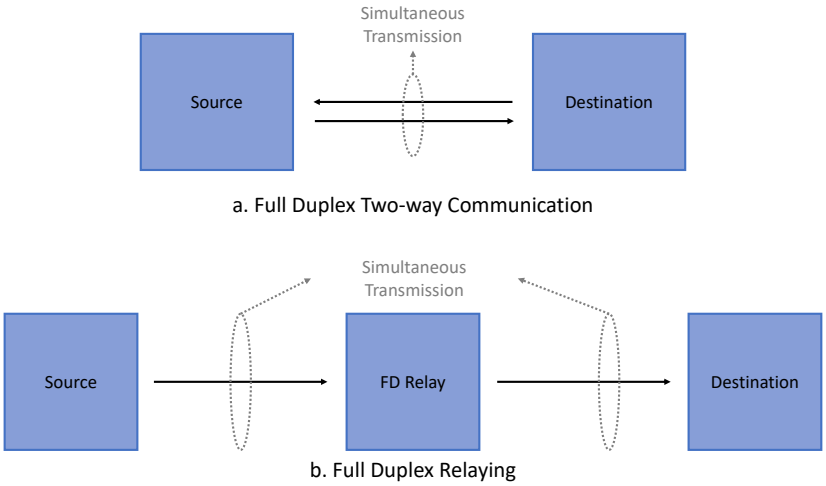

Figure 2.1: Two modes of FD communication: (a)FD Two-way Communication and (b) FD Relaying.

IBFD operation) can double their SE, as measured by the number of information bits reliably communicated per second per Hz. Additionally, two communication modes can be selected for FD communications for any wireless terminal with a FD radio, namely full-duplex relay mode and two-way communication (TWC) mode as illustrated in Fig. 2.1. Thus, IBFD operation is of great interest for next-generation wireless networks [8, 9].

2.1.3 Full-Duplex Relaying

Relaying techniques have gained considerable attraction over the past decade for their ability to extend connectivity and network coverage and provide higher capacity and better energy efficiency. In a dual-hop network, the source and destination are connected through an intermediate terminal acting as a relay. In conventional relaying networks, two orthogonal channels are required for effective communication. Usually, time-division duplexing (TDD) or frequency-division duplexing (FDD) is utilized to provide out-of-band FD operations. However, this results in a significant loss of precious spectral resources. Utilizing the same time-frequency resource for concurrent transmission and reception, i.e., FD relaying (FDR), can theoretically double the SE of the conventional HD relaying systems [5].

2.1.4 Self-Interference

Full-duplex operation is not new and has long been used successfully in wireline communications. The interference, also known as line echo, is caused by the transmitting and receiving

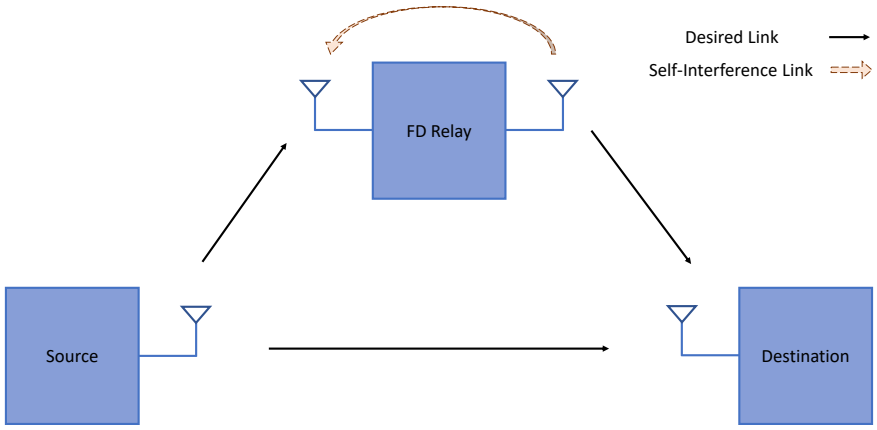

Figure 2.2: Schematic for the Full-Duplex Relaying.

wires' coupling. This line echo is 3 to 6 dB lower than the intended signal, requiring a relatively low cancellation level of 20-30 dB [10].

However, the receiver is co-located with the transmitter within the transceiver in FD wireless systems. Thus, this self-interference (SI) has a magnitude that is several orders higher than the magnitude of the intended signal because the latter crosses a longer distance than the SI. For example, if two transceivers are 500 meters apart, the intended signal from the remote transceiver is attenuated by approximately 120 dB. Further, if there is 20 dB isolation within the transmit and receive paths of the FD transceiver, the SI will be 100 dB higher than the intended signal. This massive difference between SI and received signal power levels increases with transceiver distance. FD wireless systems require higher SI cancellation than wireline systems. This power difference dictates SI-cancellation techniques and strategies for high-SI-cancellation requirements. A schematic of an FD-relay system is shown in Fig. 2.2, with the relay transmitting the source signal in FD mode to the destination. The relay experiences SI in the received signal since the transmission and reception occur within the same time-frequency resource block.

2.1.5 Self-Interference Cancellation Techniques

The literature has reported extensive work for suppressing SI [11–13]. These techniques include passive and active RF, analog suppression, and digital cancellation schemes. As a first step, passive techniques like antenna separation, isolation, etc., mitigate a significant part of SI [11]. Subsequently, passive techniques are generally followed by active RF, and analog cancellation [12]. The leftover SI is alleviated through a digital cancellation scheme [13].

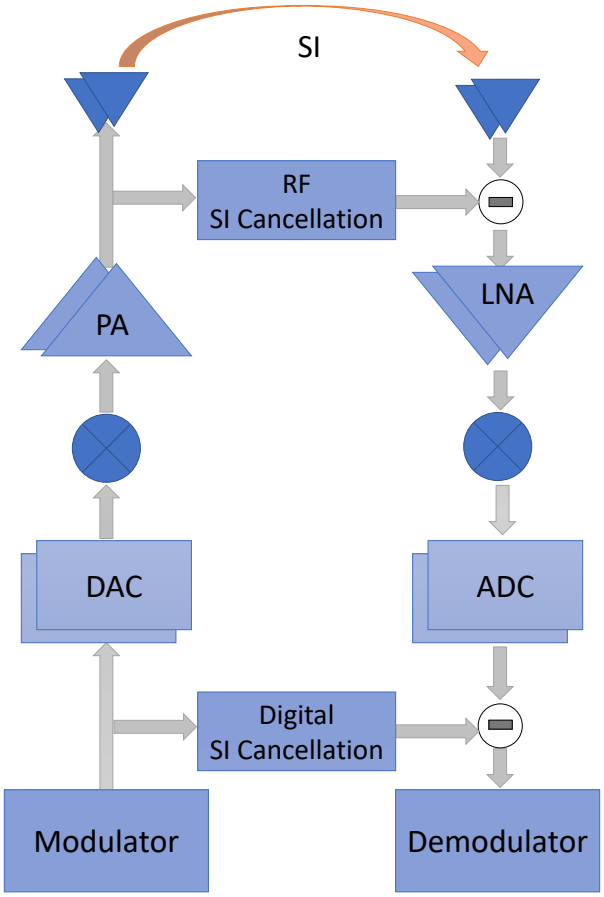

Figure 2.3: Schematic for the FD transceiver with RF and Digital Self-Interference Cancellation Stages.

Given that the transmitted SI is known at the transceiver, it might be utilized to mitigate the SI from the received signal. However, if this operation is directly performed in the digital domain at the baseband, the dynamic range of the analog-to-digital converter (ADC) will be the substantial bottleneck. Since the RF input is scaled down, the strong SI level matches the ADC's dynamic range. For example, for a 10-bit ADC, the resulting quantization noise is 6.02*10 + 1.76 = 61.96 dB. Thus, if the SI is 100 dB higher than the desired signal, the quantization noise will be around 38 dB higher. As a result, even if the SI is totally canceled at the ADC output, the receiver can no longer comprehend the intended signal. To avoid this issue, the SI must first be decreased at the receiver's input before the low-noise amplifier (LNA) and ADC, as shown in Fig. 2.3. The SI can be further lowered at the baseband after the ADC to improve signal detection. As a result, simply subtracting the SI based on the known transmitted symbols in the digital domain can result in a significant residual SI [14].

2.1.6 Residual Self Interference

In FD systems, SI cancellation is usually achieved in multiple stages. Passive SI suppression techniques like antenna separation, antenna isolation, etc., can eliminate SI by $50 \sim 80$ dB. Further, analog and digital domain cancellations can mitigate up to $50 \sim 60$ dB SI [15]. However, due to hardware imperfections in the transmit RF chain and SI cancellation circuitry, complete mitigation of SI is inevitable. The leftover SI is termed as RSI, which can be modeled in two ways.

- Fading Model: RSI is characterized through a statistical fading model like Rayleigh/Rician fading [16].
- Complex Gaussian Random Model: RSI is characterized as a Gaussian random variable with its variance depending on the underlying SIC methods [17].

Practical measurements have confirmed the Gaussian model, which has been widely used in literature, thanks to its generality in modeling the RSI [18–20]. As per the central limit theorem (CLT), the Gaussian assumption stands valid. Even if the assumptions are incorrect, the Gaussian characterization can be considered as the lower bound of the performance [21].

2.1.7 Signal Model for a FDR-aided Communication System under RSI

Considering the system model as depicted in Fig. 2.2 where a single antenna source communicates with a single antenna destination with the help of a FD relay. The FD relay is assumed to have a pair of antennas for simultaneous transmission and reception. The received signal y_r at

the FD relay can be expressed as

$$y_r = h_{sr}x_s + h_{rr}x_r + n_R, \tag{2.1}$$

where h_{sr} and h_{rd} are the source-to-FD relay and FD relay-to-destination channel. Likewise, x_s and x_r are the transmitted symbol of source and relay. Because the relay is in FD mode, the SI channel is $h_r r$. Further, n_r is the additive white Gaussian noise (AWGN) at the FD-relay. The received signal at the destination, y_d, can be expressed as

$$y_d = h_{rd}x_r + n_d, \tag{2.2}$$

where n_d denotes the AWGN at the destination.

Now the self-interference component can be estimated at the FD relay since x_r is known to the FD relay. The estimated SI can be subtracted from the received signal. However, the complete cancellation of SI is inevitable due to the various imperfections associated with the estimation and cancellation. After subtracting the estimated SI from the received signal y_r in (2.1), the updated received signal can be rewritten as

$$\mathbf{y}_r = h_{sr}x_s + d_r + n_r, \tag{2.3}$$

where d_r denotes the RSI where $d_R \sim \mathscr{CN}(0, \sigma^2_{rsi})$ and $\sigma^2_{rsi} = \alpha P_r^{\nu}$. The value of constants α and ν $(0 \leq \nu \leq 1)$ depends on the efficacy of the employed SI cancellation technique [19].

2.1.8 Related Work

FD relay-based systems have been widely studied in literature [16, 18–20, 22–24]. A multi-hop FD relay-based system is analyzed in [16], where the authors have evaluated the number of FD relays corresponding to the minimum outage. An optimal relay selection scheme for a multi-relay scenario has been considered in [18], where the relay selection is optimized for maximizing the signal-to-interference and noise ratio (SINR) in a two-way FD relay network. The impact of RSI on the error and diversity performances of a FD amplify-and-forward (AF) relay system has been investigated in [19]. Further, in [20], authors have proposed an optimal power allocation scheme for maximizing the capacity of an AF-based FD relay system under the impact of RSI. In [22], a FD AF relay system is optimized for minimizing symbol error rate (SER) in terms of power allocation and relay location. Further in [23], authors have optimized power allocation and relay position for the FD decode-and-forward (DF) relay system for minimizing the outage probability. A novel two-timeslot two-way FD relaying has

been proposed in [24], where the authors have evaluated the rate and outage performance of the access and backhaul links served by a FD relay.

Since RF waves are capable of transmitting information as well as transferring energy, simultaneous wireless information and power transfer (SWIPT) protocol, which combines power transfer and information transmission, have also been recently investigated. The fundamental trade-off between energy and information transmission with respect to SWIPT has been explored in the seminal work of [25]. In [26], authors have discussed the application of SWIPT in improving the EE and the trade-offs between the performance and system complexity. Several works have been reported in the literature that analyzed the performance of SWIPT-based FD relay systems [27–29]. Specifically, [27] proposed optimal and sub-optimal solutions for maximizing throughput in a MIMO-FD relay system employing a time-switching protocol for energy transfer to the relay. In [28], authors studied the performance of wireless-powered dual-hop AF relaying systems and the impact of channel state information and antenna correlations on system performance. A SWIPT-based FD system has been analyzed in [29], where the authors have evaluated throughput performance considering both the AF and DF relaying protocol.

S-ER-based FD relay systems have been studied in [30] for efficient energy transfer and relay of information. Joint transmission in uplink and downlink for an S-ER-based FD system has been investigated in [31] for power allocation and data transmission. The impact of the time split parameter on the EE of the S-ER-based FD downlink system has been studied in [32]. Further [33] discusses a quality-of-service aware beamforming design in S-ER based FD relay system. As evident from above, a considerable amount of literature is available on the impact of S-ER in FD systems. However, to the best of our knowledge, the stand-alone impact of S-ER in a FD system has yet to be investigated. Further, most of the prior work on FD overlooked the impact of hardware impairments while assuming the presence of an ideal transceiver at the transmitter.

2.2 Intelligent Reflecting Surface

2.2.1 Motivation for IRS

With the global commercialization of 5G networks, the research community has focused on the sixth-generation (6G) wireless communication networks. The significant drivers of 6G networks are the increased demand for wireless networks, the technology-driven paradigm shift, and the constraints and performance limitations of the 5G networks [34]. As discussed in Ref. [35], the three critical communication scenarios that will dominate the 6G networks

are ubiquitous mobile ultra-broadband (uMUB), ultra-high data density (uHDD) and ultra-high-speed with low-latency communications (uHSLLC). Based on this, the key performance indicators (KPIs) for the 6G networks would be; a peak data rate of 1∼10 Tbit/s and an EE of 10∼100 times that of 5G networks, along with the connection density of 10^7 devices/km^2 [36].

IRS is specifically a reconfigurable array of passive reflecting elements wherein each of the elements can independently alter the phase and/or attenuation of the incident signal. Cumulatively, the reflected signal is altered so that the desired channel response can be realized through proper phase shifting at each of the reflecting elements. The reflected signal can be combined constructively from all the paths to enhance the received signal power or can be combined destructively to mitigate the undesired interference, thus improving the overall performance of the wireless system. Reconfigurable intelligent surfaces (RISs) and large intelligent surfaces (LISs) are also commonly referred terminologies for IRSs and are used interchangeably in the literature. With these benefits, IRS has been acknowledged as one of the critical enablers technology for the 6G wireless network [37–39].

Moreover, due to the low-cost hardware and low energy consumption, IRS enables inexpensive, reconfigurable and software-controlled wireless communication for a green future [7]. The low hardware footprint of the IRS structure facilitates the broader deployment across the different urban structures in the outdoor environment, such as buildings, factory ceilings, rooftops, etc. Consequently, IRS can seamlessly integrate into the existing wireless communication environment without altering its infrastructure or operational standards. Thus, IRS may be densely deployed in wireless networks at a low and scalable cost while also providing a high level of flexibility, and interoperability [40, 41].

Contrary to conventional relaying, the beamforming gain in the IRS is achieved through intelligent reflection and without consuming additional energy for re-transmission. IRS reflects the incoming signal by suitably adjusting the phase of the reflected signal from each of the reflecting elements in order to have a constructive combination of the signal at the desired receiver. Additionally, the IRS does not require dedicated time/frequency resources to re-transmit the incoming signal. Since IRS does not employ a power amplifier, the circuit power consumption is much less than that in a regular AF relay. Thus, from an energy consumption standpoint, the IRS is far more energy-efficient as compared to conventional relaying [6, 7].

2.2.2 System Architecture for IRS

The IRSs' hardware implementation is based on the concept of a meta-surface, which is a controlled two-dimensional meta-material. According to the operating frequency, the meta-surface consists of a planar array with a high number of meta-atoms with a sub-wavelength electrical thickness (as illustrated in Fig. 2.4). Meta-atoms are metals or dielectrics that may

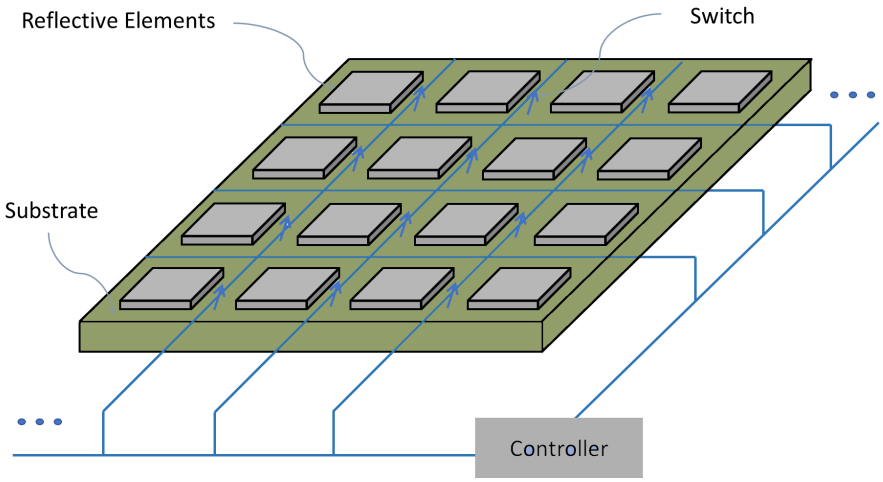

Figure 2.4: Illustration of a meta-surface made up of an array of passive reflective elements.

change electromagnetic radiation. The properties of these elements and the array's structural layout influence the transformations of the incident waves. PIN diodes, ferroelectric devices, or varactor diodes are used to implement the tunable chips implanted in the meta-surface to interact with the scattering element and communicate with an IRS controller. Further, with the advent of Micro-Electrical-Mechanical Systems (MEMS) and metamaterials, a real-time reconfiguration of the phase shifts of IRS has already been demonstrated. The real-time reconfiguration of IRS phase-shift has widely enhanced its applicability for deployment across various wireless networks [42].

2.2.3 Signal Model for a IRS-assisted Communication System

Consider a scenario where a source node communicates with a destination node via IRS, as illustrated in Fig. 2.5. The IRS comprises of M number of REs. Further, it is assumed that the direct link between the source and destination is unavailable due to a blockage. At the destination, the received reflected signal from IRS, y_d, can be expressed as

$$y_d = \sum_{i=1}^{M} h_i g_i r_i \tilde{x}_s + n_d, \tag{2.4}$$

where h_i and g_i are the fading channel between the source-to-ith-RE and ith-RE-to-destination. Further, x_s is the transmitted symbol from the source, and n_d denotes the AWGN noise modeled as a zero-mean complex Gaussian process having a variance of σ^2.

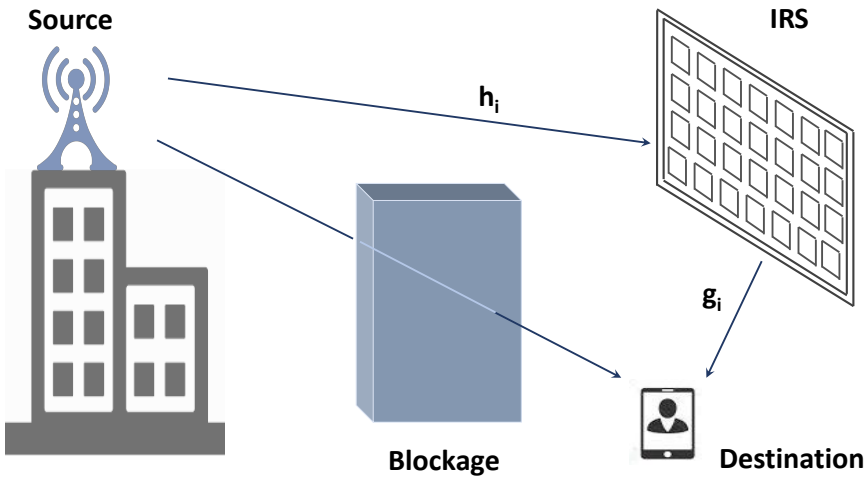

Figure 2.5: Schematic for the IRS-Assisted Wireless System.

Now representing the equivalent source-to-IRS-to-destination channel by $\mathscr{G}$, (2.4) can be represented as

$$y_d = \mathscr{G} r_i x_s + n_d, \tag{2.5}$$

with

$$\mathscr{G} = \sum_{i=1}^{M} |h_i| |g_i|, \tag{2.6}$$

where, r_i represents the response of the ith RE and it can be obtained as

$$r_i = |r_i| \exp(j\varphi_i), \tag{2.7}$$

where φ_i denotes the phase shift that is applied by the ith-RE of the IRS. Further, without losing generality, we assume that $|r_i| = 1$. This assumption aligns with realistic implementations, as discussed in [43].

The IRS can be configured to provide optimal phase shift, assuming that the perfect channel estimates are available at IRS. Thus, the optimal phase can be adjusted as

$$\varphi_i = -(\varphi_{h_i} + \varphi_{g_i}), \tag{2.8}$$

so, for the optimal phase at IRS, (2.7) can be rewritten as

$$r_i = \exp(-j(\varphi_{h_i} + \varphi_{g_i})). \tag{2.9}$$

Now by substituting (2.9) into (2.4), the received signal at the destination can be expressed as

$$y_d = \mathscr{G} x_s + n_d. \tag{2.10}$$

2.2.4 Related Work

IRS was first introduced as a novel concept in [44] and has gotten much buzz in the wireless communication world. Initially, the authors in [45, 46] show that IRS technology can be used in wireless data transfer and position estimation. In [47], the authors have investigated the approximate achievable data rate assuming that the channels between transmitter-to-IRS and IRS-to-receiver are independent and Rician distributed. In [48], authors have analyzed the asymptotic uplink sum rate of an IRS-assisted system in the Rician channel. IRS is adopted for downlink communication in the multi-user scenario to enhance EE in [7]. Specifically, in [7], the authors have reported a 300% increase in the EE of IRS vis-a-vis traditional AF relaying-based resource allocation. Similarly, the authors in [7, 40] considered the IRS for assisting downlink transmission scenarios for multiple users and worked on maximizing the sum rate. Further, in [6] and [49], the authors have derived the upper bound for the error performance of IRS-assisted wireless systems. These upper bounds are pretty tight for IRS with a large number of reflecting elements; however, the lower bound is not entirely accurate when the number of reflecting elements is small. Further, in [50], authors have provided bit error rate (BER) analysis for IRS-assisted non-orthogonal multiple access (NOMA) systems. However, the authors employed the CLT to characterize the distribution of the equivalent channel; the results are precise for IRS having a large number of reflecting elements.

In [51], IRS has been employed in a SWIPT-aided system, where the IRS enhances energy harvesting. Further, a self-sustainable IRS has been proposed for a wireless powered communication network (WPCN), where IRS improves downlink energy transfer, and uplink information transmission for multiple users [52]. Similarly, in [53], IRS has been proposed to the realm of index modulation (IM), where the author has proposed IRS-space shift keying (SSK) and IRS-spatial modulation (SM) schemes for future wireless communication systems. The joint passive and active beamforming at IRS has been studied in [54] for obtaining the average received power at the user. IRS has also been explored for physical layer security (PLS) in [55]. Lastly, [56] employs IRS for vehicular communications, where the IRS enhances the link-performance of both the vehicle-to-vehicle (V2V) and vehicle-to-infrastructure (V2I) link. The seminal work of Renzo et al. comprehensively discussed the concept and state-of-art research for IRSs [57]. Further, it also presented the communication-theoretic framework based on electromagnetic theory for modeling, analysis, optimization and deployment of a futuristic

IRS-empowered smart radio environment. In addition, the work of [6, 37, 58, 59] presented a comprehensive review of IRS-empowered communication.

Performance comparison of IRS with an ideal AF relay was studied in [7], where the IRS shows a large EE. Further, in [43], the performance IRS-assisted system is compared with the ideal AF relay in terms of outage probability, SER and ergodic capacity. Here also, the IRS-assisted system outperforms the conventional AF relaying. Likewise, in [60], Bjornson et al. have compared the performance of IRS-assisted systems against DF relaying. The authors have shown that the IRS-aided transmission only sometimes outweighs the conventional DF relaying. However, for a very large number of REs, the IRS can outperform the DF relaying. Moreover, in [61], the authors have considered some novel 5G channel models and revised the results for IRSs. DF relays, where they have shown that the IRS and DF relay can complement each other's strengths and can both have a place in 5G and beyond 5G (B5G) architectures. Finally, Renzo et al. have summarized the key differences and similarities between IRSs and the relays in [62].

However, these works have considered the unrealistic assumption of ideal hardware, whereas omitting the impact of HIs for a practical IRS implementation could lead to misleading design conclusions. Specifically, for the IRS-assisted systems, two major categories of HIs are transceiver HIs (T-HIs) and IRS-HI. T-HI accounts for the combined impact of all the non-ideal hardware across the transceiver chain, such as a high-power amplifier, oscillator, ADC or digital-to-analog converter (DAC) etc., and can be modeled as an additive Gaussian distributed noise. Further, the IRS-HI results are due to the inability of infinite precision of the IRS phase shifts. Consequently, the impact of both T-HIs and IRS-HIs should be considered while analyzing the performance of IRS-enabled wireless communication systems.

Chapter 3

Performance Analysis of Full-Duplex Communication System

This chapter investigates the performance of FD systems under the impact of RSI. In the first part of this chapter we have considered a single user scenario, where a multi-antenna FD relay is assisting the BS to communicate with the user. Further, in part I, we consider a DF protocol for the FD relay. Likewise, in the second part of this chapter we generalized it to a multiuser scenario. Further, in part II, the performance of a multiuser-based FD system is studied under non-ideal hardware and RSI. The analytical evaluation comprises of deriving the closed-form expressions for the OP, SE and EE for both parts.

Part I - Single User Scenario

3.1 Overview of Part I

In this part of the chapter, we investigate the performance of a FD-MIMO-DF relay system under RSI. The proposed analysis considers a multi-antenna-based FD relay system where the FD relay facilitates the transfer of information between a single antenna source and destination. The proposed scenario suits well for a typical wireless cellular architecture, wherein the multi-antenna BS works as a relay facilitating the exchange of information among the UEs. In general, the UEs are constrained by form-factor and complexity issues, so the half-duplex mode is preferred for UEs. Further, it is assumed that BS has enough computational and hardware resources to support FD operations. The multiple antennas at the FD relay have also been utilized for S-ER, along with information transmission and reception. It has been shown that allocating more antennas for S-ER increases the EE by contributing more towards EH

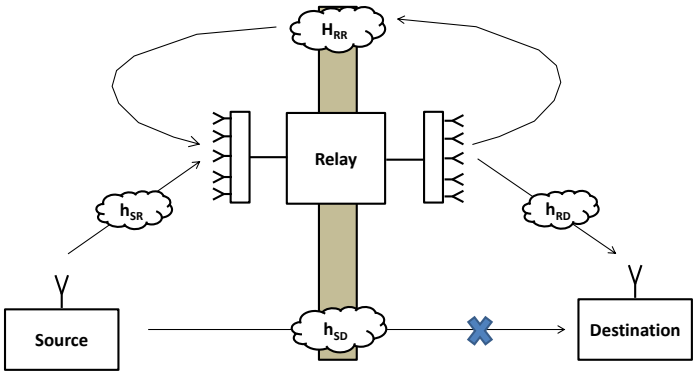

Figure 3.1: Schematic for the FD-MIMO-DF Relay System Model.

and reducing circuit power consumption. However, this also reduces the antenna array gain, adversely impacting the system's SE and OP. The impact of S-ER on the SE, EE and OP in the FD-MIMO-DF relay-based system is studied in this part.

The major contributions of this part of the proposed work is as follows

- The performance of a FD-MIMO-DF relay system in the presence of S-ER has been investigated. It has been shown that the source-to-FD relay link dictates the system performance since the SI impacts the source-to-FD relay link, whereas the relay-to-destination link is interference-free. Hence, the antennas at the transmit-end of the FD relay can efficiently be utilized for S-ER, which improves the EE of the system.

- It has been shown that S-ER improves the EE of the system, but it also slightly degrades the SE and OP. Further, an adaptive S-ER scheme is proposed, improving the EE and compensating for the degradation in the SE and OP.

- It has also been shown that the EE of the FD-MIMO-DF relay system depends on the total circuit power, which in turn depends on the number of active RF chains. Hence, employing S-ER further enhances the EE of the system by reducing the circuit power consumption by lowering the number of active RF chains.

- Closed-form expressions of OP, SE and EE have been derived for the FD-MIMO-DF relay system for both fixed and adaptive S-ER schemes.

3.2 System Model for FD-MIMO-DF Relay

In this work, we consider a dual-hop communication between source and destination via relay, and this can also be illustrated as Fig. 3.1. The source and destination are considered to be single-antenna and operating in a HD mode. In contrast, the relay is multi-antenna with N_t antennas at the transmit end and N_r antennas at the receiving end and is operating in a FD mode. Since the performance of the FD relay is impacted by the RSI, the received signal through the source-to-FD relay link experience interference from the SI. However, the relay-to-destination link is interference-free, i.e., the transmission of information from the FD relay node is not impacted by RSI. To exploit the above scenario, the proposed antenna allocation (AA) scheme allocates antennas at the FD relay node for information transmission/reception in an adaptive manner. Further, apart from information relaying, the FD relay also recycles a part of transmitted power through harvesting the SI by S-ER, which enhances the EE of the overall FD relay system.

3.2.1 Antenna Allocation

The antennas at the FD relay can either be allotted for S-ER or information relaying at both transmit and receive end of the relay. The allocation of antennas at the FD relay is defined by an antenna allocation ratio, η_a, where $a \in (t,r)$ and t,r refers to the transmit and receiving ends of the FD relay respectively. This can be mathematically represented as: $\eta_a = N_a^{\text{S-ER}}/N_a$. Hence, the number of antennas for S-ER is $N_a^{S-ER} = \eta_a N_a$, and $N_a^I = (1-\eta_a)N_a$ antennas are used for information relaying at both the transmit and receive-end of the FD relay. This has also been illustrated in Fig. 3.2.

3.2.2 Channel Model

The source-to-FD relay channel as well as FD relay-to-destination channel is modeled as flat Rayleigh fading channel denoted by $\mathbf{h}_{SR}$ and $\mathbf{h}_{RD}$ with dimensions $N_r^I \times 1$ and $1 \times N_t^I$ respectively. The channel elements of both $\mathbf{h}_{SR}$ and $\mathbf{h}_{RD}$ are independent and identically distributed (i.i.d.) with $\mathscr{CN}(0,1)$. The transmit data symbol x_S is transmitted from the source. In contrast, the relay transmits $N_t^I \times 1$ transmit data vector, denoted as $\mathbf{x}_R$, which may be thought of as the time-delayed and refined version of the data transmitted by the source. The elements of the transmit data are assumed to be i.i.d. with zero mean and variance $P_s = \mathrm{E}\left\{x_S x_S^H\right\}$ and $P_r = \mathrm{tr}\left(\mathrm{E}\left\{\mathbf{x}_R \mathbf{x}_R^H\right\}\right)$ respectively, where P_s and P_r are constrained by the total transmit power constraint at the source and the FD relay respectively. Furthermore, the $(\eta_t N_t + \eta_r N_r) \times N_t^I$ S-ER channel is modeled as flat Rayleigh fading channel denoted by $\mathbf{H}_{RR}$

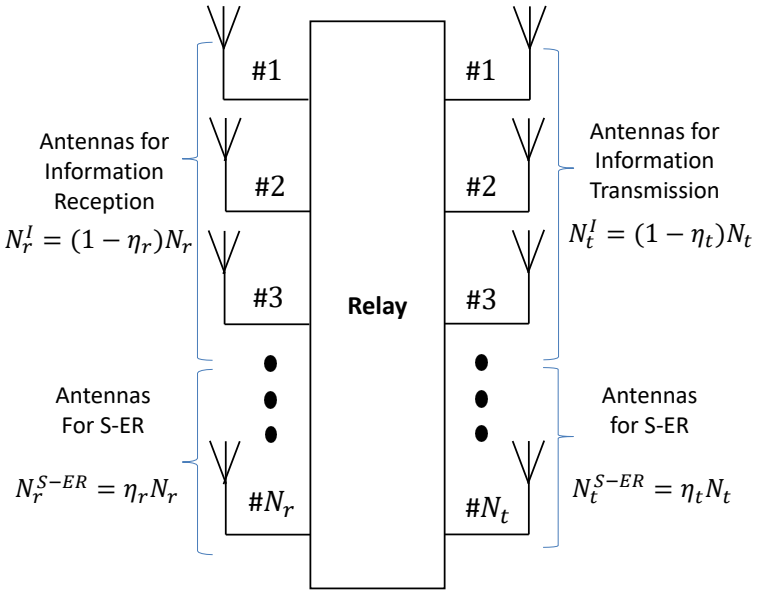

Figure 3.2: Illustration for the antenna allocation at the FD Relay for S-ER and information transmission and reception.

with i.i.d. elements, $h_{i,j} \sim \mathscr{CN}(0,1)$ [63]. Further, we assume that the direct link between the source and destination does not exist, or the direct path between the source and destination is blocked due to obstacles, i.e., $h_{SD} = 0$. Hence, the transmission occurs through the relay only [24]. It is also assumed that full channel state information (CSI) of source-to-FD relay channel ($\mathbf{h}_{SR}$), FD relay-to-destination channel ($\mathbf{h}_{RD}$) and the relay-to-relay channel ($\mathbf{H}_{RR}$) is available at the FD relay [64].

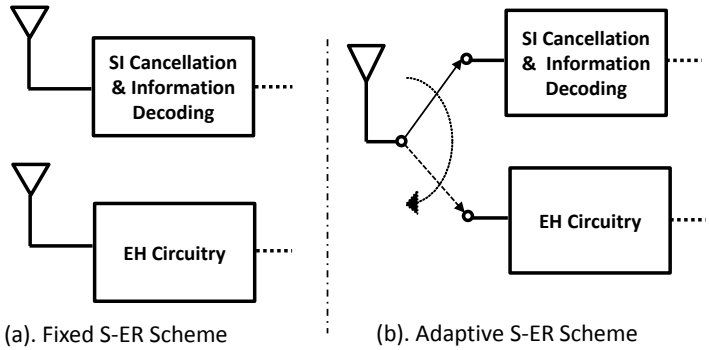

Figure 3.3: Utilizing antenna for S-ER: (a) Fixed and (b) Adaptive S-ER Scheme.

3.2.3 S-ER Schemes

Two different ways are proposed to implement the S-ER scheme, namely adaptive and fixed S-ER schemes. This has also been illustrated in Fig. 3.3

Adaptive S-ER Scheme: In the adaptive S-ER scheme, the N_t antennas at the transmit end of the FD relay are arranged in the decreasing order of channel gain. Then, the $N_t^I = (1-\eta_t)N_t$ antennas corresponding to the largest channel gains are taken adaptively for information transmission while the remaining $N_t^{S-ER} = \eta_t N_t$ are utilized for S-ER.

Fixed S-ER Scheme: In case of fixed S-ER scheme, the initial $N_t^I = (1-\eta_t)N_t$ antennas out of N_t antennas are used for transmission purpose, while the remaining $N_t^{S-ER} = \eta_t N_t$ are utilized for S-ER scheme.

Similarly, the N_r antennas at the receive-end of the relay can be allocated for both the S-ER schemes.

3.2.4 Received Signal Model

The $N_r^I \times 1$ received signal vector $\mathbf{y}_R$ at the relay can be expressed as

$$\mathbf{y}_R = \mathbf{h}_{SR} x_S + \mathbf{H}_{RR}\mathbf{x}_R + \mathbf{w}_R, \tag{3.1}$$

where $\mathbf{w}_R$ is the AWGN noise vector of dimension $N_r^I \times 1$ with its element being $\mathscr{CN}(0,\sigma^2)$. The received signal at the destination, y_D, can be expressed as

$$y_D = \mathbf{h}_{RD}\mathbf{x}_R + w_D, \tag{3.2}$$

where $w_D \sim \mathscr{CN}(0,\sigma^2)$ denotes the AWGN.

The self-interference component can be estimated at the FD relay since $\mathbf{x}_R$ is known to the relay. The estimated SI can be subtracted from the received signal. However, the complete cancellation of SI is inevitable due to the various imperfections associated with the estimation and cancellation. After subtracting the estimated SI from the received signal y_R in (3.1), the updated received signal can be rewritten as

$$\mathbf{y}_R = \mathbf{h}_{SR} x_S + \mathbf{d}_R + \mathbf{w}_R, \tag{3.3}$$

where $\mathbf{d}_R$ denotes the RSI vector of dimension $N_r^I \times 1$ with its element $d_R \sim \mathscr{CN}(0,\sigma_{rsi}^2)$ and $\sigma_{rsi}^2 = \alpha P_r^{\nu}$. The value of constants α and ν $(0 \leq \nu \leq 1)$ depends on the efficacy of the employed SI cancellation technique [19].

3.3 Performance Analysis of the proposed FD-MIMO-DF Relay System

In this section, we derive the analytical expressions for the SE, outage, symbol error rate (SER) performance and EE for the adaptive S-ER and fixed S-ER schemes. Initially, the rate equations are formulated for both the source-to-FD relay and FD relay-to-destination links, which are utilized in deriving the SE and outage probability. Further, a circuit power consumption model is also discussed in detail. The EE expressions are derived based on the SE, S-ER and the power consumption model.

3.3.0.1 Spectral Efficiency

The normalized instantaneous rate R_{in} for the source-to-FD relay link can be formulated from (3.3) and can be expressed as

$$\begin{aligned} R_{SR}^{in} &= \log_2\left(1+\rho_1(g)\right), \\ &= \log_2\left(1+\frac{g_1 P_s}{\sigma_{rsi}^2+\sigma^2}\right), \end{aligned} \tag{3.4}$$

where $\rho_1(g)$ is the SINR at the FD relay, $g_1 = \sum_{i=1}^{N_r^I} |h_i|^2$ denotes the channel gain for the source-to-FD relay link based on maximal ratio combining and σ^2 denotes the additive noise variance. The average SE (ASE) of the source-to-FD relay link can be defined as

$$ASE_{SR} = \mathrm{E}\left[R_{SR}^{in}\right] = \mathrm{E}\left[\log_2\left(1+\frac{g_1 P_s}{\sigma_{rsi}^2+\sigma^2}\right)\right]. \tag{3.5}$$

The closed-form expression for ASE of the source-to-FD relay link can be evaluated by solving the expectation over the distribution of channel gain g_1.

$$ASE_{SR} = \int_0^\infty \log_2\left(1+\frac{g_1 P_s}{\sigma_{rsi}^2+\sigma^2}\right) f_G(g_1)\mathrm{dg}_1. \tag{3.6}$$

Similarly, the normalized instantaneous rate R_{in} for the FD relay-to-destination link can be expressed as

$$\begin{aligned} R_{RD}^{in} &= \log_2\left(1+\rho_2(g)\right) \\ &= \log_2\left(1+\frac{g_2 P_r}{\sigma^2}\right), \end{aligned} \tag{3.7}$$

where $\rho_2(g)$ denotes the signal-to-noise ratio (SNR) at the destination, $g_2 = \sum_{i=1}^{N_I} |h_i|^2$, is the channel gain for the FD relay-to-destination link based on maximal ratio transmission. The ASE of the FD relay-to-destination link can be defined as

$$\begin{aligned} ASE_{RD} &= \mathrm{E}\left[R_{RD}^{in}\right], \\ &= \mathrm{E}\left[\log_2\left(1+\frac{g_2 P_r}{\sigma^2}\right)\right], \\ &= \int_0^{\infty} \log_2\left(1+\frac{g_2 P_r}{\sigma^2}\right) f_G(g_2)\mathrm{d}g_2. \end{aligned} \tag{3.8}$$

Now based on DF protocol, the end-to-end (e2e) ASE of the source-to-destination link via FD relay can expressed as

$$ASE_{e2e} = \min\left\{ASE_{SR}, ASE_{RD}\right\}. \tag{3.9}$$

3.3.0.2 Outage

The e2e outage from source-to-destination via FD relay P_{e2e} can be defined in the terms of P_{SR}^{out} and P_{RD}^{out} as

$$\begin{aligned} P_{e2e} =& 1-\left(1-P_{SR}^{out}\right)\left(1-P_{RD}^{out}\right), \\ =& P_{SR}^{out} + P_{RD}^{out} - P_{SR}^{out} P_{RD}^{out}, \end{aligned} \tag{3.10}$$

where P_{SR}^{out} is the outage probability for the source-to-FD relay link and P_{RD}^{out} is the outage probability for the FD relay-to-destination link.

The e2e outage can be evaluated in terms of a rate threshold, R_{th}, as discussed below. As a first step, we calculate the outage probability for the source-to-FD relay link, P_{SR}^{out}, which can be formulated as

$$P_{SR}^{out} = \Pr\left[R_{SR}^{in} < R_{th}\right]. \tag{3.11}$$

From (3.4), P_{SR}^{out} can be given as

$$\begin{aligned} P_{SR}^{out} &= \Pr\left[\log_2\left(1+\frac{g_1 P_s}{\sigma_{rsi}^2+\sigma^2}\right) < R_{th}\right], \\ &= \Pr\left[\frac{g_1 P_s}{\sigma_{rsi}^2+\sigma^2} < 2^{R_{th}}-1\right], \\ &= \Pr\left[g_1 < \frac{\left(2^{R_{th}}-1\right)\left(\sigma_{rsi}^2+\sigma^2\right)}{P_s}\right], \\ &= \Pr\left[g_1 < z_1\right], \end{aligned} \tag{3.12}$$

where $z_1 = \frac{\left(2^{R_{th}}-1\right)\left(\sigma_{rsi}^2+\sigma^2\right)}{P_s}$.

Thus, the closed-form expression of the outage probability for the source-to-FD relay link can be evaluated as

$$P_{SR}^{out} = \int_0^{z_1} f_G(g_1)\mathrm{d}g_1. \tag{3.13}$$

Similarly, in the second step, outage probability for the FD relay-to-destination link, P_{RD}^{out}, can be formulated as

$$P_{RD}^{out} = \Pr\left[R_{RD}^{in} < R_{th}\right]. \tag{3.14}$$

From (3.7), P_{RD}^{out} can be evaluated as

$$\begin{aligned} P_{RD}^{out} &= \Pr\left[\log_2\left(1+\frac{g_2 P_r}{\sigma^2}\right) < R_{th}\right], \\ &= \Pr\left[\frac{g_2 P_r}{\sigma^2} < 2^{R_{th}}-1\right], \\ &= \Pr\left[g_2 < \frac{2^{R_{th}}-1}{P_r/\sigma^2}\right], \\ &= \Pr\left[g_2 < z_2\right], \end{aligned} \tag{3.15}$$

where $z_2 = \frac{2^{R_{th}}-1}{P_r/N_o}$. Thus, the closed-form expression of the outage probability for the relay-to-destination link can be evaluated as

$$P_{RD}^{out} = \int_0^{z_2} f_G(g_2)\mathrm{d}g_2. \tag{3.16}$$

3.3.0.3 Energy Efficiency

The average EE (AEE) can now be defined in bits/Joule/Hz as the ratio of ASE over the total power budget

$$AEE = \frac{ASE}{P_{tot} - P_{ser}}, \tag{3.17}$$

where P_{tot} is the total power consumed in transmission and circuitry at the source, FD relay and the destination, and P_{ser} is the harvested power through S-ER. The modelling of P_{tot} and P_{ser} are described as below.

Power Consumption Modelling: The power consumption at the source comprises of the transmission power, P_s, the power consumed by the high power amplifier (HPA) at the source P^S_{amp}, and the other circuit power P^S_c (excluding the HPA power consumption)[1]. The power consumption of HPA is modeled as $P^S_{amp} = \beta P_s$, where $\beta = \frac{\varepsilon}{\varsigma} - 1$ and ε, ς are the peak-to-average ratio and the drain efficiency of HPA, respectively. The value of β depends on the modulation scheme and the associated constellation size.

The other circuit power P^S_c can be expressed as

$$P^S_c = P^S_{mix} + P^S_{syn} + P^S_{DAC} + P^S_{ecc} \tag{3.18}$$

where the P^S_{mix} is the mixer power consumption, the P^S_{syn} is the frequency synthesizer power consumption, P_{DAC} is the digital-to-analogy converter power consumption, and the P_{ecc} is the encoder power consumption. Therefore, the source power consumption can be written as

$$P^S_{tot} = (1+\beta)P_s + P^S_c, \tag{3.19}$$

which is a linear function over the transmission power at the source P_s. Since the HPA is not present at the destination, the power consumption at the destination can be expressed as

$$P^D_{tot} = P^D_c, \tag{3.20}$$

where P^D_c is the circuit power consumption at the destination.

Since the relay is equipped with multiple antennas, for ease of exposition and without any loss of generality, it is assumed that each active RF-chain consumes identical power [65]. So,

[1]The other circuit power accounts for the power consumed by other blocks such as mixer, DAC, frequency synthesizer.

the power consumption at the relay can be given as

$$P_{tot}^{R} = (1+\beta)P_r + P_c^{R}, \tag{3.21}$$

where P_c^R is the circuit power consumption (excluding the HPA power consumption) at the FD relay.

Further, since the relay needs extra power to cancel the RSI, denoting it as P_{SIC}. Based on state-of-the-art SI cancellation technologies discussed in the literature, P_{SIC} can be modeled as a linear function over the P_r. So, it can be expressed as below,

$$P_{SIC} = \alpha(1+\beta)P_r + P_{c0}, \tag{3.22}$$

where α is the isolating factor, and P_{c0} comprises of all other constant power consumption in the analog and digital SI cancellation circuit [66].

Thus, the total circuit power consumption of the FD relay system can be expressed as

$$P_c^{FD} = P_c^{S} + P_c^{R} + P_c^{D} + P_{SIC}. \tag{3.23}$$

Further, expressing $P_t = P_s + P_r$ as the total transmit power, the total power consumption in the FD relay system, P_{tot}, can be written as:

$$P_{tot} = (1+\beta)P_t + P_c^{FD}. \tag{3.24}$$

Self-Energy Recycling: The FD relay node not only collects the transmitted signal from the source node but also recycles part of its transmitted power as few of the antennas are being activated simultaneously for the energy harvesting purpose. The FD relay employs self-interference cancellation techniques in the remaining antennas to eliminate the SI signal [30]. The harvested energy at the relay will be stored in the battery, which prolongs the battery life at the FD-relay [67]. So, in the S-ER process, ηN_t antennas are allotted for S-ER out of N_t antennas at the FD relay transmit-end. The amount of power harvested through S-ER can be expressed as

$$\begin{aligned} P_{ser} =& \kappa \times \mathrm{E}\left[\mathrm{tr}\left\{\mathbf{H}_{RR}\mathbf{Q}_{xx}(\mathbf{H}_{RR})^{H}\right\}\right], \\ =& \kappa(\eta_t N_t + \eta_r N_r)(1-\eta_t)N_t P_r, \end{aligned} \tag{3.25}$$

where $\mathbf{Q}_{xx} = \mathrm{E}\left\{\mathbf{x}_R\mathbf{x}_R^H\right\}$ is the covariance matrix for relay transmitted signal $\mathbf{x}_R$ and κ is the RF-to-DC conversion efficiency [68]. Since the strength of received SI is several orders larger

than the strength of the received signal from the source, its contribution can be neglected in the harvested energy.

Based on the above formulations of SE, OP and EE, the subsequent subsections present the detailed derivation of the closed-form expressions of these quantities.

3.3.1 Adaptive S-ER Scheme

In the adaptive S-ER scheme, the antennas for information transmission at the FD relay are allocated adaptively based on the channel gain. So, the distribution of the channel gain for transmit antenna selection can be invoked utilizing the results derived in ordered statistics. From [69], the effective probability density function (PDF) for the sum of L_s largest exponentially distributed random variable out of L random variables can be given as

$$f_{\Sigma}(\gamma) = \binom{L}{L_s}\left[\frac{\exp(-\gamma)\gamma^{L_s-1}}{(L_s-1)!} + \sum_{\tau=1}^{L-L_s}(-1)^{L_s+\tau-1}\binom{L-L_s}{\tau}\right.$$
$$\left.\times\left(\frac{L_s}{\tau}\right)^{L_s-1}\exp(-\gamma)\left\{\exp\left(\frac{-(\tau\gamma)}{L_s}\right) - \sum_{m=0}^{L_s-2}\frac{1}{m!}\left(\frac{-\tau\gamma}{L_s}\right)^m\right\}\right]. \quad (3.26)$$

The above PDF, as described in (3.26), is utilized to evaluate the performance of the adaptive S-ER scheme in terms of SE, OP and EE.

3.3.1.1 Spectral Efficiency for Adaptive S-ER Scheme

From (3.6), the closed-form expression for ASE of the source-to-FD relay link can be evaluated as

$$ASE_{SR} = \int_0^{\infty}\log_2\left(1+\frac{g_1P_s}{\sigma_{rsi}^2+\sigma^2}\right)f_G(g_1)\mathrm{d}g_1, \quad (3.27)$$

or equivalently

$$ASE_{SR} = \frac{1}{\ln 2}\int_0^{\infty}\ln(1+g_1A_1)\,f_G(g_1)\mathrm{d}g_1, \quad (3.28)$$

where $A_1 = \frac{P_s}{\sigma_{rsi}^2+\sigma^2}$.

Now by substituting (3.26), the above expression can be expanded as

$$ASE_{SR} = \frac{1}{\ln 2}\int_0^{\infty} \ln\left(1+g_1A_1\right)\binom{N_r}{N_r^I}\exp\left(-g_1\right)\left[\frac{g_1^{N_r^I-1}}{\left(N_r^I-1\right)!}+\sum_{\tau=1}^{\eta N_r}(-1)^{N_r^I+\tau-1}\left(\frac{N_r^I}{\tau}\right)^{N_r^I-1}\binom{\eta N_r}{\tau}\right.$$
$$\left.\times\left\{\exp\left(\frac{-(\tau g_1)}{N_r^I}\right)-\sum_{m=0}^{N_r^I-2}\frac{1}{m!}\left(\frac{-\tau g_1}{N_r^I}\right)^m\right\}\right]\mathrm{d}g_1. \tag{3.29}$$

After some mathematical manipulations, (3.29) can be reformulated as

$$ASE_{SR} = \frac{1}{\ln 2}\binom{N_r}{N_r^I}\left[\int_0^{\infty}\frac{\exp\left(-g_1\right)\ln\left(1+g_1A_1\right)g_1^{N_r^I-1}}{\left(N_r^I-1\right)!}\mathrm{d}g_1\right.$$
$$+\sum_{\tau=1}^{\eta N_r}\Xi_1\left(\tau\right)\left\{\int_0^{\infty}\ln\left(1+g_1A_1\right)\exp\left(-g_1\right)\exp\left(\frac{-(\tau g_1)}{N_r^I}\right)\mathrm{d}g_1\right.$$
$$\left.\left.-\sum_{m=0}^{N_r^I-2}\Xi_2\left(m\right)\int_0^{\infty}\ln\left(1+g_1A_1\right)\exp\left(-g_1\right)g_1^m\mathrm{d}g_1\right\}\right], \tag{3.30}$$

where

$$\Xi_1\left(\tau\right) = (-1)^{N_r^I+\tau-1}\left(\frac{N_r^I}{\tau}\right)^{N_r^I-1}\binom{\eta N_r}{\tau} \tag{3.31}$$

and

$$\Xi_2\left(m\right) = \frac{1}{m!}\left(\frac{-\tau}{N_r^I}\right)^m, \tag{3.32}$$

or equivalently

$$ASE_{SR} = \frac{1}{\ln 2}\binom{N_r}{N_r^I}\left[\frac{1}{\left(N_r^I-1\right)!}\mathscr{I}_1+\sum_{\tau=1}^{\eta N_r}\Xi_1\left(\tau\right)\left\{\mathscr{I}_2-\sum_{m=0}^{N_r^I-2}\Xi_2\left(m\right)\mathscr{I}_3\right\}\right], \tag{3.33}$$

with

$$\mathscr{I}_1 = \int_0^{\infty}\exp\left(-g_1\right)\ln\left(1+g_1A_1\right)g_1^{N_r^I-1}\mathrm{d}g_1, \tag{3.34}$$

$$\mathscr{I}_2 = \int_0^{\infty}\ln\left(1+g_1A_1\right)\exp\left(\frac{-(\tau+N_r^I)}{N_r^I}g_1\right)\mathrm{d}g_1 \tag{3.35}$$

and

$$\mathscr{I}_3 = \int_0^{\infty} \ln(1+g_1A_1)\exp(-g_1)g_1^m \mathrm{d}g_1. \tag{3.36}$$

Using [70, Appendix A] and [71, eq. (4.337.2)], $\mathscr{I}_1, \mathscr{I}_2$ and $\mathscr{I}_3$ can be evaluated as

$$\mathscr{I}_1 = (N_r-1)!\exp\left(\frac{1}{A_1}\right)\sum_{k=0}^{N_r^I-1} \mathrm{E}_{k+1}\left(\frac{1}{A_1}\right), \tag{3.37}$$

$$\mathscr{I}_2 = -\frac{N_r^I}{\tau+N_r^I}\exp\left(\frac{\tau+N_r^I}{N_r^IA_1}\right)\mathrm{E}_i\left(\frac{-(\tau+N_r^I)}{N_r^IA_1}\right) \tag{3.38}$$

and

$$\mathscr{I}_3 = (m)!\exp\left(\frac{1}{A_1}\right)\sum_{k=0}^{m} \mathrm{E}_{k+1}\left(\frac{1}{A_1}\right), \tag{3.39}$$

where the exponential integral $\mathrm{E}_{\vartheta}(\theta)$ denotes a special case of complementary incomplete gamma function defined as [70]

$$\mathrm{E}_{\vartheta}(\theta) = \theta^{(\vartheta-1)}\Gamma(1-\vartheta,\theta), \tag{3.40}$$

for $\varpi = 0,1,2\ldots$ and $Re(\theta) > 0$.

Finally by substituting $\mathscr{I}_1, \mathscr{I}_2, \mathscr{I}_3$, Ξ_1 and Ξ_2 in (3.33) and rearranging the terms, the closed-form expression for ASE of the source-to-FD relay link can be expressed as

$$ASE_{SR} = \frac{1}{\ln 2}\binom{N_r}{N_r^I}\left[\exp\left(\frac{1}{A_1}\right)\sum_{k=0}^{N_r^I-1}\mathrm{E}_{k+1}\left(\frac{1}{A_1}\right) + \sum_{\tau=1}^{N_r-N_r^I}(-1)^{N_r^I+\tau-1}\binom{N_r-N_r^I}{\tau}\left(\frac{N_r^I}{\tau}\right)^{N_r^I-1}\right.$$
$$\left.\times\left\{\frac{-N_r^I}{\tau+N_r^I}\exp\left(\frac{\tau+N_r^I}{N_r^IA_1}\right)\mathrm{E}_i\left(\frac{-(\tau+N_r^I)}{N_r^IA_1}\right) - \sum_{m=0}^{N_r^I-2}\left(\frac{-\tau}{N_r^I}\right)^m\exp\left(\frac{1}{A_1}\right)\sum_{k=0}^{m}\mathrm{E}_{k+1}\left(\frac{1}{A_1}\right)\right\}\right]. \tag{3.41}$$

Now the closed-form expression for ASE of the FD relay-to-destination link as defined in (3.8) can be formulated identically by utilizing (3.26) as

$$ASE_{RD} = \int_0^{\infty}\log_2\left(1+\frac{g_2P_r}{\sigma^2}\right)f_G(g_2)\mathrm{d}g_2, \tag{3.42}$$

or equivalently

$$ASE_{RD} = \frac{1}{\ln 2}\int_0^{\infty} \ln\left(1+g_2A_2\right) f_G(g_2)\mathrm{d}g_2, \tag{3.43}$$

where $A_2 = \frac{P_r}{\sigma^2}$. Now by substituting (3.26), the above expression can be expanded as

$$ASE_{RD} = \frac{1}{\ln 2}\int_0^{\infty} \ln\left(1+g_2A_2\right)\binom{N_t}{N_t^I}\exp\left(-g_1\right)\left[\frac{g_2^{N_t^I-1}}{(N_t^I-1)!}\right.$$
$$\left. + \sum_{\tau=1}^{\eta N_t}(-1)^{N_t^I+\tau-1}\binom{\eta N_t}{\tau}\left(\frac{N_t^I}{\tau}\right)^{N_t^I-1}\left\{\exp\left(\frac{-(\tau g_2)}{N_t^I}\right) - \sum_{m=0}^{N_t^I-2}\frac{1}{m!}\left(\frac{-\tau g_2}{N_t^I}\right)^m\right\}\right]\mathrm{d}g_2, \tag{3.44}$$

which can be solved based on a similar approach that has been undertaken above while evaluating the expression in (3.29). Thus, the closed-form expression for the ASE of the FD relay-to-destination link, ASE_{RD}, can be expressed as

$$ASE_{RD} = \frac{1}{\ln 2}\binom{N_t}{N_t^I}\left[\exp\left(\frac{1}{A_2}\right)\sum_{k=0}^{N_t^I-1}\mathrm{E}_{k+1}\left(\frac{1}{A_2}\right) + \sum_{\tau=1}^{N_t-N_t^I}(-1)^{N_t^I+\tau-1}\binom{N_t-N_t^I}{\tau}\left(\frac{N_t^I}{\tau}\right)^{N_t^I-1}\right.$$
$$\left.\times\left\{\frac{-N_t^I}{\tau+N_t^I}\exp\left(\frac{\tau+N_t^I}{N_t^IA_2}\right)\mathrm{E}_i\left(\frac{-\left(\tau+N_t^I\right)}{N_t^IA_2}\right) - \sum_{m=0}^{N_t^I-2}\left(\frac{-\tau}{N_t^I}\right)^m\exp\left(\frac{1}{A_2}\right)\sum_{k=0}^{m}\mathrm{E}_{k+1}\left(\frac{1}{A_2}\right)\right\}\right], \tag{3.45}$$

where $A_2 = \frac{P_r}{\sigma^2}$.

So, the e2e ASE of the source-to-destination link for adaptive S-ER scheme, ASE_{e2e}^{adp} can now be expressed as

$$ASE_{e2e}^{adp} = \min\left\{ASE_{SR}, ASE_{RD}\right\}. \tag{3.46}$$

3.3.1.2 Energy Efficiency for Adaptive S-ER Scheme

The AEE for adaptive S-ER scheme, AEE_{e2e}^{adp}, as defined in (3.17) can now be evaluated by utilizing (3.24), (3.25), and (3.46). Hence, it can be written as

$$AEE_{e2e}^{adp} = \frac{ASE_{e2e}^{adp}}{(1+\beta)P_t + P_c^{FD} - \kappa(\eta_tN_t+\eta_rN_r)(1-\eta_t)N_tP_R}. \tag{3.47}$$

3.3.1.3 Outage for Adaptive S-ER Scheme

The outage probability for the source-to-FD relay link P_{SR}^{out} as defined in (3.13) can be evaluated as

$$P_{SR}^{out} = \int_0^{z_1} f_G(g_1)\mathrm{d}g_1, \tag{3.48}$$

which by utilizing (3.26) can be re-written as

$$P_{SR}^{out} = \int_0^{z_1} \binom{N_r}{N_r^I} \left[\frac{g_1^{N_r^I-1}}{(N_r^I-1)!}\exp(-g_1) + \sum_{\tau=1}^{\eta N_r} (-1)^{N_r^I+\tau-1} \binom{\eta N_r}{\tau} \left(\frac{N_r^I}{\tau}\right)^{N_r^I-1} \right.$$
$$\left. \times \exp(-g_1) \left\{ \exp\left(\frac{-(\tau g_1)}{N_r^I}\right) - \sum_{m=0}^{N_r^I-2} \frac{1}{m!} \left(\frac{-\tau g_1}{N_r^I}\right)^m \right\} \right] \mathrm{d}g_1. \tag{3.49}$$

After some mathematical manipulations (3.49) can be reformulated as

$$P_{SR}^{out} = \binom{N_r}{N_r^I} \left[\frac{1}{(N_r^I-1)!} \int_0^{z_1} g_1^{N_r^I-1} \exp(-g_1)\mathrm{d}g_1 \right.$$
$$\left. + \sum_{\tau=1}^{\eta N_r} \Xi_1(\tau) \left\{ \int_0^{z_1} \exp\left(\frac{-(\tau g_1)}{N_r^I}\right) \exp(-g_1)\mathrm{d}g_1 - \sum_{m=0}^{N_r^I-2} \Xi_2 \int_0^{z_1} (m)\, g_1^m \exp(-g_1)\mathrm{d}g_1 \right\} \right], \tag{3.50}$$

where

$$\Xi_1(\tau) = (-1)^{N_r^I+\tau-1} \left(\frac{N_r^I}{\tau}\right)^{N_r^I-1} \binom{\eta N_r}{\tau} \tag{3.51}$$

and

$$\Xi_2(m) = \frac{1}{m!} \left(\frac{-\tau}{N_r^I}\right)^m, \tag{3.52}$$

or equivalently

$$P_{SR}^{out} = \binom{N_r}{N_r^I} \left[\frac{1}{(N_r^I-1)!} \mathscr{J}_1 + \sum_{\tau=1}^{\eta N_r} \Xi_1(\tau) \left\{ \mathscr{J}_2 - \sum_{m=0}^{N_r^I-2} \Xi_2(m)\, \mathscr{J}_3 \right\} \right], \tag{3.53}$$

with

$$\mathscr{J}_1 = \int_0^{z_1} g_1^{N_r^I-1} \exp(-g_1) \mathrm{d}g_1, \tag{3.54}$$

$$\mathscr{J}_2 = \int_0^{z_1} \exp\left(\frac{-(\tau+1)g_1}{N_r^I}\right) \mathrm{d}g_1, \tag{3.55}$$

and

$$\mathscr{J}_3 = \int_0^{z_1} g_1^m \exp(-g_1) \mathrm{d}g_1. \tag{3.56}$$

Now by using [71, eq. (3.351.1)], $\mathscr{J}_1$, $\mathscr{J}_2$ and $\mathscr{J}_3$ can be evaluated as:

$$\mathscr{J}_1 = \left(N_r^I - 1\right)! - \exp(-z_1) \sum_{\omega=0}^{N_r^I-1} \frac{\left(N_r^I-1\right)!}{\omega!} z_1^{\omega}, \tag{3.57}$$

$$\mathscr{J}_2 = \frac{1 - \exp\left\{-z_1\left(1+\frac{\tau}{N_r^I}\right)\right\}}{\left(1+\frac{\tau}{N_r^I}\right)} \tag{3.58}$$

and

$$\mathscr{J}_3 = (m)! - \exp(-z_1) \sum_{\omega=0}^{m} \frac{(m)!}{\omega!} z_1^{\omega}. \tag{3.59}$$

Finally by substituting $\mathscr{J}_1$, $\mathscr{J}_2$, $\mathscr{J}_3$, Ξ_1 and Ξ_2 in (3.53) and rearranging the terms, the closed form expression for the outage probability for the source-to-FD relay, P_{SR}^{out} can now be expressed as

$$P_{SR}^{out} = \binom{N_r}{N_r^I} \left[1 - \exp(-z_1) \sum_{\omega=0}^{N_r^I-1} \frac{z_1^{\omega}}{\omega!} + \sum_{\tau=1}^{\eta N_r} (-1)^{N_r^I+\tau-1} \binom{\eta N_r}{\tau} \left(\frac{N_r^I}{\tau}\right)^{N_r^I-1} \right.$$
$$\left. \times \left\{ \frac{1 - \exp\left\{-z_1\left(1+\frac{\tau}{N_r^I}\right)\right\}}{\left(1+\frac{\tau}{N_r^I}\right)} - \sum_{m=0}^{N_r^I-2} \left(\frac{-\tau}{N_r^I}\right)^m \left(1 - \exp(-z_1) \sum_{\omega=0}^{m} \frac{z_1^{\omega}}{\omega!}\right) \right\} \right]. \tag{3.60}$$

Similarly, the outage probability for the FD relay-to-destination link P_{RD}^{out} as defined in (3.16) can be formulated as

$$P_{RD}^{out} = \int_0^{z_2} f_G(g_2)\mathrm{d}g_2, \tag{3.61}$$

which by utilizing (3.26) can be re-written as

$$P_{RD}^{out} = \int_0^{z_2} \binom{N_t}{N_t^I} \left[\frac{\exp(-g_1) g_2^{N_t^I-1}}{(N_t^I-1)!} + \sum_{\tau=1}^{\eta N_t} (-1)^{N_t^I+\tau-1} \binom{\eta N_t}{\tau} \left(\frac{N_t^I}{\tau}\right)^{N_t^I-1} \times \exp(-g_1) \left\{ \exp\left(\frac{-(\tau g_2)}{N_t^I}\right) - \sum_{m=0}^{N_t^I-2} \frac{1}{m!} \left(\frac{-\tau g_2}{N_t^I}\right)^m \right\} \right] \mathrm{d}g_2. \tag{3.62}$$

Similar to (3.49), the integral in (3.62) can be evaluated; thus, the closed form expression for the outage probability for the FD relay-to-destination link, P_{RD}^{out}, can be expressed as

$$P_{RD}^{out} = \binom{N_t}{N_t^I} \left[1 - \exp(-z_2) \sum_{\omega=0}^{N_t^I-1} \frac{z_2^\omega}{\omega!} + \sum_{\tau=1}^{\eta N_t} (-1)^{N_t^I+\tau-1} \binom{\eta N_t}{\tau} \left(\frac{N_t^I}{\tau}\right)^{N_t^I-1} \times \left\{ \frac{1 - \exp\left\{-z_2\left(1+\frac{\tau}{N_t^I}\right)\right\}}{\left(1+\frac{\tau}{N_t^I}\right)} - \sum_{m=0}^{N_t^I-2} \left(\frac{-\tau}{N_t^I}\right)^m \left(1 - \exp(-z_2) \sum_{\omega=0}^{m} \frac{z_2^\omega}{\omega!}\right) \right\} \right]. \tag{3.63}$$

So the e2e outage probability, i.e., of the source-to-destination link via relay, for adaptive S-ER scheme P_{e2e}^{adp} can be evaluated by substituting (3.60) and (3.63) in (3.10). Hence, this can be expressed as

$$P_{e2e}^{adp} = P_{SR}^{out} + P_{RD}^{out} - P_{SR}^{out} P_{RD}^{out}. \tag{3.64}$$

3.3.2 Fixed S-ER Scheme

In the fixed S-ER scheme, the antennas for information transmission are selected sequentially. The combined channel gain g is the sum of N_r^I independent Rayleigh fading channel gains. So, from [72], the distribution of resultant g is chi-square distribution with $2N_r^I$ degrees of freedom, which can be expressed as

$$f_G(g) = \frac{1}{(N_r^I-1)!} \exp(-g) g^{N_r^I-1}. \tag{3.65}$$

3.3.2.1 Spectral Efficiency for Fixed S-ER Scheme

Using (3.65), the ASE of the source-to-FD relay link as defined in (3.6) can be evaluated as

$$ASE_{SR} = \int_0^{\infty} \log_2\left(1+\frac{g_1 P_s}{\sigma_{rsi}^2+\sigma^2}\right)\frac{\exp(-g_1)g_1^{N_r^I-1}}{(N_r^I-1)!}\mathrm{dg}_1. \tag{3.66}$$

After some mathematical manipulations and using [70, Appendix A], (3.66) can be evaluated and the simplified closed-form expression for ASE of the source-to-FD relay link for the fixed S-ER scheme can be expressed as below:

$$ASE_{SR} = \frac{1}{\ln 2}\binom{N_r}{N_r^I}\exp\left(\frac{1}{A_1}\right)\sum_{k=0}^{N_r^I-1} E_{k+1}\left(\frac{1}{A_1}\right), \tag{3.67}$$

where $A_1 = \frac{P_s}{\sigma_{rsi}^2+\sigma^2}$.

Similarly, the ASE for FD relay-to-destination link for the fixed S-ER scheme can be evaluated from (3.8) utilizing (3.65),

$$\begin{aligned} ASE_{RD} &= \int_0^{\infty} \log_2\left(1+\frac{g_2 P_r}{\sigma^2}\right)\frac{\exp(-g_1)g_2^{N_t^I-1}}{(N_t^I-1)!}\mathrm{dg}_2, \\ &= \frac{1}{\ln 2}\binom{N_t}{N_t^I}\exp\left(\frac{1}{A_2}\right)\sum_{k=0}^{N_t^I-1} E_{k+1}\left(\frac{1}{A_2}\right), \end{aligned} \tag{3.68}$$

where $A_2 = \frac{P_r}{\sigma^2}$.

The e2e ASE of the source-to-destination link for fixed S-ER scheme, ASE_{e2e}^{fix}, can now be expressed as

$$ASE_{e2e}^{fix} = \min\left\{ASE_{SR}, ASE_{RD}\right\}. \tag{3.69}$$

3.3.2.2 Energy Efficiency for Fixed S-ER Scheme

The AEE for fixed S-ER scheme as defined in (3.17) can now be evaluated utilizing (3.24), (3.25) and (3.69)

$$AEE_{e2e}^{fix} = \frac{ASE_{e2e}^{fix}}{(1+\beta)P_t + P_c^{FD} - \kappa(\eta_t N_t + \eta_r N_r)(1-\eta_t)N_t P_R}. \tag{3.70}$$

3.3.2.3 Outage for Fixed S-ER Scheme

Now, P_{SR}^{out} and P_{RD}^{out} as defined in (3.13) and (3.16) respectively, can be evaluated for the fixed S-ER schemes as below:

Solving (3.13) by utilizing (3.65), the outage probabilities P_{SR}^{out} can be evaluated as

$$\begin{aligned} P_{SR}^{out} &= \int_0^{z_1} \frac{1}{(N_r^I-1)!} \exp(-g_1) g_1^{N_r^I-1} \mathrm{d}g_1, \\ &= 1 - \frac{\Gamma(N_r^I, z_1)}{\Gamma(N_r^I)}. \end{aligned} \tag{3.71}$$

Similarly by utilizing (3.65) for solving (3.16), the outage probabilities P_{RD}^{out} can be evaluated as

$$\begin{aligned} P_{RD}^{out} &= \int_0^{z_2} \frac{1}{(N_t^I-1)!} \exp(-g_1) g_2^{N_t^I-1} \mathrm{d}g_2, \\ &= 1 - \frac{\Gamma(N_t^I, z_2)}{\Gamma(N_t^I)}. \end{aligned} \tag{3.72}$$

Further, the e2e outage probability for the source-to-destination link via relay, P_{e2e} can be evaluated by substituting (3.71) and (3.72) in (3.10). After simplification the outage probability for fixed S-ER scheme, P_{e2e}^{fix} can be expressed as,

$$\begin{aligned} P_{e2e}^{fix} =& P_{SR}^{out} + P_{RD}^{out} - P_{SR}^{out} P_{RD}^{out}, \\ =& 1 - \frac{\Gamma(N_r^I, z_1)}{\Gamma(N_r^I)} \frac{\Gamma(N_t^I, z_2)}{\Gamma(N_t^I)}. \end{aligned} \tag{3.73}$$

From (3.73), it can be observed that as N_r^I or N_t^I increases, the overall outage probability decreases. Since N_r^I and N_t^I are inversely proportional to η_r and η_t respectively, hence that outage increases along with increasing η_r and η_t.

3.4 Simulation Results

In this section, we show the ASE, OP and AEE results for the FD-MIMO-DF relay system in the presence of proposed S-ER schemes. As discussed before, the channel assumed is flat Rayleigh fading. Further, the transmit power at the source and FD-relay is taken as $P_s = P_r = P_T$. Similarly, the circuit power consumption at the source, destination, self interference cancellation circuit and the relay is assumed to be P_c, i.e., $P_c^S = P_c^R = P_c^D = P_{co} = P_c$. The remaining simulation parameters are listed in Table 3.1.

Table 3.1: Simulation Parameters for FD-MIMO-DF Relaying System

Parameter	**Simulation Values**
Antennas at the FD Relay	N_t=10, N_r=10
Rate Threshold	R_{th} = 3 bps/Hz
RF-to-DC conversion efficiency	$\kappa = 0.5$
Variance of AWGN Noise	$\sigma^2 = 0$ dB
Variance of channel elements	1
RSI parameter	ν =1 , $\alpha = 0.01$
Co-efficient for HPA Power Consumption Model	$\beta = 0.8$

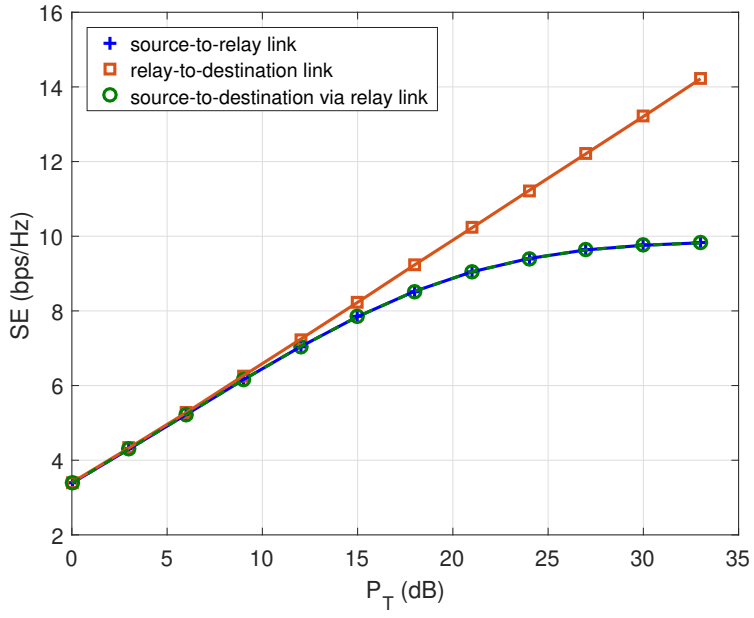

Figure 3.4: Analytical (solid lines) and simulation (marker points) shows the SE for the source-to-FD relay, relay-to-destination, and source-to-destination link various distinct transmit power level.

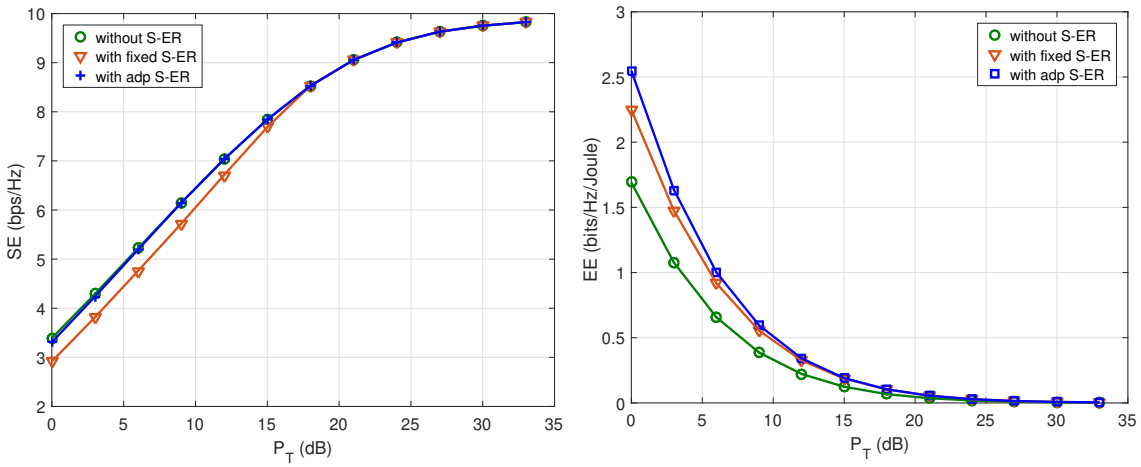

(a) SE (b) EE

Figure 3.5: Analytical (solid lines) and simulation (marker points) results of SE and EE with respect to P_T for various S-ER cases at $\eta_r = 0$, $\eta_t = 0.3$ and $P_c = 0$.

3.4.0.1 SE and EE results

Fig. 3.4 shows the ASE of the source-to-FD relay link, FD relay-to-destination and source-to-destination link via the FD relay. From the result, it can be observed that the ASE of the e2e source-to-destination link primarily depends on the source-to-FD relay link. For instance, at $P_T = 20$ dB, the ASE of the source-to-FD relay link is 9 bps/Hz, whereas for the FD relay-to-destination link ASE is 10 bps/Hz and the source-to-destination link is also 9 bps. This is because the SI impacts the source-to-FD relay link, and the FD relay-to-destination link is free from interference. Thus, the antennas at the transmit side of the FD relay can be employed for S-ER.

Fig. 5.2 shows the impact of S-ER on ASE and AEE for $\eta_r = 0$, $\eta_t = 0.3$ and $P_c = 0$. The results show that the adaptive S-ER scheme provides the best AEE compared to fixed S-ER and without S-ER. Further, $\eta_t = 0.3$ implies that $N_t^I = 7$ antennas are utilized for information transmission. The remaining 3 antennas are used for S-ER at the transmit end of the FD relay, whereas $\eta_r = 0$ implies that all the antennas are used for information reception at the receiving end of the FD relay. As discussed earlier, the e2e ASE primarily depends on the source-to-FD relay link. Thus, nearly the same ASE can be observed with, and without S-ER, as evident from Fig. 5.3(a), specifically the ASE for adaptive S-ER is almost equivalent to the ASE without S-ER. However, there is a considerable gain in AEE. For instance, as shown in Fig. 5.3(b), the AEE at $P_T = 10$ dB is 0.3 bits/Hz/Joule without S-ER, whereas, with S-ER, it increases to 0.6 bits/Hz/Joule.

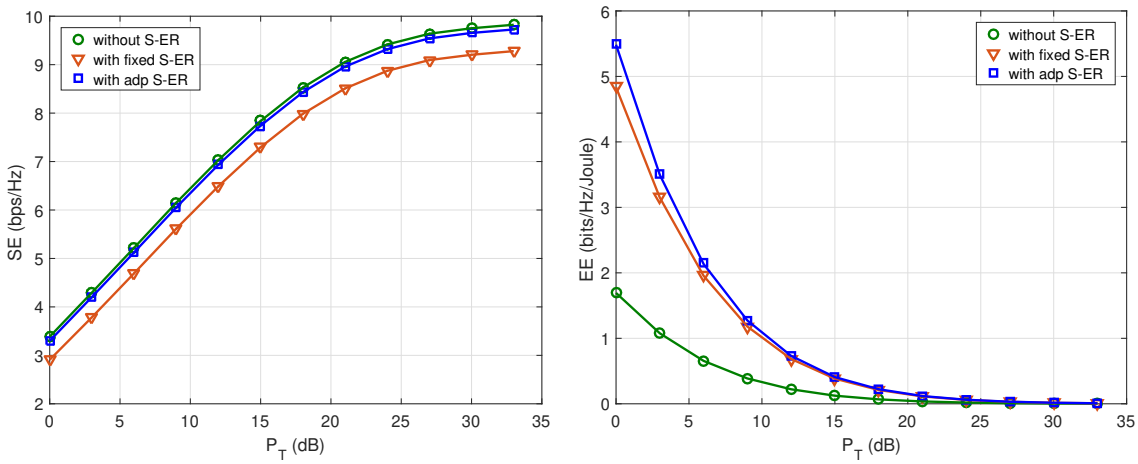

(a) SE (b) EE

Figure 3.6: Analytical (solid lines) and simulation (marker points) results of SE and EE with respect to P_T for various S-ER cases at $\eta_r = 0.3$, $\eta_t = 0.3$ and $P_c = 0$.

Fig. 5.3 shows the ASE and AEE for $\eta_r = 0.3$, $\eta_t = 0.3$, which implies that S-ER is employed at both transmit and receive end of relay. As discussed before, this will reduce the antenna array gain of the source-to-FD relay link, and hence, there would be a slight degradation in SE, as shown in Fig. 5.3(c). However, by utilizing the adaptive S-ER scheme, the loss due to antenna array gain can be compensated, as shown through the results. Fig. 5.3 also validates that adaptive S-ER provides nearly equal ASE vis-a-vis full antenna transmission and contributes to the AEE compared to the case without S-ER. For instance, in Fig. 5.3(c), at $P_T = 15$ dB, the ASE without S-ER is 7.8 bps/Hz; however, with a fixed S-ER scheme, the ASE reduces to 7.2 bps/Hz. The degradation in ASE can somewhat be compensated through an adaptive S-ER scheme, which results in an ASE of 7.7 bps/Hz, nearly equal to the ASE of without S-ER case. Similarly, from Fig. 5.3(d) the AEE at $P_T = 10$ dB for without S-ER case is 0.3 bit/Hz/Joule, whereas with S-ER AEE increases significantly to 1 bit/Hz/Joule. The results confirm that the adaptive S-ER scheme provides the best performance in terms of AEE while also providing the ASE, which is nearly equivalent to the case of without S-ER.

3.4.0.2 Impact of circuit power on EE

Fig. 3.7 shows the impact of circuit power on the AEE of a FD-MIMO-DF relay system for $\eta = 0.3$. Fig. 3.7(a) and 3.7(b) shows the AEE of various S-ER schemes at $P_c = 3$ dB and $P_c = 10$ dB respectively. It can be observed from Fig. 3.7(b) that at $P_T = 10$ dB, the AEE without S-ER is 0.10 bits/Hz/Joule, whereas, with S-ER, it increases to 0.13 bits/Hz/Joule for fixed S-ER scheme and 0.14 bits/Hz/Joule for adaptive S-ER scheme. This improvement in

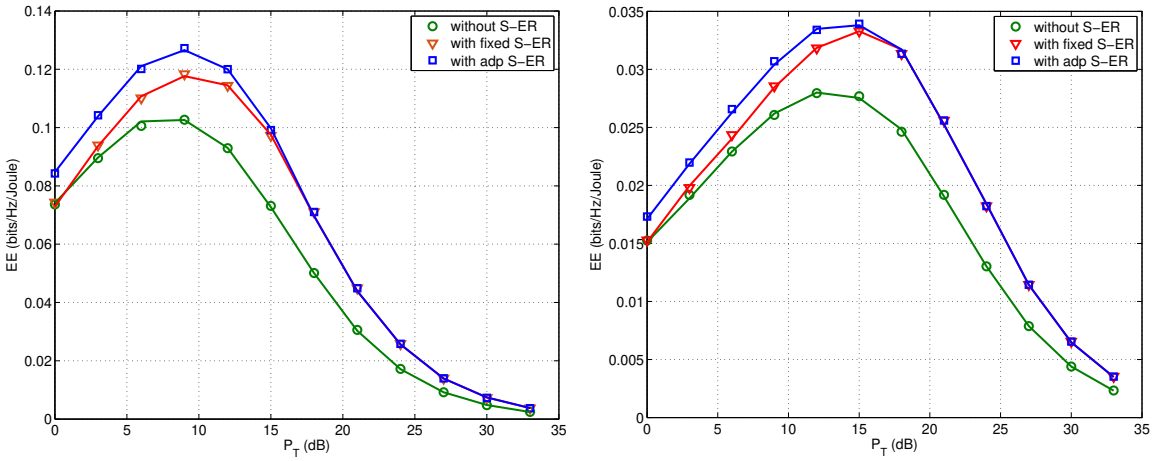

(a) EE at $P_c = 3$ dB

(b) EE at $P_c = 10$ dB

Figure 3.7: Analytical (solid lines) and simulation (marker points) results of EE with respect to P_T for various S-ER cases at $\eta = 0.3$ and different P_c

AEE is also due to the fact that in the case of adaptive S-ER, there is a reduction in circuit power consumption as the number of active RF chains is reduced, and the antennas corresponding to the inactive RF chains are being utilized for S-ER. It can be observed that initially, AEE increases and then decreases with P_T. This is because P_T increases exponentially, whereas the SE increases linearly with respect to the P_T. Thus when P_T is small, AEE increases due to an increase in ASE, whereas for larger values, the exponential increase of P_T dominates, and hence AEE decreases again. This can also be observed from (3.17). It is obvious from Fig. 3.7 that, for $P_c = 3$ dB the maximum AEE is at $P_T = 9$ dB, whereas when the circuit power is increased to $P_c = 10$ dB the maximum AEE shifts between 12 to 15 dB of P_T.

3.4.0.3 Trade-off between the EE and SE

The trade-off between the EE and the SE in the context of the proposed S-ER scheme is shown in Fig. 3.8. It can be observed from the results that increasing the SE reduces the EE of the FD-relay system. However, the adaptive S-ER scheme provides the best EE for a fixed SE. Specifically, Fig. 3.8(a) shows the FD relay system performance trade-off between the EE and SE without considering the impact of circuit power. As evident from the result, the adaptive S-ER scheme provides the best EE for any given SE. Further, it can also be observed that increasing the SE reduces the EE, whereas the most energy-efficient region is the one that corresponds to the least SE.

The impact of circuit power on the trade-off of the EE with the SE can be seen in Fig. 3.8(b). It can be observed from the result that the most energy-efficient region is not the one

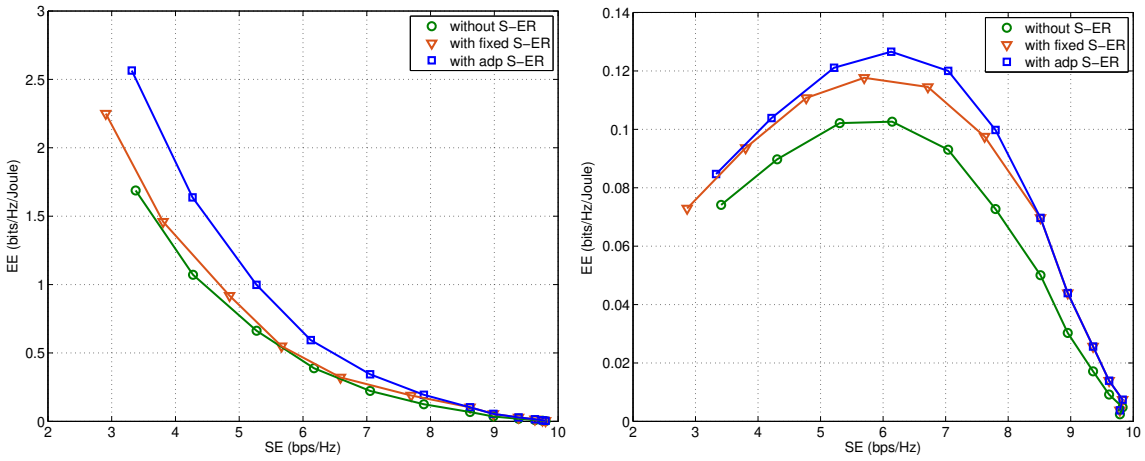

(a) EE versus SE without P_c

(b) EE versus SE with $P_c = 3$ dB

Figure 3.8: Analytical (solid lines) and simulation (marker points) shows the trade-off between the SE and the EE with respect to antenna allocation for both the S-ER schemes at $\eta = 0.3$ and different P_c.

corresponding to the least SE. However, the maximum EE is obtained at the SE of around 6 bps/Hz, whereas a further increase in SE leads to reduced EE in the FD-relay system. Moreover, the adaptive S-ER scheme provides the best EE for any given SE, consistent with the earlier observations.

3.4.0.4 Outage Performance

Fig. 3.9 shows the outage performance for both fixed S-ER and adaptive S-ER schemes. The analytical results agree with the simulation results, which validate the closed-form expressions obtained in the paper. It can be observed from Fig. 3.9(a) that the outage increases with η. This is due to the fact that increasing η implies that N_{S-ER} increases and subsequently N_I decreases, which lowers the diversity gain, consequently increasing the outage. Fig. 3.9(a) also shows that the outage performance for the adaptive S-ER scheme outperforms the fixed S-ER scheme. For instance, at $\eta = 0.5$ the outage probability for $P_T = 15$dB is 10^{-5} for adaptive S-ER scheme, whereas for fixed S-ER scheme it is 10^{-2}. Further, it can also be observed that for $P_T = 15$ dB, the outage probability for the case of without S-ER, i.e., $\eta = 0$ is 10^{-6} which is quite closer to what can be achieved by adaptive S-ER scheme. Thus, as evident from the results, the adaptive S-ER scheme compensates for the performance loss observed in the fixed S-ER scheme. Since in the adaptive S-ER, adaptive antenna allocation based on channel gain provides additional diversity gain for the same number of antennas as compared to fixed antenna allocation, hence, the adaptive S-ER scheme performs considerably better than the fixed S-ER scheme.

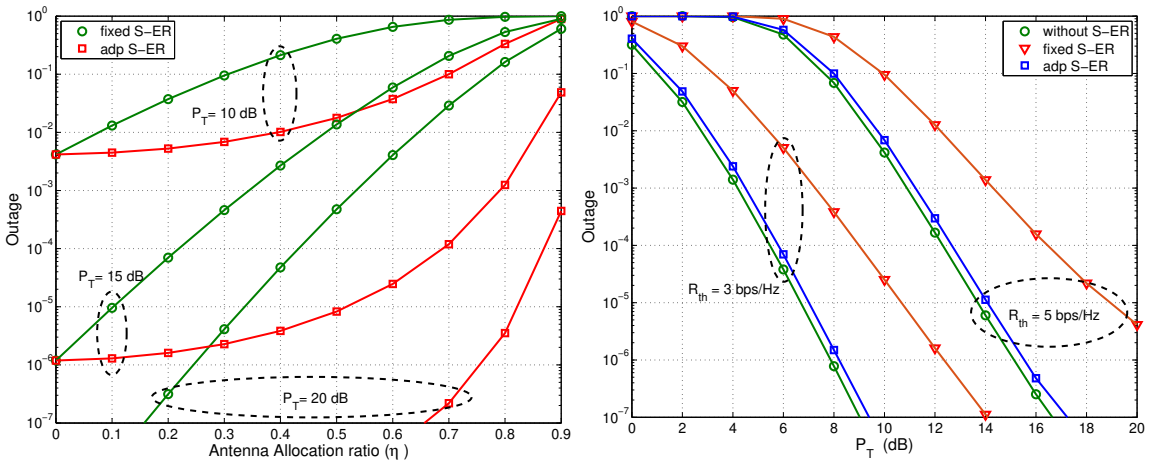

(a) Outage versus η (b) Outage versus transmit power P_T

Figure 3.9: Analytical (solid lines) and simulation (marker points) shows the outage performance with respect to η and various distinct transmit power levels for both the two S-ER schemes.

Fig. 3.9(b) shows the outage probability with respect to transmit power. It can be observed from the result that S-ER increases the outage probability. However, in the adaptive S-ER scheme, the degradation in outage performance is somewhat compensated. For instance, at $P_T = 6$ dB for $R_{th} = 3$ bps/Hz the outage probability for without S-ER case is 3×10^{-5} and for the fixed S-ER the outage increases to 4×10^{-3}. However, the adaptive S-ER scheme nearly compensates for the degradation in the outage. Specifically, the outage probability for adaptive S-ER for the same parameters is 5×10^{-5}. Further, it can also be observed that the outage increases when the rate threshold R_{th} increases. Thus as evident from the results, the adaptive S-ER provides nearly the same outage performance as without S-ER case. Thus, the adaptive S-ER technique enhances the EE and maintains the outage performance.

3.5 Conclusion of Part I

This part of the chapter investigates the impact of S-ER on the SE, OP and EE of a FD-MIMO-DF relaying system. Two S-ER schemes, namely fixed S-ER scheme and adaptive S-ER scheme, are proposed and analyzed. The closed-form expressions for OP, ASE and EE are also derived for the proposed S-ER schemes. As the number of antennas for S-ER at the FD relay increases, there is a corresponding gain in the EE due to recycling a part of transmitted signal power. However, this reduces array gain and leads to a slight degradation in the ASE and OP. Further, we have shown that the degradation in ASE and OP can be compensated via the proposed adaptive S-ER scheme while increasing the EE. The results also confirm that the

adaptive S-ER scheme enhances the EE while maintaining the ASE and the OP. Along with the analytical expressions, simulation results were also presented to verify the efficacy of the proposed analytical framework.

Part II - Multiuser Scenario

3.6 Overview of Part II

In the previous part, we presented the performance of a FD-MIMO-DF relay system with S-ER under RSI. However, the study was limited to point-to-point communication where two terminals were communicating with the help of a FD-MIMO-DF relay. In contrast, in this part, we consider a MU-MIMO set-up where the FD BS serves multiple users. Specifically, the performance of the FD MU-MIMO system is evaluated in terms of OP, SE and EE. Further, the multiple antennas at the BS can be utilized for S-ER and information transmission in the downlink. The number of antennas reserved for S-ER depends on the QoS requirement. Allocating more antennas for S-ER increases the EE and reduces circuit power consumption. However, this also reduces the antenna array gain, which impacts the system's SE. Consequently, there is a trade-off in EE-SE with respect to the number of antennas allocated for S-ER.

In this part, a comprehensive study is conducted to analyze the trade-off between SE and EE, with and without S-ER, for a linear and nonlinear FD MU-MIMO-OFDM system. The significant contributions of this part of work is as follows:

- This work investigates the impact of S-ER on the SE and EE of the FD MU-MIMO-OFDM system. Reserving a few antennas for the S-ER improves the EE of the system and reduces the circuit power consumption; however, it reduces the antenna array gain and consequently affects the SE.
- The proposed analytical formulation consists of closed-form derivation for SE, EE and outage probability for both linear and nonlinear FD MU-MIMO-OFDM systems.
- From the derived expressions, it has been shown that initially, EE increases with an increase in the number of antennas for S-ER. However, after attaining the maximum value, it again starts decreasing for both linear and nonlinear FD MU-MIMO-OFDM systems. Further, the maximum value of EE is also a function of circuit power.
- The proposed work also shows that the HPA nonlinearity severely impacts both SE and EE of the FD MU-MIMO OFDM system. The results confirm that the HPA nonlinearity reduces the SE, thus consequently affecting the EE of the system.

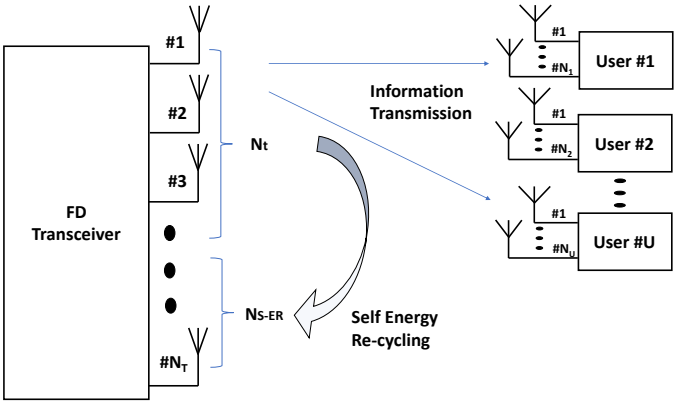

Figure 3.10: Transceiver architecture of the downlink FD MU-MIMO-OFDM System

3.7 System Model for FD MU-MIMO-OFDM

In this section, we describe the transceiver architecture of the downlink FD MU-MIMO-OFDM system. As shown in Fig.3.10, we consider a FD BS having N_T antennas and U users each having N_u receive antennas. At the BS, $N_{S\text{-}ER}$ antennas are allocated for S-ER and the remaining $N_t = N_T - N_{S\text{-}ER}$ antennas are used for data transmission. The allocation of antennas for S-ER is based on the desired QoS requirement, whereas N_t is preconditioned on the inter-user interference cancellation requirement, which is described in the subsequent sections.

Let $\mathbf{b}_u(k)$ represents the $L_u \times 1$ transmit data symbol vector at k^{th} subcarrier for u^{th} user where L_u represents the number of parallel data symbols for the u^{th} user, where the index u refer to u^{th} user $(u = 1, \ldots, U)$. Without loss of generality, it is assumed that transmit complex data symbols are i.i.d. with zero mean and variance P_u. The $\mathbf{b}_u(k)$ is passed through a transmit precoder matrix, $\mathbf{G}_u(k)$ of dimension $N_t \times L_u$ to eliminate the inter-user interference. The corresponding output can be expressed as:

$$\mathbf{z}_u(k) = \mathbf{G}_u(k)\mathbf{b}_u(k), \tag{3.74}$$

where $\mathbf{z}_u(k)$ is a $N_t \times 1$ precoded transmit vector for the u^{th} user at the k^{th} subcarrier. The power of each element of the precoded transmit vector $\mathbf{z}_u(k)$ is P_{z_u}, which can be given as [73]:

$$P_{z_u} = \frac{L_u P_u}{N_t}. \tag{3.75}$$

The data of all the users are combined before passing through the OFDM modulator; hence the combined precoded data can be represented as:

$$\mathbf{z}(k) = \sum_{u=1}^{U} \mathbf{z}_u(k). \tag{3.76}$$

The time domain representation of an OFDM modulation with N subcarriers, appended with the guard interval, N_{GI}, and the discrete-time index n $(-N_{GI} \leq n \leq N-1)$, can be expressed as:

$$x^t[n] = \frac{1}{N} \sum_{k=0}^{N-1} z^t(k) \exp(j2\pi kn/N), \tag{3.77}$$

where $z^t(k)$ is a complex data symbol at the t^{th} transmit antenna on the k^{th} subcarrier. By the CLT, when the number of subcarriers N is large, $x^t[n]$ can be assumed to be a complex Gaussian process with zero mean and $P_T = P_z/N$ variance. P_z is the variance of $z^t(k)$ and it can be evaluated as $P_z = \mathrm{E}\left[\left|z^t(k)\right|^2\right]$. Using (3.76), we have

$$\begin{aligned} P_z &= \sum_{u=1}^{U} \mathrm{E}\left[\left|z_u^t(k)\right|^2\right], \\ &= \sum_{u=1}^{U} P_{z_u}, \\ &= \sum_{u=1}^{U} \frac{L_u}{N_t} P_u. \end{aligned} \tag{3.78}$$

Hence, P_T can be re-written as:

$$P_T = \frac{1}{N} \sum_{u=1}^{U} \frac{L_u}{N_t} P_u. \tag{3.79}$$

The MIMO channel between N_t transmit antennas and $N_{S\text{-}ER}$ receive antennas can be denoted as $\mathbf{H}_{S\text{-}ER}$ with dimension $N_{S\text{-}ER} \times N_t$ whose elements are assumed to be i.i.d. with $\mathscr{CN}(0, \sigma^2_{S\text{-}ER})$ [74]. On the other hand, the MIMO channel between N_t transmit antennas and u^{th} user is assumed to be a multipath Rayleigh fading channel denoted as $\overline{\mathbf{H}}_u[n]$ and can be expressed as:

$$\overline{\mathbf{H}}_u[n] = \sum_{l=1}^{L} \overline{\mathbf{H}}_u^l \delta[n-l], \tag{3.80}$$

where L denotes the total number of delay taps. $\overline{\mathbf{H}}_u^l$ with dimension $N_u \times N_t$ is the channel response between BS and u^{th} user at the l^{th} tap delay with elements being i.i.d. and $\mathscr{CN}(0,1)$. At the receiver of u^{th} user, the received signal can be written as:

$$\overline{\mathbf{r}}_u[n] = \sum_{l=1}^{L} \overline{\mathbf{H}}_u^l \overline{\mathbf{x}}[n-l] + \overline{\mathbf{w}}_u[n], \tag{3.81}$$

where $\overline{\mathbf{r}}_u[n]$ is $N_u \times 1$ received signal vector at u^{th} user, $\overline{\mathbf{x}}[n]$ is $N_t \times 1$ transmit OFDM symbol vector, and $\overline{\mathbf{w}}_u[n]$ is a $N_u \times 1$ AWGN noise vector, whose elements are i.i.d. and $\mathscr{CN}(0,\sigma^2)$.

After the removal of the guard interval and applying discrete Fourier transform (DFT) at the receiver, the $N_u \times 1$ complex data symbol vector for u^{th} user of the k^{th} subcarrier can be expressed as [73]:

$$\mathbf{r}_u(k) = \mathbf{H}_u(k)\mathbf{x}(k) + \mathbf{w}_u(k), \tag{3.82}$$

where $\mathbf{H}_u(k)$ is $N_u \times N_t$ effective MIMO channel related to the k^{th} subcarrier for u^{th} user whose elements can be obtained by taking DFT of $\overline{\mathbf{H}}_u^l$ over all the delay taps, and $\mathbf{w}_u(k)$ is the noise vector at k^{th} subcarrier and u^{th} user. Using (3.74) and (3.76), the $N_t \times 1$ signal vector $\mathbf{x}(k)$ in (3.82) can be expressed as:

$$\begin{aligned}
\mathbf{x}(k) =& DFT\left[\sum_{i=1}^{U} \overline{\mathbf{x}}_i[n]\right] \\
=& \sum_{i=1}^{U} \mathbf{z}_i(k) \\
=& \sum_{i=1}^{U} \mathbf{G}_i(k)\mathbf{b}_i(k).
\end{aligned} \tag{3.83}$$

Using (3.83), the received vector $\mathbf{r}_u(k)$ in (3.82) can be written as:

$$\begin{aligned}
\mathbf{r}_u(k) &= \mathbf{H}_u(k) \sum_{i=1}^{U} \mathbf{G}_i(k)\mathbf{b}_i(k) + \mathbf{w}_u(k), \\
&= \underbrace{\mathbf{H}_u(k)\mathbf{G}_u(k)\mathbf{b}_u(k)}_{\text{I}} + \underbrace{\mathbf{H}_u(k) \sum_{i=1, i\neq u}^{U} \mathbf{G}_i(k)\mathbf{b}_i(k)}_{\text{II}} + \mathbf{w}_u(k).
\end{aligned} \tag{3.84}$$

The I term is the intended signal for the u^{th} user, whereas the II term is an inter-user interference to u^{th} user from the remaining $U-1$ users. This interference can be eliminated

through a transmit preprocessing technique, which selects U nonzero precoding matrices $(\mathbf{G}_1(k), \mathbf{G}_2(k), \ldots, \mathbf{G}_U(k))$ for all U users. The matrix $\mathbf{G}_u(k)$ can be expressed as [75]

$$\mathbf{G}_u(k) = \mathbf{V}_u(k)\mathbf{T}_u(k), \tag{3.85}$$

where $\mathbf{V}_u(k)$ is a $N_t \times N_q$ matrix whose columns are the orthonormal basis for the null space of $\hat{\mathbf{H}}_u(k)$ and $\mathbf{T}_u(k)$ is a nonzero $N_q \times L_u$ equivalent transmit precoding matrix. The sufficient condition to guarantee the existence of the nonzero precoding matrix $\mathbf{G}_u(k)$ is that the number of the transmit antennas should always be greater than the total number of receive antennas of all the users[75]. This can be given as [75]

$$N_t > \max\left\{ \sum_{i=1, i\neq u}^{U} N_i, u = 1, 2, \ldots, U \right\}. \tag{3.86}$$

Under the sufficient condition given in (3.86), N_q can be defined as:

$$N_q = N_t - \sum_{i=1, i\neq u}^{U} N_i. \tag{3.87}$$

The matrix $\mathbf{V}_u(k)$ can be computed through the singular value decomposition (SVD) of $\hat{\mathbf{H}}_u(k)$ as:

$$\hat{\mathbf{H}}_u(k) = \mathbf{F}_u(k) \begin{bmatrix} \mathbf{\Sigma}_u(k) & \mathbf{0} \\ \mathbf{0} & \mathbf{0} \end{bmatrix} \begin{bmatrix} \hat{\mathbf{V}}_u(k)^{\mathrm{H}} \\ \mathbf{V}_u(k)^{\mathrm{H}} \end{bmatrix}, \tag{3.88}$$

where the matrix $\hat{\mathbf{H}}_u(k)$ can be defined as [75]:

$$\hat{\mathbf{H}}_u(k) = \begin{bmatrix} \mathbf{H}_1(k) \\ \vdots \\ \mathbf{H}_{u-1}(k) \\ \mathbf{H}_{u+1}(k) \\ \vdots \\ \mathbf{H}_U(k) \end{bmatrix},$$

$\mathbf{F}_u(k)$ is a unitary matrix of dimension $N_t - N_q \times N_t - N_q$, $\blacksquare_u(k)$ is a $N_t - N_q \times N_t - N_q$ diagonal matrix and $\hat{\mathbf{V}}_u(k)$ is an orthonormal matrix of dimension $N_t \times N_t - N_q$, whose columns are the

row space of $\hat{\mathbf{H}}_u(k)$. Using (3.85), the received vector $\mathbf{r}_u(k)$ can be rewritten as:

$$\mathbf{r}_u(k) = \mathbf{H}_u(k)\mathbf{V}_u(k)\mathbf{T}_u(k)\mathbf{b}_u(k) + \mathbf{w}_u(k). \tag{3.89}$$

Note that the MU-MIMO system as represented by (3.89) has now been resolved to U parallel SU-MIMO systems. A closer inspection of (3.89) also reveals that the equivalent SU-MIMO channel of user u is $\tilde{\mathbf{H}}_u(k) = \mathbf{H}_u(k)\mathbf{V}_u(k)$, where the dimension of $\tilde{\mathbf{H}}_u(k)$ is $N_u \times N_q$. $\mathbf{T}_u(k)$ is the equivalent transmit processing matrix and it consists of the right singular vectors of $\tilde{\mathbf{H}}_u(k)$. Hence, (3.89) can be rewritten as:

$$\mathbf{r}_u(k) = \tilde{\mathbf{H}}_u(k)\mathbf{T}_u(k)\mathbf{b}_u(k) + \mathbf{w}_u(k). \tag{3.90}$$

The received signal in (3.90) is processed by $L_u \times N_u$ decoding matrix $\mathbf{D}_u(k)$, which can be expressed as:

$$\check{\mathbf{r}}_u(k) = \mathbf{D}_u(k)^{\mathrm{H}}\mathbf{r}_u(k). \tag{3.91}$$

Since $\tilde{\mathbf{H}}_u(k)$ is known at receiver, $\mathbf{D}_u(k)$ can be obtained as:

$$\tilde{\mathbf{H}}_u(k) = \mathbf{D}_u(k)\mathbf{\Lambda}_u(k)\mathbf{T}_u(k)^{\mathrm{H}}, \tag{3.92}$$

where $\mathbf{D}_u(k)$ and $\mathbf{T}_u(k)$ are left and right singular matrices, and $\mathbf{\Lambda}_u(k)$ can be denoted as a diagonal matrix comprising of the singular values.

The preprocessing technique converts the MIMO channel into an equivalent parallel SISO channel for each user. On substituting (3.90) and (3.92) in (3.91), we obtain

$$\begin{aligned}
\check{\mathbf{r}}_u(k) =& \mathbf{D}_u(k)^{\mathrm{H}}\mathbf{D}_u(k)\mathbf{\Lambda}_u(k)\mathbf{T}_u(k)^{\mathrm{H}}\mathbf{T}_u(k)\mathbf{b}_u(k) + \mathbf{D}_u(k)^{\mathrm{H}}\mathbf{w}_u(k) \\
=& \mathbf{\Lambda}_u(k)\mathbf{b}_u(k) + \tilde{\mathbf{w}}_u(k) \\
=& \begin{bmatrix} \sqrt{\lambda_u^{(1)}(k)}\, b_u^{(1)}(k) \\ \sqrt{\lambda_u^{(2)}(k)}\, b_u^{(2)}(k) \\ \vdots \\ \sqrt{\lambda_u^{(L_u)}(k)}\, b_u^{(L_u)}(k) \end{bmatrix} + \begin{bmatrix} \tilde{w}_u^{(1)}(k) \\ \tilde{w}_u^{(2)}(k) \\ \vdots \\ \tilde{w}_u^{(L_u)}(k) \end{bmatrix},
\end{aligned} \tag{3.93}$$

where $\sqrt{\lambda_u(k)}$ are the singular values of the equivalent channel matrix $\tilde{\mathbf{H}}_u(k)$. Since $\mathbf{D}_u(k)$ is a unitary matrix, the elements of $\tilde{\mathbf{w}}_u(k)$ are also i.i.d and $\mathscr{CN}(0, \sigma^2)$.

3.8 Outage Analysis

In this section, the outage probability expressions are formulated for linear and nonlinear FD MU-MIMO-OFDM systems with S-ER. The desired outage performance dictates the allocation of antennas for S-ER. As discussed in Section II, the $N_{S\text{-}ER}$ antennas are allocated for S-ER out of the total N_T antennas at the BS. The remaining $N_t = N_T - N_{S\text{-}ER}$ antennas are used for data transmission. This allocation can be represented through η $(0 \leq \eta < 1)$, which can be defined as: $\eta = N_{S\text{-}ER}/N_T$. Thus, $N_{S\text{-}ER}$ and N_t can be written as:

$$N_{S\text{-}ER} = \eta N_T; \quad N_t = (1-\eta)N_T. \tag{3.94}$$

The outage expressions are derived for both linear and nonlinear systems in the following subsections.

3.8.1 Linear System

The SNR of the q^{th} data stream for u^{th} user at the k^{th} subcarrier can be defined from the received symbol expression of (3.93) and can be expressed as:

$$SNR_u^{(q)}(k) = \frac{\lambda_u^{(q)}(k)P_u}{\sigma^2}. \tag{3.95}$$

The normalized instantaneous rate for the k^{th} subcarrier can be defined as:

$$\begin{aligned} R_{inst}(k) =& \log_2\left(1 + SNR_u^{(q)}(k)\right) \\ =& \log_2\left(1 + A_o\lambda_u^{(q)}(k)\right), \end{aligned} \tag{3.96}$$

where $A_o = \frac{P_u}{\sigma^2}$.

The outage probability per subcarrier per user can be defined in terms of the desired rate threshold, R_o, where R_o is the per subcarrier desired rate threshold for each user. The outage probability for the k^{th} subcarrier can be expressed as:

$$P_{out}(k) = \Pr\left[R_{inst}(k) < R_o\right]. \tag{3.97}$$

From (3.96) and (3.97), the outage probability expression can be written as:

$$\begin{aligned} P_{out}(k) &= \Pr\left[\log_2\left(1+A_o\lambda_u^{(q)}(k)\right) < R_o\right], \\ &= \Pr\left[A_o\lambda_u^{(q)}(k) < 2^{R_o}-1\right], \\ &= \Pr\left[\lambda_u^{(q)}(k) < \frac{2^{R_o}-1}{A_o}\right], \\ &= \int_0^{\frac{2^{R_o}-1}{A_o}} p_{\lambda_u}(\lambda_u(k))\,\mathrm{d}(\lambda_u(k)), \end{aligned} \tag{3.98}$$

where $\lambda_u(k)$ is randomly selected from $\lambda_u^{(q)}(k)$ whose distribution function is given as [70]:

$$p_\lambda(\lambda_u(k)) = \frac{1}{L_u}\sum_{q=0}^{L_u-1}\sum_{\tau=0}^{q}\sum_{\rho=0}^{2\tau}\left\{\frac{(-1)^\rho}{2^{2q-\rho}\tau!\rho!}\frac{(2\tau)!}{(\zeta+\tau)!}\binom{2q-2\tau}{q-\tau}\binom{2\tau+2\zeta}{2\tau-\rho}\lambda_u^{\rho+\zeta}(k)\exp(-\lambda_u(k))\right\}, \tag{3.99}$$

where ζ is the difference between the maximum and minimum of N_q and N_u, i.e., $\zeta = max(N_q,N_u) - min(N_q,N_u)$.

Hence by utilizing (3.99), (3.98) can be evaluated as:

$$\begin{aligned} P_{out}(k) = \frac{1}{L_u}\sum_{q=0}^{L_u-1}\sum_{\tau=0}^{q}\sum_{\rho=0}^{2\tau}\Bigg\{&\frac{(-1)^\rho}{2^{2q-\rho}\tau!\rho!}\frac{(2j)!}{(\zeta+\tau)!}\binom{2q-2\tau}{q-\tau} \\ &\times\binom{2\tau+2\zeta}{2\tau-\rho}\int_0^{\frac{2^{R_o}-1}{A_o}}\lambda_u^{\zeta+\rho}(k)\exp(-\lambda_u(k))\mathrm{d}\lambda_u(k)\Bigg\}. \end{aligned} \tag{3.100}$$

After some mathematical manipulations and solving (3.100), the average outage probability per user and subcarrier can be expressed as below:

$$\begin{aligned} P_{out} = \frac{1}{UL_u}\sum_{u=1}^{U}\sum_{q=0}^{L_u-1}\sum_{\tau=0}^{q}\sum_{\rho=0}^{2\tau}\Bigg\{&\frac{(-1)^\rho}{2^{2q-\rho}\tau!\rho!}\frac{(2\tau)!}{(\zeta+\tau)!}\binom{2q-2\tau}{q-\tau} \\ &\times\binom{2\tau+2\zeta}{2\tau-\rho}\gamma\left(\zeta+\rho+1,\frac{2^{R_o}-1}{A_o}\right)\Bigg\}. \end{aligned} \tag{3.101}$$

From (3.87) and (3.94), increasing η decreases N_t, which further reduces the value of N_q. Hence, ζ decreases on increasing η and thus, the outage probability in (3.101) increases with increasing η. This implies that as the number of antennas for S-ER increases, the outage probability also increases. Thus, $N_{S\text{-}ER}$ antennas can be allocated based on the desired outage requirement from (3.101).

3.8.2 Nonlinear System

In the nonlinear FD MU-MIMO-OFDM system, there would be an impairment due to the nonlinearity of HPA. For ease of analysis, we assume the HPAs in all transmit chains have identical behavioral characteristics [76]. The nonlinear HPA can be characterized by a memory polynomial model, which is given as [77]:

$$y^t[n] = \sum_{p=1}^{P} \sum_{m=0}^{M-1} c_{p,m} x^t[n-m] \left| x^t[n-m] \right|^{p-1}, \tag{3.102}$$

where $y^t[n]$ is the output of nonlinear HPA of the OFDM signal $x^t[n]$. $c_{p,m}$ is the nonlinearity coefficient of HPA, P is the nonlinearity order, and M corresponds to the memory depth. After DFT and removing the cyclic prefix, the received data signal $y^t(k)$ can be canonically decomposed into attenuation factor, which multiplies with the desired signal, and an additive nonlinear interference. It can be expressed as [76]:

$$y^t(k) = \mu(k) x^t(k) + \Psi^t(k), \tag{3.103}$$

where $\mu(k)$ is the attenuation factor. $\Psi^t(k)$ is the additive nonlinear interference, modeled as a zero-mean Gaussian process uncorrelated to the input signal, whose variance is defined as P_I. Restricting the nonlinearity to the third order, the expressions of $\mu(k)$ and $\Psi^t(k)$ can be defined as [76]:

$$\begin{aligned} \mu(k) &= \sum_{m=0}^{M-1} (c_{1,m} + 2c_{3,m} P_T) \exp(-j2\pi km/N), \\ \Psi^t(k) &= \sum_{n=1}^{N} \sum_{m=0}^{M-1} \left(c_{1,m} x^t[n-m] + c_{3,m} x^t[n-m] \times \left| x^t[n-m] \right|^2 \right) \exp(-j2\pi kn/N) - \mu(k) x^t(k). \end{aligned} \tag{3.104}$$

Based on (3.104), the SINR of the q^{th} data stream for u^{th} user in the nonlinear FD MU-MIMO-OFDM system can be defined as:

$$SINR_u^{(q)}(k) = \frac{\lambda_u^{(q)}(k) |\mu(k)|^2 P_u}{\lambda_u^{(q)}(k) P_I + \sigma^2}. \tag{3.105}$$

The normalized instantaneous rate for the q^{th} stream of u^{th} user can be defined as:

$$\begin{aligned} R_{inst}(k) =& \log_2\left(1+SINR_u^{(q)}(k)\right), \\ =& \log_2\left(1+\frac{A_1(k)\lambda_u^{(q)}(k)}{A_2(k)\lambda_u^{(q)}(k)+1}\right). \end{aligned} \tag{3.106}$$

where $A_1(k)=\frac{P_u|\mu(k)|^2}{\sigma^2}$ and $A_2(k)=\frac{P_I}{\sigma^2}$. The outage probability for nonlinear FD MU-MIMO-OFDM system can be evaluated utilizing (3.97) and (3.106) as below:

$$\begin{aligned} P_{out}(k) &= \Pr\left[\log_2\left(1+\frac{A_1(k)\lambda_u^{(q)}(k)}{A_2(k)\lambda_u^{(q)}(k)+1}\right) < R_o\right], \\ &= \Pr\left[\frac{A_1(k)\lambda_u^{(q)}(k)}{A_2(k)\lambda_u^{(q)}(k)+1} < 2^{R_o}-1\right], \\ &= \Pr\left[\lambda_u^{(q)}(k) < \frac{1}{\frac{A_1(k)}{2^{R_o}-1}-A_2(k)}\right], \\ &= \int_0^{\frac{1}{\frac{A_1(k)}{2^{R_o}-1}-A_2(k)}} p_{\lambda_u}(\lambda_u(k))\,\mathrm{d}\lambda_u(k). \end{aligned} \tag{3.107}$$

On substituting $p_{\lambda_u(\lambda_u(k))}$ from (3.99) and solving the above equation (3.107), the average outage probability per user and per subcarrier for nonlinear FD MU-MIMO-OFDM system can be expressed as:

$$\begin{aligned} P_{out} = \frac{1}{NUL_u}\sum_{k=1}^{N}\sum_{u=1}^{U}\sum_{q=0}^{L_u-1}\sum_{\tau=0}^{q}\sum_{\rho=0}^{2\tau}\Bigg\{ & \frac{(-1)^\rho}{2^{2q-\rho}\tau!\rho!}\frac{(2\tau)!}{(\zeta+\tau)!}\binom{2q-2\tau}{q-\tau} \\ & \times\binom{2\tau+2\zeta}{2\tau-\rho}\gamma\left(\zeta+\rho+1,\left(\frac{A_1(k)}{2^{R_o}-1}-A_2(k)\right)^{-1}\right)\Bigg\}. \end{aligned} \tag{3.108}$$

3.9 EE with S-ER

In this section, we evaluate the EE for the FD MU-MIMO-OFDM system for both linear and nonlinear cases.

3.9.1 Linear System

The per subcarrier SE of the linear FD MU-MIMO-OFDM system can be defined from (3.95) as:

$$SE = \frac{1}{N}\sum_{u=1}^{U}\sum_{k=0}^{N-1}\mathrm{E}\left[\log_2\left(1+A_o\lambda_u(k)\right)\right]. \tag{3.109}$$

The SE in (3.109) can be evaluated as:

$$SE = \frac{1}{N}\sum_{u=1}^{U}\sum_{k=0}^{N-1}\int_0^{\infty}\log_2\left(1+A_o\lambda_u(k)\right)p_{\lambda}\left(\lambda_u(k)\right)\mathrm{d}\lambda_u(k). \tag{3.110}$$

From (3.99), we can re-write the above as:

$$SE = \frac{1}{NL_u}\sum_{u=1}^{U}\sum_{k=0}^{N-1}\sum_{q=0}^{L_u-1}\sum_{\tau=0}^{q}\sum_{\rho=0}^{2\tau}\left\{\frac{(-1)^{\rho}}{2^{2q-\rho}\tau!\rho!}\frac{(2\tau)!}{(\zeta+\tau)!}\binom{2q-2\tau}{q-\tau}\binom{2\tau+2\zeta}{2\tau-\rho}\right.$$
$$\left.\times\int_0^{\infty}\log_2\left(1+A_o\lambda_u(k)\right)\lambda_u^{\rho+\zeta}(k)\exp\left(-\lambda_u(k)\right)\mathrm{d}\lambda_u(k)\right\}. \tag{3.111}$$

After some mathematical manipulation, the above expression can be further simplified as [70]

$$SE = \frac{1}{NL_u\ln 2}\exp\left(\frac{1}{A_o}\right)\sum_{u=1}^{U}\sum_{k=0}^{N-1}\sum_{q=0}^{L_u-1}\sum_{\tau=0}^{q}\sum_{\rho=0}^{2\tau}\left\{\frac{(-1)^{\rho}(2\tau)!}{\tau!\rho!2^{2q-\rho}}\frac{(\zeta+\rho)!}{(\zeta+\tau)!}\right.$$
$$\left.\times\binom{2q-2\tau}{q-\tau}\binom{2\tau+2\zeta}{2\tau-\rho}\sum_{\beta=0}^{\zeta+\rho}\mathrm{E}_{\beta+1}\left(\frac{N_t}{A_o}\right)\right\}, \tag{3.112}$$

where $\mathrm{E}_n(z)=\int_1^{\infty}\exp(-zx)x^{-n}\mathrm{dx}$ is the exponential integral function of order n [71].

We can now define the EE in terms of bits/Joule/Hz as the ratio of SE over the total consumed power (P_{total}) [78]. P_{total} comprises of circuit power P_c and the transmitted power P_t. P_c includes the power consumed by the filter, mixer, digital-to-analog converter and power amplifier. Without any loss of generality, we assume that the power consumed in each RF-chain

is identical [65]. Hence, the EE of the system can be expressed as:

$$\begin{aligned} EE &= \frac{SE}{P_{total}} = \frac{SE}{N_t P_c + N_t P_T}, \\ &= \frac{\exp(1/A_o)}{N \ln 2 \,(N_t P_c + P_t)} \sum_{u=1}^{U} \sum_{k=0}^{N-1} \sum_{q=0}^{L_u-1} \sum_{\tau=0}^{q} \sum_{\rho=0}^{2\tau} \left\{ \frac{(-1)^{\rho}\,(2\tau)!}{\tau!\rho!\,2^{2q-\rho}} \frac{(\zeta+\rho)!}{(\zeta+\tau)!} \right. \\ &\qquad \left. \times \binom{2q-2\tau}{q-\tau} \binom{2\tau+2\zeta}{2\tau-\rho} \sum_{\beta=0}^{\zeta+\rho} \mathrm{E}_{\beta+1}\left(\frac{N_t}{A_o}\right) \right\}, \end{aligned} \tag{3.113}$$

where $P_t = N_t P_T$ is the total transmit power. In the S-ER process, the amount of power harvested can be expressed as [67]

$$P_{S\text{-}ER} = \kappa \sigma^2_{S\text{-}ER} (1-\eta)\, \eta N_T^2 P_t, \tag{3.114}$$

where κ is the conversion efficiency for RF-to-DC conversion. The value of κ is assumed to be constant, $0 < \kappa \leq 1$, depending on rectification and circuitry design. As the contribution of noise power in harvested energy is negligible compared to signal power, noise power is not considered.

This harvested energy contributes to the transmitted power so that we can rewrite (3.113) as:

$$\begin{aligned} EE &= \frac{SE}{N_t P_c + P_t - P_{S\text{-}ER}} \\ &= \frac{\exp(1/A_o)}{N \ln 2 \,(N_t P_c + P_t - P_{S\text{-}ER})} \sum_{u=1}^{U} \sum_{k=0}^{N-1} \sum_{q=0}^{L_u-1} \sum_{\tau=0}^{q} \sum_{\rho=0}^{2\tau} \\ &\qquad \times \left\{ \frac{(-1)^{\rho}}{2^{2i-\rho}} \frac{(2\tau)!\,(\zeta+\rho)!}{\tau!\rho!\,(\zeta+j)!} \binom{2q-2\tau}{q-\tau} \binom{2\tau+2\zeta}{2\tau-\rho} \sum_{\beta=0}^{\zeta+\rho} \mathrm{E}_{\beta+1}\left(\frac{N_t}{A_o}\right) \right\}. \end{aligned} \tag{3.115}$$

The expression for EE in (3.115) shows that increasing η increases $P_{S\text{-}ER}$ till $\eta = 0.5$. Further, increasing η also decreases $N_t P_c$, the total circuit power consumption. Consequently, the EE of the system increases with η.

3.9.2 Non-Linear System

In the nonlinear system, there would be impairment due to the nonlinearity of HPA. Thus, the interference due to nonlinearity has to be considered while evaluating the performance of nonlinear systems. The overall SE of the nonlinear system can be evaluated by summing over

all the users and the data stream to each user; hence the SE can now be defined from (3.105) as:

$$SE = \frac{1}{N}\sum_{u=1}^{U}\sum_{k=0}^{N-1}\mathrm{E}\left[\log_2\left(1+\frac{A_1\lambda_u^{(q)}(k)}{A_2\lambda_u^{(q)}(k)+1}\right)\right]. \tag{3.116}$$

The expectation operator is defined over $\lambda_u^{(q)}(k)$. Here, the nonlinear interference term is also impacted by the fading, which is why this derivation differs from the linear system's derivation. Hence, SE can be evaluated as:

$$SE = \frac{1}{N}\sum_{u=1}^{U}\sum_{k=0}^{N-1}\int_0^{\infty}\log_2\left(1+\frac{A_1\lambda_u^{(q)}(k)}{A_2\lambda_u^{(q)}(k)+1}\right)p_{\lambda}\left(\lambda_u(k)\right)\mathrm{d}\lambda_u(k). \tag{3.117}$$

After some mathematical manipulations, (3.117) can be re-written as:

$$SE = \frac{1}{N}\sum_{u=1}^{U}\sum_{k=0}^{N-1}\int_0^{\infty}\left[\log_2\left(1+(A_1+A_2)\lambda_u^{(q)}(k)\right)-\log_2\left(1+A_2\lambda_u^{(q)}(k)\right)\right]p_{\lambda}\left(\lambda_u(k)\right)\mathrm{d}\lambda_u(k). \tag{3.118}$$

Utilizing (3.99), the SE can be formulated as:

$$SE = \frac{1}{NL_u}\sum_{u=1}^{U}\sum_{k=0}^{N-1}\sum_{q=0}^{L_u}\sum_{\tau=0}^{q}\sum_{\rho=0}^{2j}\left[\frac{(-1)^{\rho}}{2^{2q-\rho}\tau!\rho!}\frac{(2\tau)!}{(\zeta+\tau)!}\binom{2q-2\tau}{q-\tau}\binom{2\tau+2\zeta}{2\tau-\rho}\right.$$
$$\left.\times\int_0^{\infty}\left(\log_2\left(1+(A_1+A_2)\lambda_u^{(q)}(k)\right)-\log_2\left(1+A_i\lambda_u^{(q)}(k)\right)\right)\lambda_u^{\zeta+\rho}(k)\exp-\lambda_u(k)\mathrm{d}\lambda_u(k)\right]. \tag{3.119}$$

The above expression can be simplified as [79]:

$$SE = \frac{1}{N\ln 2}\sum_{u=1}^{U}\sum_{k=0}^{N-1}\sum_{q=0}^{L_u-1}\sum_{\tau=0}^{q}\sum_{\rho=0}^{2\tau}\left[\frac{(-1)^{\rho}(2\tau)!}{2^{2q-\rho}\tau!\rho!}\frac{(\zeta+\rho)!}{(\zeta+\tau)!}\binom{2q-2\tau}{q-\tau}\right.$$
$$\left.\times\binom{2\tau+2\zeta}{2\tau-\rho}\left\{\exp\left(\frac{1}{A_1+A_2}\right)\sum_{\beta=0}^{\zeta+\rho}\mathrm{E}_{\beta+1}\left(\frac{N_t}{A_1+A_2}\right)-\exp\left(\frac{1}{A_2}\right)\sum_{\beta=0}^{\zeta+l}\mathrm{E}_{\beta+1}\left(\frac{N_t}{A_2}\right)\right\}\right]. \tag{3.120}$$

Hence, the EE of the nonlinear system can be evaluated as:

$$EE = \frac{SE}{N_tP_c+P_t-P_{S\text{-}ER}}. \tag{3.121}$$

Table 3.2: Simulation Parameters for FD MU-MIMO-OFDM System

Parameter	Simulation Values
Antennas at BS (N_T)	20
Antennas at u^{th} user (N_u)	2
Users (U)	5
Sub carrier (N)	1024
Guard Interval (N_{GI})	256
Memory depth (M)	4
Nonlinearity Order (P)	3
Delay Taps (L)	6
Rate Threshold (R_o)	2
RF-to-DC conversion efficiency (κ)	0.5
Variance of AWGN Noise (σ^2)	0 dB
Variance of channel elements of $\mathbf{H}_{S\text{-}ER}$ ($\sigma^2_{S\text{-}ER}$)	-20 dB

Substituting SE from (3.120), the EE of the nonlinear FD MU-MIMO-OFDM system can be expressed as:

$$EE = \frac{1}{N\ln 2\left(N_t P_c + P_t - P_{S\text{-}ER}\right)} \sum_{u=1}^{U} \sum_{k=0}^{N-1} \sum_{q=0}^{L_u-1} \sum_{\tau=0}^{q} \sum_{\rho=0}^{2\tau} \left[\frac{(-1)^{\rho}(2\tau)!}{2^{2q-\rho}\tau!\rho!} \frac{(\zeta+\rho)!}{(\zeta+\tau)!} \binom{2q-2\tau}{q-\tau} \right.$$
$$\left. \times \binom{2\tau+2\zeta}{2\tau-\rho} \left\{ \exp\left(\frac{1}{A_1+A_2}\right) \sum_{\beta=0}^{\zeta+\rho} \mathrm{E}_{\beta+1}\left(\frac{N_t}{A_1+A_2}\right) - \exp\left(\frac{1}{A_2}\right) \sum_{\beta=0}^{\zeta+\rho} \mathrm{E}_{\beta+1}\left(\frac{N_t}{A_2}\right) \right\} \right]. \tag{3.122}$$

As formulated above, the EE of the nonlinear FD MU-MIMO-OFDM system consists of an additional term, which accounts for the impact of nonlinear interference. Thus it reduces the EE of the system compared to the linear case. The analytical expressions for EE and SE for linear and nonlinear systems are derived. Furthermore, the EE and SE for the S-ER case are also considered.

3.10 Simulation Results

This section presents the simulation results for the SE and EE of FD MU-MIMO-OFDM systems with and without S-ER. The simulation parameters are listed in Table 3.2.

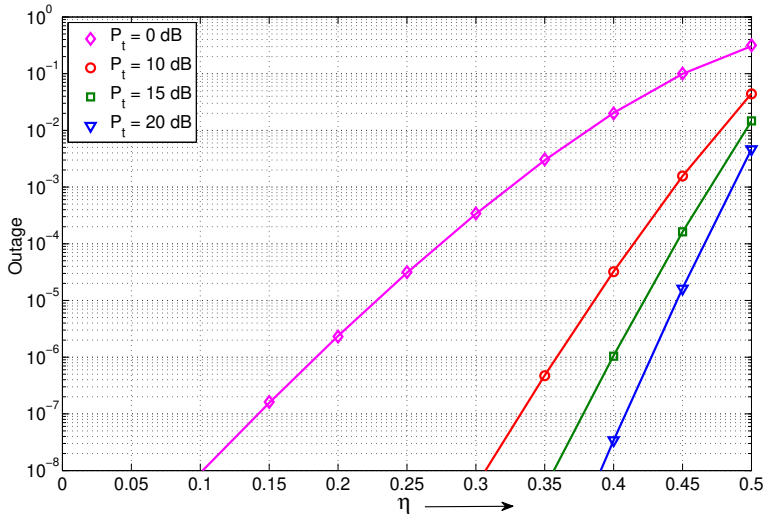

Figure 3.11: Outage performance for the linear FD MU-MIMO-OFDM system in a multipath Rayleigh fading channel with varying η.

The HPA nonlinearity is modeled through the memory polynomial model with a memory depth of 4 and a nonlinearity order of 3. The impact of nonlinearity can be reduced by operating the system with input backoff (IBO), which can be defined as IBO $= A^2/P_T$, where A is the input voltage that saturates the HPA output power. The MIMO channel between each user and BS is assumed to be a multipath Rayleigh fading channel with six delay taps and a uniform power delay profile. In the following subsections, the outage performance, SE and EE results are discussed for the linear and nonlinear FD MU-MIMO-OFDM systems. Further, it is followed by insights on the trade-off between SE and EE with respect to different parameters.

3.10.1 Linear FD MU-MIMO-OFDM System

This section presents the outage performance, SE and EE result for the linear FD MU-MIMO-OFDM system. Fig. 3.11 shows the outage performance of linear FD MU-MIMO-OFDM system with respect to η[2]. The simulation results align with the analytical results, which validates the above analysis. It can be observed from Fig. 3.11 that the outage decreases by increasing the value of η. This is because the higher value of η leads to the low number of antennas for data transmission, i.e., N_t, which reduces the system's instantaneous rate.

Hence, depending on the desired outage probability, we can fix the value of η. For instance, if the QoS requirement for the linear system is 10^{-6} outage, then from Fig. 3.11, we can select $\eta = 0.35$ at $P_t = 10$ dB. This implies that $N_{S\text{-}ER} = 7$, i.e., seven antennas can be spared for

[2]From (3.86), the required number of transmit antennas should be more than $20-4*2=8$ for data transmission; thus η can vary from 0 to 0.55.

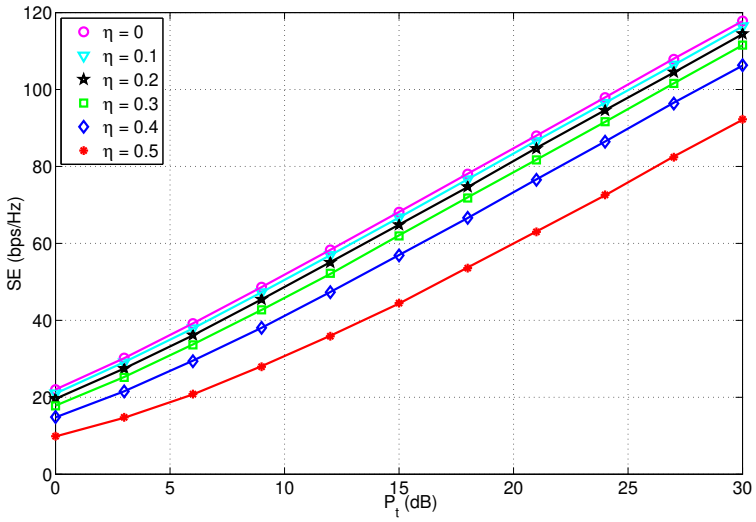

Figure 3.12: SE for linear FD MU-MIMO-OFDM system for different values of η.

S-ER purposes. Further, the outage performance improves when P_t is increased. For a $P_t = 15$ dB, as depicted from the Fig. 3.11, the outage performance of 10^{-6} corresponds to $\eta = 0.4$, which implies that now we can have $N_{S\text{-}ER} = 8$, i.e., eight antennas for S-ER purpose. The outage performance shows the QoS variation with respect to η for a fixed transmit power P_t. Similar observations can be made if we vary the transmit power P_t while fixing η as some constant.

Fig. 3.12 shows the SE for linear FD MU-MIMO-OFDM system with respect to transmit power P_t for different values of η. The curves show that SE reduces gradually along with increasing η due to the low number of antennas for data transmission. For instance at $P_t = 15$ dB, the SE is 68 bps/Hz for $\eta = 0$, while it reduces to 67, 65, 63, 56, and 44 bps/Hz for $\eta = 0.1, 0.2, 0.3, 0.4$ and 0.5, respectively.

Fig. 3.13 shows the EE results for the FD linear MU-MIMO-OFDM system with respect to η for two different values of P_c. The results show that EE initially increases with P_t, and after maximum EE, it again starts decreasing. This is due to the fact that for lower values of P_t, $N_t P_c$ term dominates as can be seen from (3.115), and also as the SE increases with increasing P_t, so EE initially increases with P_t. For larger values of P_t, P_t dominates as it increases exponentially, whereas the corresponding SE increases linearly; thus, the overall effect decreases the EE while increasing P_t. Specifically, these results show the maximum energy efficient region of the system in terms of P_t for a particular value of P_c. Moreover, while increasing P_c, P_t corresponding to the maximum EE region also increases.

The results in Fig. 3.13 also show that EE can be improved through S-ER, as EE increases with increasing η till $\eta = 0.4$. However, further increasing η reduces the EE due to considerable degradation in corresponding SE while going from $\eta = 0.4$ to $\eta = 0.5$. The results confirm

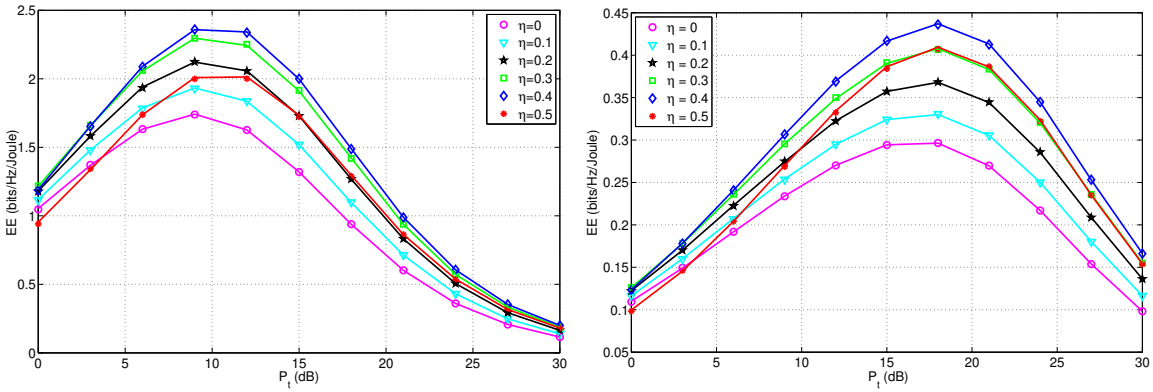

(a) $P_c = 0$ dB. (b) $P_c = 10$ dB.

Figure 3.13: Analytical (solid lines) and simulation (marker points) results of EE for the linear FD MU-MIMO-OFDM system for different values of η.

that although S-ER degrades the system's SE, it improves the EE of the system. Therefore, as long as the degradation in SE is within acceptable limits and satisfies the QoS requirement, S-ER can be used to improve the EE of the system.

Fig. 3.14 shows the joint impact of η and transmit power P_t on the EE of the linear FD MU-MIMO-OFDM system with $P_c = 10$ dB. As discussed above, the EE increases with η till a maximum value of EE is reached; afterward, it starts degrading. The EE corresponding to the region $\eta = 0.4$ to $\eta = 0.5$ and $P_t = 15$ dB to $P_t = 21$ dB is maximum as depicted in the Fig. 3.14.

The EE and SE trade-off for the linear FD MU-MIMO-OFDM system is shown in Fig. 3.15. It can be observed here that $\eta = 0.5$ provides the best EE for lower values of SE. However, as the SE value increases, $\eta = 0.4$ and $\eta = 0.3$ are the most energy efficient, respectively. As the EE of the system depends on both SE and P_{total}, the overall EE varies along with η. Increasing η decreases P_{total}; however, it also decreases the SE, as discussed previously. Hence, there is a trade-off between EE and SE with respect to η.

3.10.2 Nonlinear FD MU-MIMO-OFDM System

This section presents the outage performance, SE and EE result for the nonlinear FD MU-MIMO-OFDM Systems. Fig. 3.16 shows the outage performance for nonlinear FD MU-MIMO-OFDM system with respect to η. A good agreement between the simulation and analytical results verifies the abovementioned analysis. As evident from the result, the outage performance of the nonlinear system is worse than that of the linear case due to nonlinear distortion. Moreover, as we increase the P_t, the outage performance improves further, as shown

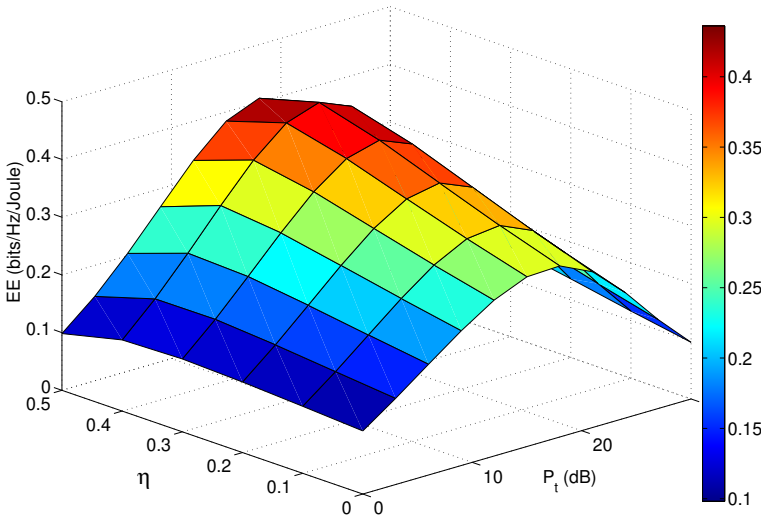

Figure 3.14: EE for linear FD MU-MIMO-OFDM system with respect to varying η and transmit power P_t.

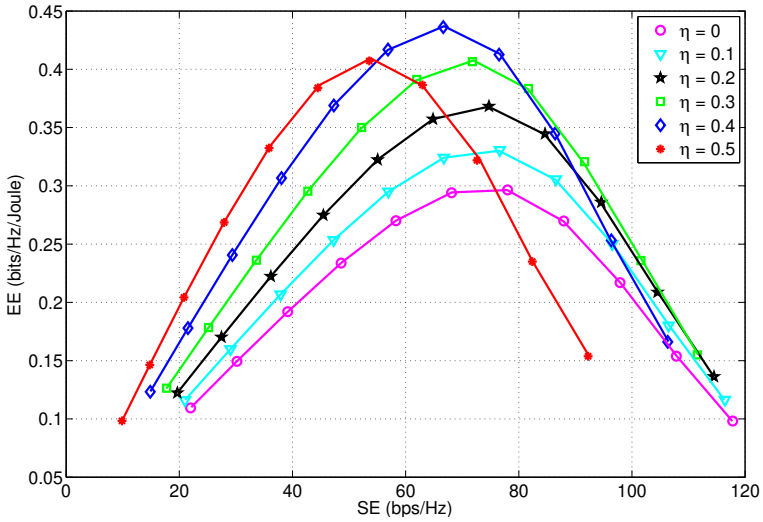

Figure 3.15: EE and SE trade-off for linear FD MU-MIMO-OFDM system for different values of η.

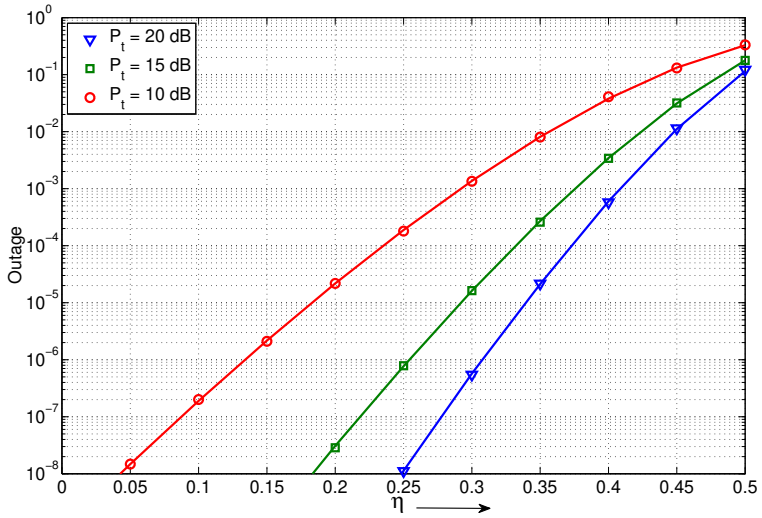

Figure 3.16: Outage performance for the nonlinear FD MU-MIMO-OFDM system in a multipath Rayleigh fading channel with varying η for IBO = 10 dB.

in Fig. 3.16. Further, depending upon the required outage performance, we can fix the value of η. For instance, if the QoS requirement is 10^{-6}, then from Fig. 3.16, we can select $\eta = 0.25$, i.e., $N_{S\text{-}ER} = 5$ at $P_t = 15$ dB.

Fig. 3.17 shows the SE for the nonlinear FD MU-MIMO-OFDM system with varying η. The results show that SE of the nonlinear system saturates and further starts decreasing at higher transmit power due to the impact of nonlinearity. Further, increasing η decreases the system's SE, as depicted in Fig. 3.17. Moreover, it can be observed that the considerable reduction in the SE is only observed for the large value of η. This is due to the fact for a higher value of η, N_t is decreased, which leads to lower channel gain, and hence SE reduces. For instance, Fig. 3.17(a) shows that SE decreases considerably while going from $\eta = 0.4$ to $\eta = 0.5$. In the nonlinear system, the impact of nonlinearity can be reduced by operating the HPA in the backoff region. IBO reduces the nonlinearity; hence, the SE performance improves, as depicted in Fig. 3.17(b), respectively.

Fig.3.18(a) and 3.18(b) shows the EE plots for the nonlinear FD MU-MIMO-OFDM system with and without IBO. It can be observed from the results that EE increases with increasing η. However, for a large value of η, it reduces slightly. As discussed earlier, EE depends on the SE as well as P_{total}, while SE decreases on increasing η, reducing the EE of the system. However, P_{total} also decreases due to reduced $N_t P_c$ and larger $P_{S\text{-}ER}$, which in turn increases the EE of the system. Therefore, a collective impact of both SE and P_{total} on EE is observed, as shown in Fig. 3.18(a). Hence, there is a trade-off between EE and SE with respect to η, and this trade-off can be observed by comparing the EE and SE results in Fig. 3.17 and Fig. 3.18. The EE results also offer insight into the impact of reasonable selection of η, and that particular

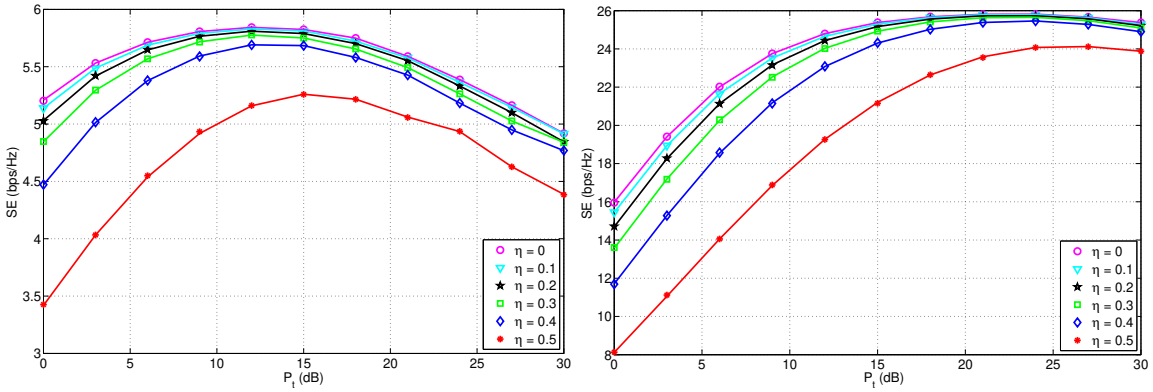

(a) SE with IBO = 0 dB. (b) SE with IBO = 10 dB.

Figure 3.17: Analytical (solid lines) and simulation (marker points) results of SE for the nonlinear FD MU-MIMO-OFDM system with $P_c = 10$ dB for different values of η.

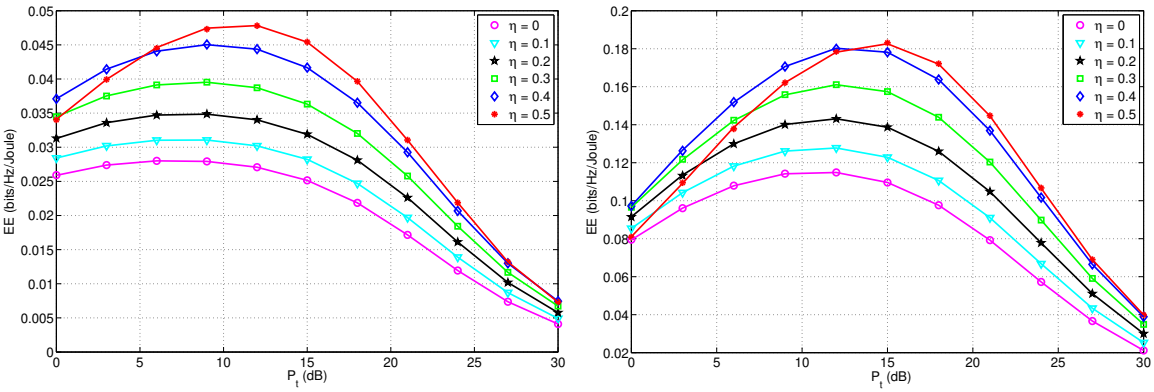

(a) EE with IBO = 0 dB. (b) EE with IBO = 10 dB.

Figure 3.18: Analytical (solid lines) and simulation (marker points) results of EE for the nonlinear FD MU-MIMO-OFDM system with $P_c = 10$ dB for different values of η.

value of η gives the best EE performance. For instance, $\eta = 0.4$ corresponds to the best EE result as depicted in Fig. 3.18(b). It can also be observed that increasing the IBO improves the EE of the nonlinear FD MU-MIMO-OFDM system, as can be seen, while comparing the result in Fig. 3.18(a) with Fig. 3.18(b).

Fig. 3.19 shows the joint impact of η and P_t on the EE of the nonlinear FD MU-MIMO-OFDM system. It can be observed that an increase in η increases the EE of the overall system. However, for the large value of η, the EE slightly degrades, similar to the linear case. This is because of the significant reduction in SE for $\eta = 0.5$ compared to $\eta = 0.4$. As depicted in the Fig. 3.19, the region corresponding to $\eta = 0.4$ to $\eta = 0.5$ and $P_t = 12$ dB to $P_t = 18$ dB is the providing the maximum EE in the nonlinear MU-MIMO-OFDM system.

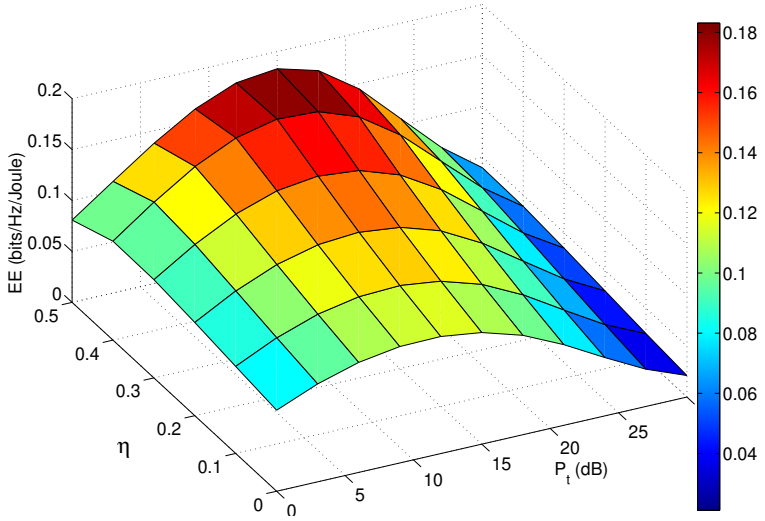

Figure 3.19: EE for nonlinear FD MU-MIMO-OFDM system with respect to varying η and transmit power P_t at IBO = 10 dB.

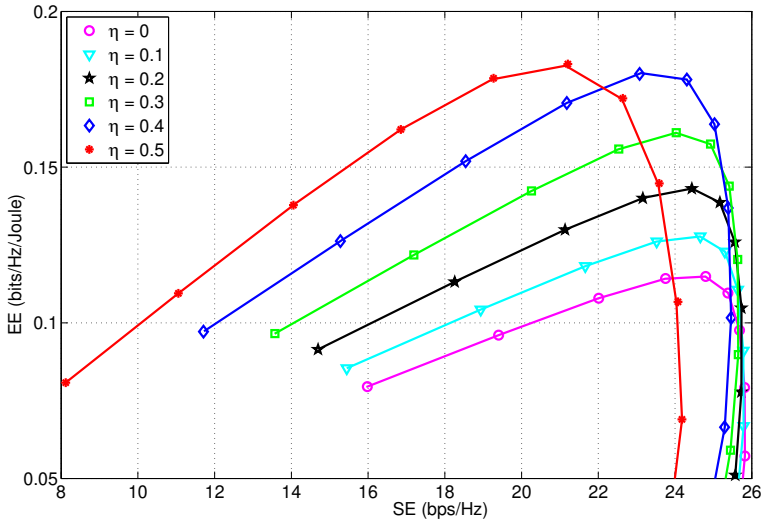

Figure 3.20: EE and SE trade-off for nonlinear FD MU-MIMO-OFDM system for different values of η at IBO = 10 dB.

However, the system's overall EE is much lower than the linear system due to the impact of nonlinearity. Fig. 3.20 shows the EE and SE trade-off for nonlinear FD MU-MIMO-OFDM system. It can be observed that $\eta = 0.5$ provides the best EE for lower SE performances. However, as the SE requirement increases, η corresponding to maximum EE decreases, as shown in Fig. 3.20. This is obvious; as the system requires more SE, fewer antennas can be allocated for S-ER. The curves also show that after a particular EE, there is a sharp decrease in EE. This is because initially SE increases with P_t, but afterward, it starts decreasing, whereas the transmit power P_t increases exponentially, which causes the EE to decrease sharply.

3.11 Conclusion of Part II

In this part, we investigated the impact of S-ER on the EE for the downlink FD MU-MIMO-OFDM system under RSI and transmitter nonlinearity. The SI present inherently in the FD systems is utilized opportunistically to harvest energy, thereby enhancing the EE of the system. However, this comes at the cost of slightly degrading the system's SE due to reduced array gain. The allocation of antennas for S-ER and information transmission can be done based on the desired QoS requirement for a FD MU-MIMO-OFDM system. Analytical expressions are derived for outage probability. Further closed-form expressions of EE and SE are formulated for both linear and nonlinear FD MU-MIMO-OFDM systems. Through the obtained results, it has been shown that S-ER improves the EE of the systems for both linear as well as a nonlinear systems. S-ER improves the EE of the system by re-cycling the transmitted energy portion at the cost of a slight degradation in the SE. As long as this degradation in SE satisfies the desired QoS, S-ER can be utilized to improve the EE of the FD MU-MIMO-OFDM system.

Chapter 4

Performance Analysis of IRS-assisted Communication System

This chapter investigates the performance of an IRS-assisted communication system. Specifically, the first part of this chapter investigates the performance of a single IRS-based communication system, while the latter deals with a dual IRS-based communication system. Further, the performance of the single and double IRS-based communication system is analyzed in the presence of HIs.

Part I - Single IRS Scenario

4.1 Overview of Part I

Recently, IRS has emerged as a revolutionary technology that can reconfigure the radio propagation environment by dynamically altering the amplitude and/or phase of wireless signals via a large number of reflecting units. In contrast to the vast literature on the performance analysis of IRS-enabled systems, this paper considers the theoretical characterization of the combined effect of IRS phase error and transceiver hardware impairments on the performance of an IRS-aided wireless communication system.

This part of the work investigates the combined impact of T-HIs and IRS-HIs on the performance of IRS-aided communication systems. The significant contributions in this part can be summarized as

- We present a model to characterize the impact of T-HIs and IRS-HIs on the performance of IRS-aided wireless systems taking into account both scenarios, viz with and without a direct link.

- Specifically, we derive the novel closed-form expressions for the SE, EE and OP for both scenarios, viz., in the presence of a direct link and when the direct link is obstructed. Further, the two special cases of high transmit SNR and large N are also discussed, where N is the number of REs at the IRS.

- The results show that the SE got saturated in the high transmit power regime and large N regimes, where N is the number of REs at the IRS. Numerical and simulation results reveal that T-HI and IRS-HI negatively impact the system's performance. However, the impact of T-HI is far more severe than the IRS-HI, as T-HI limits the received signal power and makes it independent of N, whereas IRS-HI reduces the order of the channel gain in the received signal power.

4.2 System Model for Single IRS-assisted Communication

Fig. 4.1 illustrates that the downlink single-antenna BS communicates with a single antenna UE. An IRS is employed to enhance the performance of UE, consisting of the N number of REs (here, $N > 1$). We consider the scenario where the direct link between the BS and UE is also present. Later, as a special case, we will consider the scenario where the direct link between the BS and UE is blocked. The channel between the BS and UE is assumed to be quasi-static and flat fading with the assumption of perfectly-known CSI. Since the IRS is deployed to have a line-of-sight (LoS) with the BS and the UE, the small-scale fading coefficients for the BS-to-IRS and IRS-to-UE, $\mathbf{h}_1$ and $\mathbf{h}_2$ can be characterized through the Rician fading model [80]. In contrast, the direct link between the BS-to-UE may not have the LoS; hence, h can be characterized through the Rayleigh fading model, thus, $h \sim \mathscr{CN}(0,1)$.

4.2.1 Transceiver Hardware Impairments

The assumption of ideal hardware when evaluating the performance of wireless communication systems is not practical. As discussed in the literature, the transceiver architecture at the RF front-end is prone to several inevitable additive impairments, such as in-phase/quadrature (I/Q) imbalance, radio front-end nonlinearity, and phase noise at the oscillator. A generic approach for modeling the combined effect characterizes the resultant 'distortion' noise to be Gaussian distributed[1].

[1] As discussed in [81], the Gaussian characterization has also been validated experimentally.

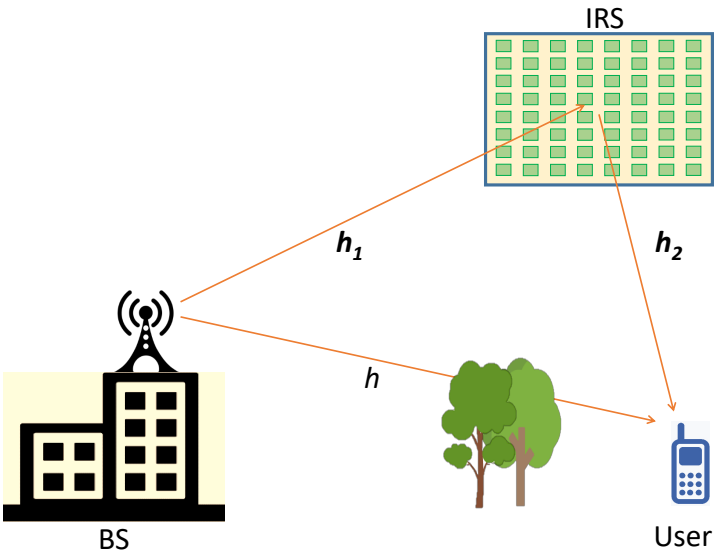

Figure 4.1: Schematic showing the proposed IRS-assisted communication scenario.

Consequently, there will be a mismatch between the actual broadcasted signal, $\tilde{x}$, and the desired signal, x, where $x \in \mathscr{CN}\left(0, \sigma^2\right)$. Thus, $\tilde{x}$ can be expressed as

$$\tilde{x} = x + w. \tag{4.1}$$

Here, w is the zero-mean complex Gaussian random variable representing the aggregated distortion noise. The variance of w can be modeled as

$$\sigma_w^2 = \kappa^2 \sigma_{in}^2, \tag{4.2}$$

where κ is the proportionality constant that dictates the severity of the HIs.

4.2.2 IRS Hardware Impairments

Ideally, the IRS is configured to provide a phase shift that cancels the overall phase shift and thus maximizes the received signal power at the desired receiver. However, a residual phase error exists in the actual phase shift imparted by the IRS due to these two possible reasons. This deviation of the actual phase shift from the ideally desired phase shift is modeled by setting the phase noise Θ, a random variable in $[-\pi, \pi)$.

- The first reason for the residual phase error is the imperfect channel estimate at the IRS and termed the phase estimation error. Specifically, Θ is modeled for this scenario as a zero-mean von Mises variable [82]. Here, τ is the concentration parameter that captures

the channel estimation accuracy. Further, in this case, the characteristic function can be expressed as

$$\varphi_p = \frac{I_p(\tau)}{I_p(\tau)}. \tag{4.3}$$

- Likewise, the second reason is the hardware imperfection due to practical hardware at the IRS. Here only a set of discrete phase shifts, 2^q ($q \geq 1$), are available instead of the ideally infinite phase shifts. Moreover, the error Θ is assumed to be uniformly distributed over $[-2^{-q}\pi, 2^{-q}\pi]$ [82]. For this case, the characteristic function can be defined as

$$\varphi_1 = \frac{\sin(2^{-q}\pi)}{2^{-q}\pi}, \tag{4.4}$$

and

$$\varphi_2 = \frac{\sin\left(2^{-q+1}\pi\right)}{2^{-q+1}\pi}. \tag{4.5}$$

4.3 Received Signal Model

This section describes the received signal model and evaluates the SNR formulation at UE for both scenarios, with and without a direct link.

4.3.1 With Direct Link

The received signal at the UE comprises the direct link as well as the reflected link via IRS. Thus, the received signal at UE, y_1, can be expressed as

$$y_1 = \left[\sqrt{\mathrm{PL}_h}\,h + \sqrt{\mathrm{PL}_{h_1}\mathrm{PL}_{h_2}}\,\mathbf{h}_2\,\Phi\,\mathbf{h}_1\right](x_s + w_s)\,\sqrt{P_s} + w_d + N_o, \tag{4.6}$$

where PL_h is the pathloss for the direct path between BS and UE, while PL_{h_1} and PL_{h_2} are the pathloss for the reflected link, i.e., BS-to-IRS and IRS-to-UE, respectively. Likewise, $w_s \in \mathscr{CN}\left(0, \kappa_s^2 P_s\right)$ is the distortion noise due to T-HI at the BS, and P_s denotes the transmit power at the BS. Further, Φ is the reflection coefficient matrix of the IRS and $w_d \in \mathscr{CN}\left(0, \kappa_d^2 \left|\sqrt{\mathrm{PL}_h}\,h + \sqrt{\mathrm{PL}_{h_1}\mathrm{PL}_{h_2}}\,\mathbf{h}_2\,\Phi\,\mathbf{h}_1\right|^2 P_s\right)$ represents the aggregated distortion noise due to the T-HIs at the UE. Also, $h = |h|\,e^{-j\phi}$ is the small-scale fading co-efficient for the direct link between the BS and the UE, where $|h|$ is the channel amplitude that can be

characterized through the Rayleigh random variable (RV) and ϕ is the channel phase. Finally, N_o is the AWGN with $N_o \in \mathscr{CN}(0,\sigma^2)$.

On expanding (4.6), we can re-write the received signal at NU as

$$y_1 = \left[\sqrt{\mathrm{PL}_h}\,h + \sqrt{\mathrm{PL}_{h_1}\mathrm{PL}_{h_2}}\sum_{i=1}^{N} h_2^i\,\Phi^i\,h_1^i\right](x_n + w_s)\sqrt{P_s} + w_d + N_o, \tag{4.7}$$

where, $h_1^i = \left|h_1^i\right| e^{-j\phi_1^i}$ is the channel co-efficient between the BS to the i-th RE of IRS with amplitude, $\left|h_1^i\right|$, and phase, ϕ_1^i. Similarly, $h_2^i = \left|h_2^i\right| e^{-j\phi_2^i}$ is the channel coefficient between the i-th RE of the IRS to UE with amplitude, $\left|h_2^i\right|$, and phase, ϕ_2^i. The envelopes of h_1^i and h_2^i for $i = 1,\cdots,N$ are i.i.d and characterized through Rician RV with a shape and scale factor of K_1, K_2 and Ω_1, Ω_2, respectively. It is also assumed that $\mathbf{h}_1$ and $\mathbf{h}_2$ are mutually independent of h and of each other.

4.3.1.1 IRS Reflection Parameters

Now by optimizing the reflection matrix, Φ, the total channel gain for the UE can be maximized, i.e., $\left|\sqrt{\mathrm{PL}_h}\,h + \sqrt{\mathrm{PL}_{h_1}\mathrm{PL}_{h_2}}\,\mathbf{h}_1\Phi\mathbf{h}_2\right|$. This can be achieved by adjusting θ^i to cancel the resultant phase of h_1^i, h_2^i and h. Thus, by applying $\theta^i = \phi - \phi_1^i + \phi_2^i$, the channel gain will be maximized and can be expressed as

$$\begin{aligned}
|\mathscr{H}_1|^2 &= \left|\sqrt{\mathrm{PL}_h}\,h + \sqrt{\mathrm{PL}_{h_1}\mathrm{PL}_{h_2}}\,\mathbf{h}_1\,\Phi\,\mathbf{h}_2\right|^2, \\
&= \left(\sqrt{\mathrm{PL}_h}\,|h| + \sqrt{\mathrm{PL}_{h_1}\mathrm{PL}_{h_2}}\sum_{i=1}^{N}\left|h_1^i\right|\left|h_2^i\right|\right)^2.
\end{aligned} \tag{4.8}$$

However, due to non-ideal hardware at the IRS, θ^i may not be able to cancel the resultant phase of h_1^i, h_2^i and h. Thus, the resultant channel gain will comprise of the phase error, which can be expressed as

$$|\mathscr{H}_1|^2 = \left(\sqrt{\mathrm{PL}_h}\,|h| + \sqrt{\mathrm{PL}_{h_1}\mathrm{PL}_{h_2}}\sum_{i=1}^{N}\left|h_1^i\right|\left|h_2^i\right| e^{j\Theta_i}\right)^2, \tag{4.9}$$

or equivalently

$$|\mathscr{H}_1|^2 = \left(\sqrt{\mathrm{PL}_h}\,|h| + \sqrt{\mathrm{PL}_{h_1}\mathrm{PL}_{h_2}}\,N\,|H|\right)^2, \tag{4.10}$$

where

$$H = \frac{1}{N}\sum_{i=1}^{N} \left|h_1^i\right| \left|h_2^i\right| e^{j\Theta_i}. \tag{4.11}$$

Utilizing (4.10), the received signal at UE in (4.7) can now be expressed as

$$y_1 = |\mathscr{H}_1|^2 \, x_s \sqrt{P_s} + w + N_o, \tag{4.12}$$

where

$$w = |\mathscr{H}_1|^2 \, w_s + w_d, \tag{4.13}$$

denotes the aggregated distortion caused by the transceiver impairments at the BS and UE.

4.3.1.2 SNR Formulation

Based on (4.12), the SDNR at UE can be expressed as

$$SDNR_1 = \frac{|\mathscr{H}_1|^2 \, P_s}{|\mathscr{H}_1|^2 \left(\kappa_s^2 + \kappa_d^2\right) P_s + \sigma^2}, \tag{4.14}$$

after rearranging the terms of 4.14, the SDNR at UE can be expressed as

$$SDNR_1 = \frac{|\mathscr{H}_1|^2 , \Upsilon_s}{|\mathscr{H}_1|^2 \left(\kappa_s^2 + \kappa_d^2\right) \Upsilon_s + 1}, \tag{4.15}$$

where $\Upsilon_s = \frac{P_s}{\sigma^2}$ is the transmit SNR.

Thus, the normalized instantaneous rate for the UE, R_1, can be evaluated from the SDNR at the UE as

$$\begin{aligned} R_1 &= \log_2 \left(1 + SDNR_1\right), \\ &= \log_2 \left(1 + \frac{|\mathscr{H}_1|^2 \, \Upsilon_s}{|\mathscr{H}_1|^2 \left(\kappa_s^2 + \kappa_d^2\right) \Upsilon_s + 1}\right). \end{aligned} \tag{4.16}$$

4.3.2 Without Direct Link

Now consider the scenario where the direct link is blocked. In this scenario, the communication between BS and UE occurs through the IRS via indirect LoS links, i.e., the BS-IRS-UE link.

Thus, the received signal at the UE, y_2, can be expressed as

$$y_2 = \sqrt{\mathrm{PL}_{h_1}\mathrm{PL}_{h_2}}\,\mathbf{h}_1\,\Phi\,\mathbf{h}_2\,(x_s + w_s)\,\sqrt{P_s} + w_d + N_o, \tag{4.17}$$

which on further expanding

$$y_2 = \sqrt{\mathrm{PL}_{h_1}\mathrm{PL}_{h_2}}\left[\sum_{i=1}^{N} h_1^i\,\Phi^i\,h_2^i\right](x_s + w_s)\,\sqrt{P_s} + w_d + N_o. \tag{4.18}$$

Similar to the scenario where the direct link is available, the maximum channel gain that can be achieved can be expressed as

$$|\mathscr{H}_2|^2 = \mathrm{PL}_{h_1}\mathrm{PL}_{h_2}\left(\sum_{i=1}^{N}\left|h_1^i\right|\left|h_2^i\right|\exp\left(j\Theta_i\right)\right)^2, \tag{4.19}$$

or equivalently,

$$|\mathscr{H}_2|^2 = N^2\,\mathrm{PL}_{h_1}\mathrm{PL}_{h_2}\,|H|^2, \tag{4.20}$$

where $H = \frac{1}{N}\sum_{i=1}^{N}\left|h_1^i\right|\left|h_2^i\right|\exp\left(j\Theta_i\right)$.

Hence, from (4.20), the received signal at UE in (4.18) can be re-written as

$$y_2 = |\mathscr{H}_2|^2\,(x_s + w_s)\,\sqrt{P_s} + w_d + N_o, \tag{4.21}$$

which, on simplification, gives

$$y_2 = |\mathscr{H}_2|^2\,x_s\,\sqrt{P_s} + w + N_o. \tag{4.22}$$

Additionally, it can also be noted here that for $\kappa_s = \kappa_d = 0$, the scenario reduces to the case of an ideal transceiver with no distortion, i.e., $w = 0$ in both (4.12) and (4.22).

Likewise, the SDNR at UE for this scenario can be expressed as

$$SDNR_2 = \frac{|\mathscr{H}_2|^2\,P_s}{|\mathscr{H}_2|^2\left(\kappa_s^2 + \kappa_d^2\right)P_s + \sigma^2}. \tag{4.23}$$

or equivalently

$$SDNR_2 = \frac{|\mathscr{H}_2|^2\,\Upsilon_s}{|\mathscr{H}_2|^2\left(\kappa_s^2 + \kappa_d^2\right)\Upsilon_s + 1}. \tag{4.24}$$

Thus, the normalized instantaneous rate for the UE in this scenario, R_2, can now be evaluated as

$$\begin{aligned} R_2 &= \log_2\left(1+SDNR_2\right), \\ &= \log_2\left(1+\frac{\left|\mathscr{H}_2\right|^2 \Upsilon_s}{\left|\mathscr{H}_2\right|^2\left(\kappa_s^2+\kappa_d^2\right)\Upsilon_s+1}\right). \end{aligned} \tag{4.25}$$

4.4 Performance Analysis of the IRS-Assisted Communication System

This section evaluates the SE, EE, and OP performance for an IRS-assisted communication system for both scenarios, i.e., with and without a direct link.

4.4.1 Spectral Efficiency

The SE for the scenario when the direct link is available can be formulated as

$$\begin{aligned} SE_1 &= \mathbb{E}\left[R_1\right], \\ &= \mathbb{E}\left[\log_2\left(1+\frac{\left|\mathscr{H}_1\right|^2 \Upsilon_s}{\left|\mathscr{H}_1\right|^2\left(\kappa_s^2+\kappa_d^2\right)\Upsilon_s+1}\right)\right], \end{aligned} \tag{4.26}$$

The PDF of $\mathscr{H}_1$ is not available in the closed form. Consequently, the ergodic rate of UE for the direct link scenario does not admit a closed-form expression. However, it can be approximated tightly by an upper bound [83].

We can evaluate an upper bound on SE_1. From (4.26), the rate can be re-written as

$$\begin{aligned} SE_1 &= \mathbb{E}\left[\log_2\left(\frac{1+\left|\mathscr{H}_1\right|^2\left(1+\kappa_s^2+\kappa_d^2\right)\Upsilon_s}{1+\left|\mathscr{H}_1\right|^2\left(\kappa_s^2+\kappa_d^2\right)\Upsilon_s}\right)\right], \\ &= \mathbb{E}\left[\log_2\left(1+\Xi_1\left|\mathscr{H}_1\right|^2\right)-\log_2\left(1+\Xi_2\left|\mathscr{H}_1\right|^2\right)\right], \\ &= \mathbb{E}\left[\log_2\left(1+\Xi_1\left|\mathscr{H}_1\right|^2\right)\right]-\mathbb{E}\left[\log_2\left(1+\Xi_2\left|\mathscr{H}_1\right|^2\right)\right], \end{aligned} \tag{4.27}$$

where Ξ_1 and Ξ_2 are constant defined as

$$\Xi_1 = \left(1+\kappa_s^2+\kappa_d^2\right)\Upsilon_s, \tag{4.28}$$

and

$$\Xi_2 = \left(\kappa_s^2 + \kappa_d^2\right) \Upsilon_s. \tag{4.29}$$

Applying Jensen's inequality, the upper bound for the ergodic rate can be evaluated as

$$SE_1 \leq SE_1^u, \tag{4.30}$$

where SE_1^u can be defined as

$$SE_1^u = \log_2\left(1 + \Xi_1 \mathbb{E}\left[|\mathscr{H}_1|^2\right]\right) - \log_2\left(1 + \Xi_2 \mathbb{E}\left[|\mathscr{H}_1|^2\right]\right). \tag{4.31}$$

Now in order to evaluate $\mathbb{E}\left[|\mathscr{H}_1|^2\right]$, we apply the binomial expansion theorem here, we have

$$\begin{aligned}\mathbb{E}\left[|\mathscr{H}_1|^2\right] &= \mathbb{E}\left[\left|\sqrt{\mathrm{PL}_h}\, h + \sqrt{\mathrm{PL}_{h_1}\mathrm{PL}_{h_2}}\, N\, |H|\right|^2\right], \\ &= \mathrm{PL}_h \underbrace{\mathbb{E}\left\{|h|^2\right\}}_{\mathscr{E}_1} + \mathrm{PL}_{h_1}\mathrm{PL}_{h_2} N^2 \underbrace{\mathbb{E}\left\{|H|^2\right\}}_{\mathscr{E}_2} + 2N\sqrt{\mathrm{PL}_h \mathrm{PL}_{h_1}\mathrm{PL}_{h_2}}\, \underbrace{\mathbb{E}\left\{|h|\,|H|\right\}}_{\mathscr{E}_3}.\end{aligned} \tag{4.32}$$

We now calculate $\mathscr{E}_1$, $\mathscr{E}_2$ and $\mathscr{E}_3$ one-by-one.

Calculating $\mathscr{E}_1$: Obviously, we have $\mathscr{E}_1 = 1$, as $h \sim \mathscr{CN}(0,1)$.

Calculating $\mathscr{E}_2$: Now, $\mathbb{E}\left\{|H|^2\right\}$ is a Gamma distributed RV (for more details, please refer to Appendix B), so $\mathbb{E}\left\{|H|^2\right\} = \Omega^2$. Thus, on further expanding,

$$\mathbb{E}\left\{|H|^2\right\} = \frac{\varphi_1^2 \pi^2}{16\left(K_1+1\right)\left(K_2+1\right)} \left\{L_{\frac{1}{2}}\left(-K_1\right)\right\}^2 \left\{L_{\frac{1}{2}}\left(-K_2\right)\right\}^2. \tag{4.33}$$

Calculating $\mathscr{E}_3$: Now, for the Rayleigh variable $|h|$, we have

$$\mathbb{E}\left\{|h|\right\} = \sqrt{\frac{\pi}{2}}, \tag{4.34}$$

while $|H|$ is a Nakagami-m RV with

$$\begin{aligned}\mathbb{E}\{|H|\} &= \frac{\Gamma\left(\vartheta+\frac{1}{2}\right)}{\Gamma(\vartheta)}\sqrt{\frac{\Omega^2}{\vartheta}},\\ &= \frac{\Gamma\left(\vartheta+\frac{1}{2}\right)}{\Gamma(\vartheta)}\frac{\varphi_1\,\pi\,L_{\frac{1}{2}}(-K_1)\,L_{\frac{1}{2}}(-K_2)}{\sqrt{4\,\vartheta\,(K_1+1)\,(K_2+1)}}.\end{aligned} \tag{4.35}$$

So, $\mathscr{E}_3$ can be expressed as

$$\sqrt{\frac{\varphi_1^2\,\pi^3}{8\,\vartheta\,(K_1+1)\,(K_2+1)}}\frac{\Gamma\left(\vartheta+\frac{1}{2}\right)}{\Gamma(\vartheta)}L_{\frac{1}{2}}(-K_1)\,L_{\frac{1}{2}}(-K_2). \tag{4.36}$$

Finally, putting $\mathscr{E}_1$, $\mathscr{E}_2$ and $\mathscr{E}_3$ all together yields $\mathbb{E}\left[|\mathscr{H}|^2\right]$ which can be expressed as

$$\begin{aligned}\mathbb{E}\left[|\mathscr{H}|^2\right] =& \mathrm{PL}_h + N^2\,\mathrm{PL}_{h_1}\mathrm{PL}_{h_2}\frac{\varphi_1^2\,\pi^2}{16\,(K_1+1)\,(K_2+1)}\left\{L_{\frac{1}{2}}(-K_1)\right\}^2\left\{L_{\frac{1}{2}}(-K_2)\right\}^2\\ &+ 2N\frac{\Gamma\left(\vartheta+\frac{1}{2}\right)}{\Gamma(\vartheta)}\sqrt{\frac{\varphi_1^2\,\pi^3\mathrm{PL}_h\mathrm{PL}_{h_1}\mathrm{PL}_{h_2}}{8\,\vartheta\,(K_1+1)\,(K_2+1)}}L_{\frac{1}{2}}(-K_1)\,L_{\frac{1}{2}}(-K_2),\end{aligned} \tag{4.37}$$

which can be put in (4.31) to give the desired upper bound. Thus, for the considered IRS-aided communication system, the SE when the direct link is available, SE_1 is upper bounded by SE_1^u, which can be expressed as

$$\begin{aligned}SE_1^u =& \log_2\left[1+\Xi_1\mathrm{PL}_h + 2N\,\Xi_1\frac{\Gamma\left(\vartheta+\frac{1}{2}\right)}{\Gamma(\vartheta)}\sqrt{\frac{\varphi_1^2\,\pi^3\mathrm{PL}_h\mathrm{PL}_{h_1}\mathrm{PL}_{h_2}}{8\,\vartheta\,(K_1+1)\,(K_2+1)}}L_{\frac{1}{2}}(-K_1)\,L_{\frac{1}{2}}(-K_2)\right.\\ &\left.+\ N^2\,\Xi_1\,\mathrm{PL}_{h_1}\mathrm{PL}_{h_2}\frac{\varphi_1^2\,\pi^2}{4\,(K_1+1)\,(K_2+1)}\left\{L_{\frac{1}{2}}(-K_1)\right\}^2\left\{L_{\frac{1}{2}}(-K_2)\right\}^2\right]\\ &-\log_2\left[1+\Xi_2\mathrm{PL}_h + 2N\,\Xi_2\frac{\Gamma\left(\vartheta+\frac{1}{2}\right)}{\Gamma(\vartheta)}\sqrt{\frac{\varphi_1^2\,\pi^3\mathrm{PL}_h\mathrm{PL}_{h_1}\mathrm{PL}_{h_2}}{8\,\vartheta\,(K_1+1)\,(K_2+1)}}L_{\frac{1}{2}}(-K_1)\,L_{\frac{1}{2}}(-K_2)\right.\\ &\left.+\ N^2\,\Xi_2\,\mathrm{PL}_{h_1}\mathrm{PL}_{h_2}\frac{\varphi_1^2\,\pi^2}{4\,(K_1+1)\,(K_2+1)}\left\{L_{\frac{1}{2}}(-K_1)\right\}^2\left\{L_{\frac{1}{2}}(-K_2)\right\}^2\right].\end{aligned} \tag{4.38}$$

Likewise, the SE for the IRS-assisted communication system for the case when the direct link is blocked can be given as

$$\begin{aligned} SE_2 =& \mathbb{E}\left[R_2\right], \\ =& \mathbb{E}\left[\log_2\left(1+\frac{\left|\mathscr{H}_2\right|^2 \Upsilon_s}{\left|\mathscr{H}_2\right|^2 \left(\kappa_s^2+\kappa_d^2\right) \Upsilon_s+1}\right)\right], \end{aligned} \tag{4.39}$$

which can be evaluated as,

$$SE_2 = \mathbb{E}\left[\log_2\left(1+SDNR_2\right)\right], \tag{4.40}$$

where $SDNR_2$ can be further expanded as

$$SDNR_2 = \frac{N^2 \mathrm{PL}_{h_{12}} \left|H\right|^2 \Upsilon_s}{N^2 \mathrm{PL}_{h_{12}} \left|H\right|^2 \left(\kappa_s^2+\kappa_d^2\right) \Upsilon_s+1}. \tag{4.41}$$

where $\mathrm{PL}_{h_{12}}$ is substituted for $\mathrm{PL}_{h_1}\mathrm{PL}_{h_2}$.

Now the cumulative distribution function (CDF) and the PDF for the channel gain $\left|H\right|^2$ can be derived as [82]

$$f_{\left|\mathscr{H}\right|^2}(h) = \frac{\vartheta^{\vartheta}}{\Gamma(m)\,\Omega^{2\vartheta}} h^{\vartheta-1} \exp\left(-\frac{\vartheta}{\Omega^2} h\right), \tag{4.42}$$

and

$$F_{\left|H\right|^2}(h) = \frac{\gamma\left(\vartheta, \frac{\vartheta}{\Omega^2} h\right)}{\Gamma\left(\vartheta\right)}, \tag{4.43}$$

respectively. Here, ϑ and Ω are constants, which are defined as

$$\vartheta = \frac{N}{2} \frac{\varphi_1^2\, \varpi^4}{1+\varphi_2-2\,\varphi_1^2\, \varpi^4} \tag{4.44}$$

and

$$\Omega = \varphi_1\, \varpi^2, \tag{4.45}$$

where $\varpi = \sqrt{\varpi_1\, \varpi_2}$ withϖ_1 andϖ_2 being the expected values of Rician RV h_1 and h_2, respectively. It can further be noticed that, for a Rician variable $h_1 \in \{0,1\}$, the expected value can

be given as

$$\begin{aligned}\varpi_1 =&\mathbb{E}\{|h_1|\}\\ =&\sqrt{\frac{\pi}{4\left(K_1+1\right)}}L_{\frac{1}{2}}\left(-K_1\right),\end{aligned} \tag{4.46}$$

similarly, ϖ_2 can be given as

$$\begin{aligned}\varpi_2 =&\mathbb{E}\{|h_2|\}\\ =&\sqrt{\frac{\pi}{4\left(K_2+1\right)}}L_{\frac{1}{2}}\left(-K_2\right),\end{aligned} \tag{4.47}$$

.

Utilizing (4.41) and (4.42) to solve the expectation in (4.40), we can have

$$SE_2 =\int_0^{\infty}\log_2\left(1+\frac{h\,\mathrm{PL}_{h_{12}}N^2\,\Upsilon_s}{h\,\mathrm{PL}_{h_{12}}N^2\left(\kappa_s^2+\kappa_d^2\right)\Upsilon_s+1}\right)f_H(h)\mathrm{dh}. \tag{4.48}$$

Now by substituting (4.42) in (4.48), the SE can be evaluated as

$$SE_2 =\frac{\vartheta^{\vartheta}}{\Gamma\left(\vartheta\right)\Omega^{2\vartheta}\ln(2)}\int_0^{\infty}\ln\left(1+\frac{h\,\mathrm{PL}_{h_{12}}N^2\,\Upsilon_s}{h\,\mathrm{PL}_{h_{12}}N^2\left(\kappa_s^2+\kappa_d^2\right)\Upsilon_s+1}\right)h^{\vartheta-1}\exp\left(-\frac{\vartheta}{\Omega^2}h\right)\mathrm{dh}, \tag{4.49}$$

which, after simplification and re-arrangement, can be expressed as

$$SE_2 =\frac{\vartheta^{\vartheta}}{\Gamma\left(\vartheta\right)\Omega^{2\vartheta}\ln(2)}\left\{\mathscr{I}_1-\mathscr{I}_2\right\}, \tag{4.50}$$

where

$$\mathscr{I}_1 =\int_0^{\infty}\ln\left(1+h\mathscr{C}_1\Upsilon_s\right)h^{\vartheta-1}\exp\left(-\frac{\vartheta}{\Omega^2}h\right)\mathrm{dh}, \tag{4.51}$$

and

$$\mathscr{I}_2 =\int_0^{\infty}\ln\left(1+h\mathscr{C}_2\Upsilon_s\right)h^{\vartheta-1}\exp\left(-\frac{\vartheta}{\Omega^2}h\right)\mathrm{dh}, \tag{4.52}$$

with

$$\mathscr{C}_1 =\mathrm{PL}_{h_{12}}N^2\left(1+\kappa_s^2+\kappa_d^2\right) \tag{4.53}$$

and

$$\mathscr{C}_2 = \mathrm{PL}_{h_{12}} N^2 \left(\kappa_s^2 + \kappa_d^2\right). \tag{4.54}$$

Now $\mathscr{I}_1$ and $\mathscr{I}_2$ can be solved by utilizing [84, eqn. 17] and can be expressed as

$$\mathscr{I}_1 = \frac{\pi}{\left(\mathscr{C}_1 \Upsilon_s\right)^{\vartheta}} \frac{{}_1\mathrm{F}_1\left(\vartheta; \vartheta+1; \frac{\vartheta}{\Omega^2}\frac{1}{\mathscr{C}_1 \Upsilon_s}\right)}{\vartheta \sin(\vartheta \pi)} - \frac{\Omega^{2\vartheta}\Gamma(\vartheta)}{\vartheta^{\vartheta}} \left[\ln\left(\frac{\vartheta}{\Omega^2}\frac{1}{\mathscr{C}_1 \Upsilon_s}\right) - \Psi(\vartheta) + \frac{\vartheta}{\Omega^2(1-\vartheta)}\frac{1}{\mathscr{C}_1 \Upsilon_s} {}_2\mathrm{F}_2\left(1,1; 2, (1-\vartheta); \frac{\vartheta}{\Omega^2}\frac{1}{\mathscr{C}_1 \Upsilon_s}\right)\right], \tag{4.55}$$

and

$$\mathscr{I}_2 = \frac{\pi}{\left(\mathscr{C}_2 \Upsilon_s\right)^{\vartheta}} \frac{{}_1\mathrm{F}_1\left(\vartheta; \vartheta+1; \frac{\vartheta}{\Omega^2}\frac{1}{\mathscr{C}_2 \Upsilon_s}\right)}{\vartheta \sin(\vartheta \pi)} - \frac{\Omega^{2\vartheta}\Gamma(\vartheta)}{\vartheta^{\vartheta}} \left[\ln\left(\frac{\vartheta}{\Omega^2}\frac{1}{\mathscr{C}_2 \Upsilon_s}\right) - \Psi(\vartheta) + \frac{\vartheta}{\Omega^2(1-\vartheta)}\frac{1}{\mathscr{C}_2 \Upsilon_s} {}_2\mathrm{F}_2\left(1,1; 2, (1-\vartheta); \frac{\vartheta}{\Omega^2}\frac{1}{\mathscr{C}_2 \Upsilon_s}\right)\right], \tag{4.56}$$

respectively. Further, $\mathscr{I}_1$ and $\mathscr{I}_2$ can be substituted in (4.50) to get the expression for SE_2. Thus, for the considered IRS-aided communication system, the SE when the direct link is blocked, SE_2, can be expressed as

$$SE_2 = \frac{\vartheta^{\vartheta}}{\Gamma(\vartheta)\,\Omega^{2\vartheta}\ln(2)} \left[\frac{\pi}{\vartheta \sin(\vartheta \pi)} \left\{\frac{{}_1\mathrm{F}_1\left(\vartheta; \vartheta+1; \frac{\vartheta}{\Omega^2}\frac{1}{\mathscr{C}_1 \Upsilon_s}\right)}{\left(\mathscr{C}_1 \Upsilon_s\right)^{\vartheta}} - \frac{{}_1\mathrm{F}_1\left(\vartheta; \vartheta+1; \frac{\vartheta}{\Omega^2}\frac{1}{\mathscr{C}_2 \Upsilon_s}\right)}{\left(\mathscr{C}_2 \Upsilon_s\right)^{\vartheta}}\right\} + \frac{\Omega^{2\vartheta}\Gamma(\vartheta)}{\vartheta^{\vartheta}} \left\{\ln\left(\frac{\mathscr{C}_1}{\mathscr{C}_2}\right) + \frac{\vartheta}{\Omega^2(1-\vartheta)} \times \left(\frac{{}_2\mathrm{F}_2\left(1,1; 2, (1-\vartheta); \frac{\vartheta}{\Omega^2}\frac{1}{\mathscr{C}_2 \Upsilon_s}\right)}{\mathscr{C}_2 \Upsilon_s} - \frac{{}_2\mathrm{F}_2\left(1,1; 2, (1-\vartheta); \frac{\vartheta}{\Omega^2}\frac{1}{\mathscr{C}_1 \Upsilon_s}\right)}{\mathscr{C}_1 \Upsilon_s}\right)\right\}\right]. \tag{4.57}$$

Remark 1: The high SNR approximation for the SE in both scenarios can be given as

$$\bar{SE}_3 = \log_2\left(1 + \frac{1}{\kappa_s^2 + \kappa_d^2}\right). \tag{4.58}$$

This approximation can be derived from (4.26) by considering the fact that for high SNR (i.e., when Υ is large) $|\mathscr{H}_1|^2\left(\kappa_s^2+\kappa_d^2\right)\Upsilon_s+1\approx|\mathscr{H}_1|^2\left(\kappa_s^2+\kappa_d^2\right)\Upsilon_s$ and thus 1 can be neglected safely. After simplification, the above relationship can easily be found. Likewise, a similar observation can also be taken from (4.39).

Remark 2: Likewise, for large M, the approximation of the SE for both scenarios can again be given as

$$\bar{SE}_4=\left[\log_2\left(1+\frac{1}{\kappa_s^2+\kappa_d^2}\right)\right]. \tag{4.59}$$

Since the proof is similar to that followed in Remark 1 and can be evaluated from (4.26), thus, it is omitted for the sake of brevity.

4.4.2 Outage Probability

An outage for the considered IRS-aided communication system can be defined as when the instantaneous achieved rate falls below the required rate threshold, R_{th}. So, the outage probability at the UE can be defined as

$$\begin{aligned}P_1=&\mathbb{P}\left\{R_1<R_{th}\right\},\\=&\mathbb{P}\left\{\log_2(1+SDNR_1)<R_{th}\right\},\end{aligned} \tag{4.60}$$

which can be simplified as

$$P_1=\mathbb{P}\left\{|\mathscr{H}_1|^2<\frac{\chi}{\Upsilon_s\left(1-\left(\kappa_s^2+\kappa_d^2\right)\chi\right)}\right\}, \tag{4.61}$$

equivalently,

$$P_1=\mathbb{P}\left\{|\mathscr{H}_1|^2\leq\mathscr{Y}_1\right\}, \tag{4.62}$$

where

$$\mathscr{Y}_1=\frac{\chi}{\Upsilon_s\left(1-\left(\kappa_s^2+\kappa_d^2\right)\chi\right)}, \tag{4.63}$$

and $\chi=2^{R_{th}}-1$. Now, the PDF of $|\mathscr{H}_1|^2$ is unknown. Hence, P_1 does not admit a closed-form solution. However, it can be evaluated numerically through simulations.

Likewise, the outage probability for the scenario where the direct link is blocked can be defined as

$$\begin{aligned} P_2 =& \mathbb{P}\left\{R_2 < R_{th}\right\}, \\ =& \mathbb{P}\left\{\log_2(1+SDNR_2) < R_{th}\right\}. \end{aligned} \tag{4.64}$$

The OP for this scenario can be evaluated from (4.64), as

$$\begin{aligned} P_2 =& \mathbb{P}\left\{SDNR_2 < 2^{R_{th}} - 1\right\}, \\ =& \mathbb{P}\left\{SDNR_2 < \chi\right\}, \end{aligned} \tag{4.65}$$

which on substituting $SDNR_2$ from (4.41) gives

$$P_2 = \mathbb{P}\left\{\frac{h\,\mathrm{PL}_{h_{12}} N^2 \Upsilon_s}{h\,\mathrm{PL}_{h_{12}} N^2 \left(\kappa_s^2+\kappa_d^2\right)\Upsilon_s + 1} < \chi\right\}. \tag{4.66}$$

After simplification, (4.66) can be re-written as

$$P_2 = \mathbb{P}\left\{h < \frac{\chi}{\mathrm{PL}_{h_{12}} N^2 \Upsilon_s \left(1-(\kappa_s^2+\kappa_d^2)\chi\right)}\right\}, \tag{4.67}$$

$$= \mathbb{P}\left\{h < \mathscr{Y}_2\right\}, \tag{4.68}$$

where

$$\mathscr{Y}_2 = \frac{\chi}{\mathrm{PL}_{h_1}\mathrm{PL}_{h_2} N^2 \Upsilon_s \left(1-(\kappa_s^2+\kappa_d^2)\chi\right)}. \tag{4.69}$$

Next, from (4.42), the outage probability,P_2, can be evaluated as

$$P_{out} = \int_0^{\mathscr{Y}_2} f_{|H|^2}(h)\mathrm{dh}, \tag{4.70}$$

or, equivalently

$$P_{out} = F_{|H|^2}(\mathscr{Y}_2). \tag{4.71}$$

Thus, for the considered IRS-aided communication system, the OP of the scenario where the direct link is not available can be expressed as

$$P_2 = \frac{\gamma\left(\vartheta, \frac{\vartheta}{\Omega^2}\mathscr{Y}_2\right)}{\Gamma(\vartheta)}. \tag{4.72}$$

4.4.3 Energy Efficiency

The EE of the considered IRS-aided communication system can be defined as the ratio of the SE over total consumed power, P_{tot}, and can be expressed as

$$EE = \frac{SE}{P_{tot}}, \tag{4.73}$$

in terms of bits/Joule/Hz [85].

Further, the total consumed power comprises the transmit power at the BS and the circuit power consumed at the BS, IRS and UE. Now, the transmit power at the BS is P_s. Thus, the dynamic power consumption of the BS power amplifier can be denoted by P_s/δ, where δ is the efficiency of the power amplifier. Likewise, the power consumed at the IRS is given as NP_{RE} where P_{RE} is consumed at each RE. Lastly, the static circuit power consumption of the BS and UE can be denoted as P_{BS} and P_U, respectively. Substituting all these in (4.73), the EE can be expressed as

$$EE = \frac{SE}{(1+1/\delta)P_s + P_{BS} + NP_{RE} + P_{UE}}. \tag{4.74}$$

Thus, the corresponding EE can be evaluated accordingly by substituting the value of SE for both scenarios, i.e., SE_1 and SE_2.

This completes the analytical evaluation of the proposed IRS-aided communication system with and without a direct link. The following remarks provide system-design insights that can be noted here 1) The performance analysis of the designed system provides insights regarding the suitable number of REs, which can be determined to strike a balance between hardware cost and system performance for different scenarios, i.e., with and without a direct link. 2) The analytical results contribute to the deployment of IRS under realistic scenarios, i.e., the BS-IRS and IRS-user links can be either LoS or non-LoS (NLoS) and the Rician fading parameter can be adjusted accordingly. 3) Based on the impact of transceiver impairments on the system performance, we know how the non-ideal transceiver limits the performance gain provided by IRS.

Table 4.1: Simulation Parameters for IRS-assisted Communication System

Parameter	Simulation Values
Antenna Gain	$G_t = 1$, $G_r = 1$
Circuit Power	P_{BS}=10 dBm, P_{UE}=10 dBm [7]
HPA Power Consumption Factor	$1/\delta = 1.2$ [86]
IRS Power Consumption	P_{RE} = 10 dBm [7]
Shape Parameter	$K_1, K_2 = 5$
Scale Parameter	$\Omega_1 = \Omega_2 = 1$
Variance of AWGN Noise	σ^2 = -120 dBm

4.5 Simulation Results

This section discusses and presents the simulation results for the performance of the considered scenario of IRS-aided communication systems. If not specified otherwise, the proportionality constant for the T-HI level is assumed to be $\kappa_s = \kappa_d$. Likewise, the distances for the BS-to-IRS and IRS-to-UE links are 50 m, while the direct link is assumed to be 70 m. In addition to the above, solid lines show the analytical results, while the marker points denote the simulation results; a similar convention is followed throughout this section. Table 5.1 lists the rest of the simulation parameters. Moreover, the pathloss associated with the direct and reflected links is evaluated through the 3GPP Urban Micro model [60]. So, at 3 GHz of carrier frequency the pathloss PL(d) (in [dB]) experienced by a LoS link of length d (in metre) can be given as

$$\mathrm{PL}(d) = G_\mathrm{t} + G_\mathrm{r} - 37.5 - 22\log_{10}(d), \tag{4.75}$$

while for the NLoS case, the corresponding pathloss would be

$$\mathrm{PL}(d) = G_\mathrm{t} + G_\mathrm{r} - 35.1 - 36.7\log_{10}(d) \tag{4.76}$$

where G_t is the antenna gain at the BS and G_r is the receive antenna gain at UE (both in [dBi]).

Fig. 4.2 shows the SE of the considered IRS-aided communication system with and without a direct link. Specifically, it shows the impact of hardware impairment on the SE, as the SE corresponding to the ideal hardware is also plotted against the transmit power for the sake of comparison. It can easily be observed here that hardware impairments saturate the SE, and no further gain can be observed in the SE by increasing the transmit power. In contrast, the SE increases linearly with transmit power in the case of the ideal hardware-based IS-aided communication system. Further, it can also be observed here that the SE saturation level

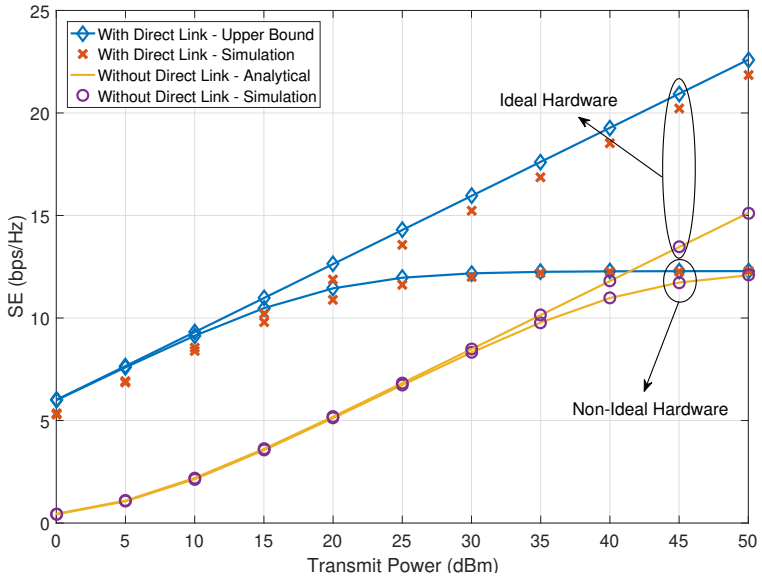

Figure 4.2: SE with respect to transmit power, here $N = 20$, $q = 3$ and $\kappa = 0.01$.

does not depend on the availability of a direct link. Rather it depends only on the transceiver hardware impairment level. This verifies the analytical findings as mentioned in Remark 1.

Fig. 4.3 shows the SE for the IRS-aided communication system with respect to N. The results show the SE for ideal and non-ideal hardware-based communication scenarios. Specifically, it shows that SE saturates with increasing N for the practical non-ideal hardware-based scenario, whereas ideally, the SE increases linearly with N. Furthermore, increasing transmit power results in saturation of SE even for moderate values of N. Likewise, it can also be observed that the SE for both scenarios with and without direct link saturates to a similar level while increasing N. For instance, at $P_s = 30$ dBm, the SE of the ideal hardware case increases with N. However, for the non-ideal hardware case, the SE saturates at 12.2 bps/Hz for both scenarios with and without a direct link. This verifies the analytical limit as discussed in Remark 2. Moreover, even as the SE is saturated, the IRS still provides leverage to reduce the transmit power by increasing N until saturation. For instance, as evident from the result, the SE at $P_s = 30$ dB can also be achieved at $P_s = 10$ dB through larger N.

Fig. 4.4 shows the joint impact of IRS phase noise and the transceiver hardware impairment on the SE of the considered IRS-aided communication system. It can be noted here that $q = 3$ provides nearly equivalent SE to that of an ideal phase shifter with infinite available phases, i.e., $q = \infty$. Further, it can also be noted that the transceiver hardware impairment impacts more severely than the IRS phase noise. For instance, for $\kappa = 0$, the SE increases with transmit SNR for all the values of q viz. 1, 3 and ∞. However, for $\kappa = 0.01$ and 0.1, the SE saturates with transmit SNR for all three values of q. Consequently, it can be inferred that the IRS-HIs result

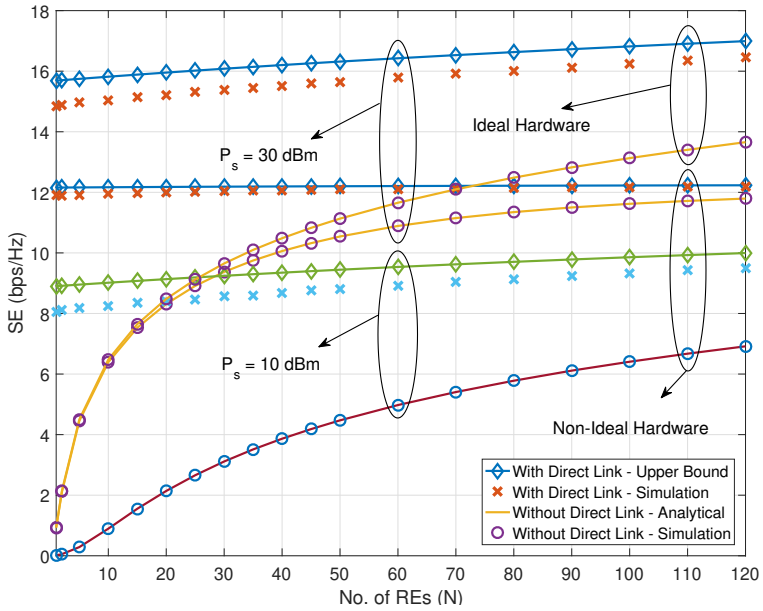

Figure 4.3: SE with respect to N, here $q = 3$.

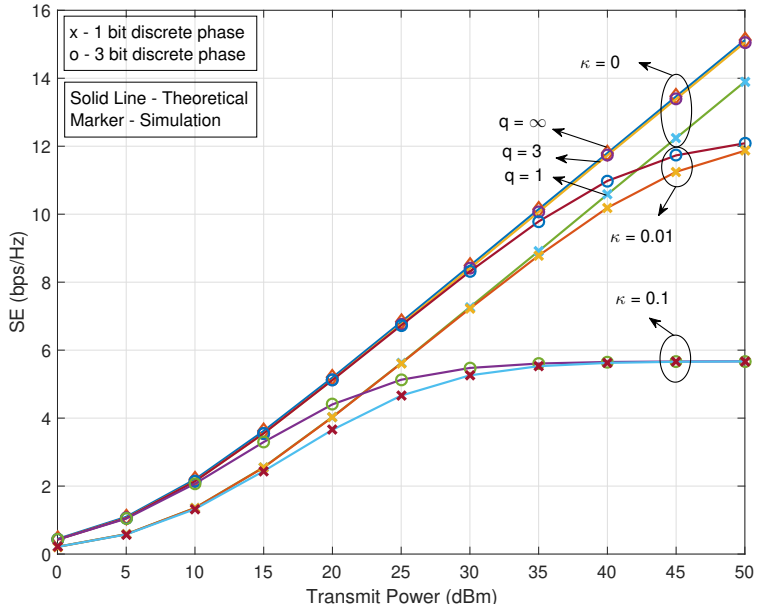

Figure 4.4: SE with respect to transmit power, here $N = 20$.

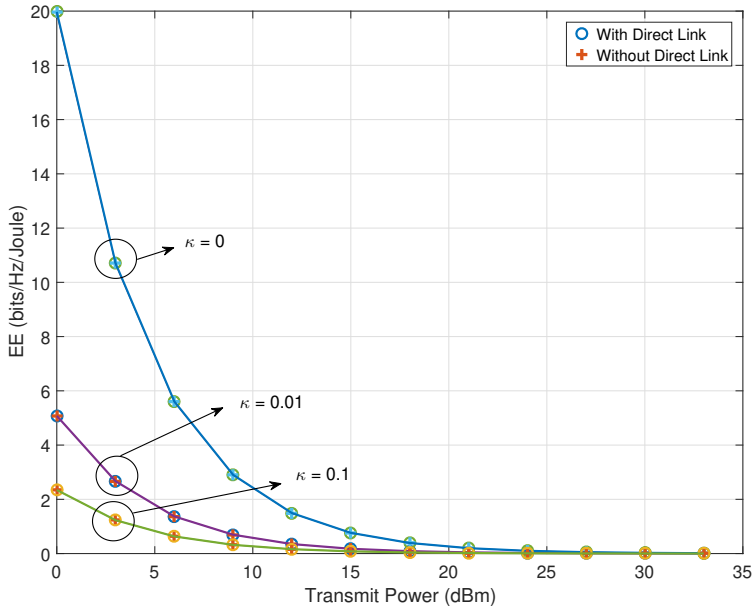

Figure 4.5: EE with respect to transmit power, here $N = 20$.

in some deterioration in performance while T-HIs severely limit the performance of IRS-aided communication. Hence, the impact of T-HIs is far more significant than that of the IRS-HIs.

Likewise, Fig. 4.5 and 4.6 show the EE of the considered IRS-aided system with IRS phase error and T-HIs. Specifically, Fig. 4.5 shows the EE with respect to the transmit power, while Fig. 4.6 shows the EE with respect to the number of REs. The following points can easily be observed here from both figures. The level of T-HIs severely impacts the EE, and for a fixed transmit power, it can not be improved by increasing N. As the level of T-HIs increases, i.e., κ increases, the EE degrades with respect to transmit power. Further, it can also be observed that the difference between the EE of the with and without direct link scenarios is insignificant. This is because the SE saturates to the same level in both scenarios and is independent of the presence of the direct link.

Fig. 4.7 shows the outage probability for the considered IRS-aided communication scenario with respect to transmit SNR. Specifically, it shows the impact of the non-ideal hardware at the IRS, which results in the phase error due to the non-availability of the continuous phase at the REs. The results show that the OP worsens as the number of discrete phases at IRS decreases. Further, it also shows that, for $q = 3$, the performance is as good as that of an ideal phase-based IRS. It can be observed that increasing N improves the OP. Moreover, it can also be noted that increasing the transmit SNR improves the OP, which is evident and intuitive.

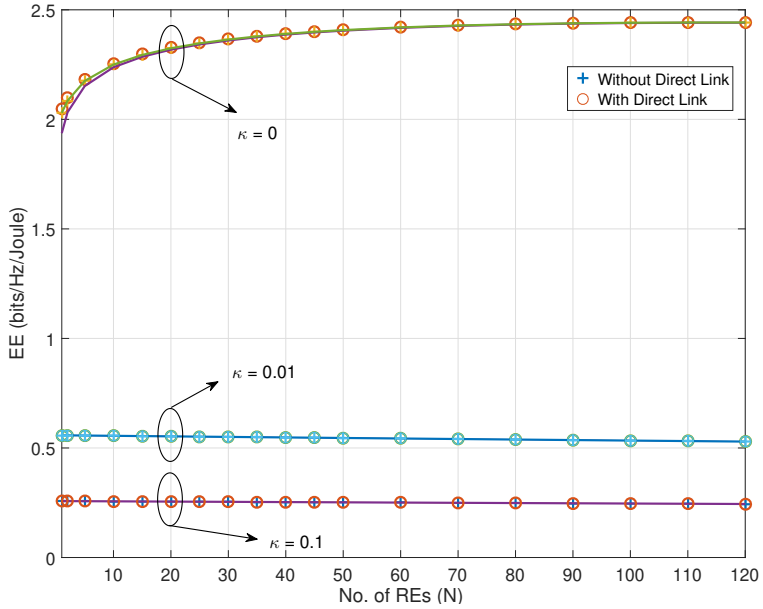

Figure 4.6: EE with respect to N, here $P_s = 10$ dBm.

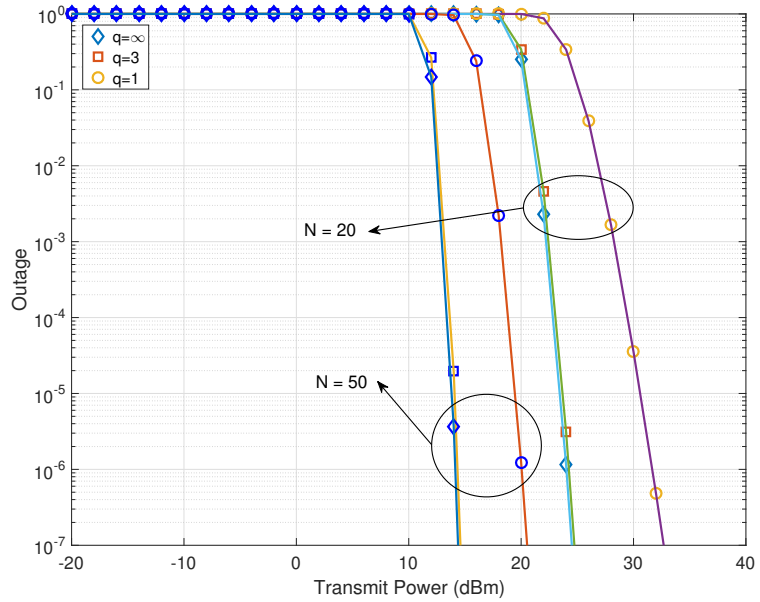

Figure 4.7: Outage performance with respect to transmit power, here $N = 20, 50$ and $\kappa = 0.01$.

4.6 Conclusion of Part I

This part of the chapter investigates the joint impact of the transceiver HIs and IRS phase error on the performance of an IRS-aided communication system with and without a direct link. Specifically, we derived the closed-form expressions for the SE, EE and OP. The result shows that although both transceiver hardware impairment and IRS phase error degrade the performance, the impact of transceiver hardware impairment is far more severe and detrimental. In particular, the transceiver hardware impairment saturates the SE, and this saturation level is independent of the number of REs in the IRS and the transmit power. Likewise, for the high transmit SNR and large N cases, the SE saturates to the level independent of the presence of direct link and transmit SNR and N. Consequently, the impact of non-ideal hardware must be addressed in a practical IRS-enabled system design.

Part II - Dual IRS Scenario

4.7 Overview of Part II

Like part I of this chapter, most of the existing IRS research has focused only on single IRS-assisted communication systems [43, 80, 83, 87–90]. However, in situations with dense blockages between the IRS and the BS or the receiver, this may not be effective, as a single IRS may not be able to establish a direct LoS path between the BS and each user. This motivates us to look beyond the paradigm of single IRS-aided communication systems.

Motivated by the above, in this part, we investigate the fundamental performance limits of a dual IRS-aided wireless communication system over the Nakagami-m fading channels in this work. Further, we have considered a generalized scenario with HIs due to a non-ideal transceiver. In particular, the performance of an ideal transceiver-based dual IRS-aided communication system is also considered. The significant contributions of this part of the work can be summarized as

- Explicitly, we invoke a CLT to characterize the received SNR for the proposed dual IRS case. Further, we derive the closed-form expression for outage probability based on the received SNR.
- We also derived the closed-form expressions for the upper and lower bounds of the SE of the proposed dual IRS-aided communication scenario.
- Finally, the proposed scenario is compared with the single IRS-aided communication as a performance benchmark. The results show that dual IRS can outperform the single IRS

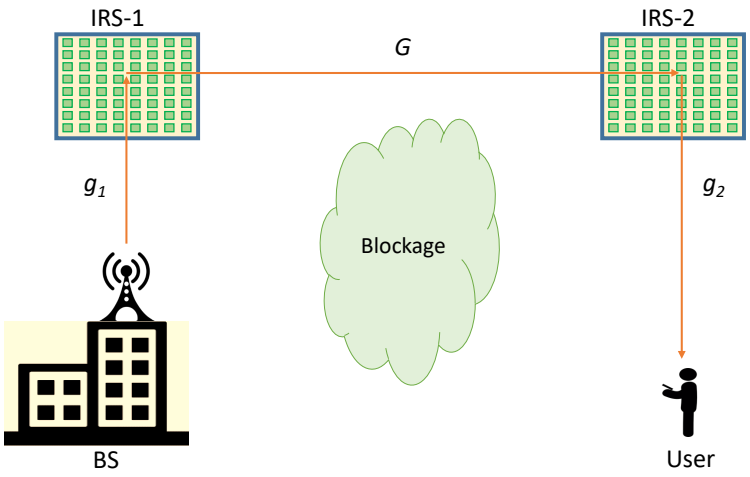

Figure 4.8: Schematic for the considered Dual IRS-assisted Communication System.

for the ideal transceiver case by increasing M. However, in the non-ideal transceiver case, the SE of the dual IRS saturates and hence increasing M does not yield any significant gain over the single IRS scenario.

4.8 System Model for Dual IRS-aided Communication

Fig. 4.8 illustrates the dual IRS-aided communication system model. As evident from Fig. 1, the direct path between the BS and the UE is blocked. To support the communication between the BS and UE, an indirect LoS path is constructed via two IRSs (one each near to the BS and UE). The proposed scheme can alleviate the limitations of higher pathloss in blockage-prone urban dense scenarios. Thus, for this particular case, instead of using a large IRS, we employ two smaller IRSs, viz., IRS-1 and IRS-2, equipped with M_1 and M_2 number of REs, respectively, where $M_1 + M_2 = N$. Likewise, for a single IRS-aided communication system, a large IRS with a N number of REs facilitates the transmission while being placed at the location of IRS-1.

4.8.1 Channel Model

The channels between BS-to-IRS-1 and IRS-2-to-UE can be modeled as deterministic LoS channels since the distances are very small and the probability of LoS is very high. However, the distance between IRS-1 and IRS-2 is large, and thus the small scale fading for the channel between i-th element of IRS1-to-j-th element of IRS-2, g_{ij}^{RR}, can be modeled as Nakagami-m fading, for all $i = 1, 2, \cdots, M_1$ and $j = 1, 2, \cdots, M_2$. Further, the distance between the BS-to-IRS-1, IRS-1-to-IRS-2 and IRS-2-to-UE are represented by d_{SR_1}, $d_{R_1R_2}$ and d_{R_2D}, respectively.

Likewise, for the single IRS-aided communication system, the channel between the BS-to-IRS is modeled as a deterministic LoS channel. In contrast, the channel between the IRS-to-UE can either be an LoS or an NLoS link. Thus, the small-scale fading between IRS-to-UE can be characterized through the Nakagami-m fading model with m_h as the fading parameter for $\mathbf{h} = [h^1 \cdots h^M]$. Furthermore, d_{SR} and d_{RD} denote the distance between BS-to-IRS and IRS-to-UE, respectively.

4.8.2 Received Signal Model for the Dual IRS Scenario

The received baseband signal at the UE, y, for the dual IRS (DIRS) scenario can be expressed as

$$y = \sqrt{\mathscr{B}} \left(\sum_{i=1}^{M_1} \sum_{j=1}^{M_2} e^{j\phi_i^{(1)}} g_{ij}^{RR} e^{j\phi_j^{(2)}} \right) \sqrt{P_t} \left(x_t + w_t \right) + w_r + N_o, \tag{4.77}$$

where $\mathscr{B}$ denotes the pathloss for the BS-to-UE link via IRS. Further, P_t is the transmit power constraint at the BS, $x_t \sim \mathscr{CN}(0,1)$ is the transmitted symbol, $N_o \sim \mathscr{CN}\left(0, \sigma^2\right)$ is AWGN. Further, $w_t \in \mathscr{CN}\left(0, \kappa_t^2 P_t\right)$ is the zero-mean complex Gaussian random variable which represents the aggregated distortion noise due to the non-ideal transceiver at the BS[2]. Further, κ_t is the proportionality constant that dictates the severity of the HIs. Likewise, $w_r \in \mathscr{CN}\left(0, \kappa_r^2 \left| \sqrt{\mathscr{B}} \sum_{i=1}^{M_1} \sum_{j=1}^{M_2} e^{j\phi_i^{(1)}} g_{ij}^{RR} e^{j\phi_j^{(2)}} \right|^2 P_t \right)$ represents the aggregated distortion noise at the UE due to non-ideal transceiver. After some manipulation, (4.77) can be rewritten as

$$y = \sqrt{\mathscr{B}} \left(\sum_{i=1}^{M_1} \sum_{j=1}^{M_2} e^{j\phi_i^{(1)}} g_{ij}^{RR} e^{j\phi_j^{(2)}} \right) x_t \sqrt{P_t} + w_d + N_o, \tag{4.78}$$

where $w_d \in \mathscr{CN}\left(0, \left(\kappa_t^2 + \kappa_r^2\right) P_t\right)$ [86].

Now, the received signal power at the UE can be maximized by adjusting the phase at IRSs to cancel the resultant phase, i.e., $\phi_i^{(1)} + \phi_j^{(2)} - \varphi_{ij} = 0$, $\forall i, j$. Thus, by substituting $\varphi_{ij} = \phi_i^{(1)} + \phi_j^{(2)}, \forall i, j$, the received signal power at the UE can be maximized. Consequently,

[2]This Gaussian characterization of the aggregated distortion noise is experimentally verified, for details, please refer to [81].

the SDNR corresponding to the optimal phase can be given as

$$\begin{aligned}\rho &= \frac{\mathscr{B}\mathscr{G}^2 P_t}{\mathscr{B}\mathscr{G}^2\left(\kappa_t^2+\kappa_r^2\right)P_t+\sigma^2} \\ &= \frac{\mathscr{B}\mathscr{G}^2\bar{\rho}}{\mathscr{B}\mathscr{G}^2\left(\kappa_t^2+\kappa_r^2\right)\bar{\rho}+1},\end{aligned} \tag{4.79}$$

where $\mathscr{G}^2 = \left[\sum_{i=1}^{M_1}\sum_{j=1}^{M_2}\left|g_{ij}^{RR}\right|\right]^2$ and $\bar{\rho} = P_t/\sigma^2$ is the transmit SNR.

Further, for a link distance d, $\mathscr{B}$ at the carrier frequency of 3 GHz can be given by [60]

$$\mathscr{B}(d)\ [\text{dB}] = \begin{cases} -37.5 - 22\log_{10}(d/1\,\text{m}) & \text{if LoS,} \\ -35.1 - 36.7\log_{10}(d/1\,\text{m}) & \text{if NLoS.} \end{cases} \tag{4.80}$$

4.8.3 Single IRS Scenario

Likewise, the SDNR at the UE for the single IRS (SIRS) scenario can be expressed as

$$\rho = \frac{\hat{\mathscr{B}}\mathscr{H}^2\bar{\rho}}{\hat{\mathscr{B}}\mathscr{H}^2\left(\kappa_t^2+\kappa_r^2\right)\bar{\rho}+1}, \tag{4.81}$$

where $\hat{\mathscr{B}}$ is the corresponding pathloss. Further, $\mathscr{H}^2 = \left[\sum_{i=1}^{M}|h_i|\right]^2$ is the maximized channel gain corresponding to the optimized phase shift at the IRS. Here, β_i is the amplitude of the small-scale fading coefficient between the i-th RE of IRS-to-UE.

4.9 Performance Analysis

This section initially evaluates the SNR for single and dual IRS scenarios. The closed-form expressions for the SE and OP are derived utilizing SNR.

4.9.1 Statistical Characterization of the Dual IRS Channel Gain

Now utilizing the CLT for $M \gg 1$, $\mathscr{G} = \sum_{i=1}^{M_1}\sum_{j=1}^{M_2}\delta_{ij}$ can be approximated through a Gaussian distribution, i.e., $\mathscr{G} \sim \mathscr{N}(\mu_y, \sigma_y^2)$

$$\mathrm{f}_{\mathscr{G}}(y) = \begin{cases} \frac{1}{\sqrt{2\pi\sigma_{\mathscr{G}}^2}}\exp\left(\frac{-(y-\mu_{\mathscr{G}})^2}{2\sigma_{\mathscr{G}}^2}\right), & \text{if } y \geq 0 \\ 0, & \text{if } y = 0 \end{cases} \tag{4.82}$$

where

$$\mu_{\mathscr{G}} = \sum_{i=1}^{M_1} \sum_{j=1}^{M_2} \mu_{ij} \tag{4.83}$$

and

$$\sigma_{\mathscr{G}}^2 = \sum_{i=1}^{M_1} \sum_{j=1}^{M_2} \sigma_{ij}^2. \tag{4.84}$$

Here, μ_{ij} and σ_{ij}^2 are the mean and variance of the random variable δ_{ij}, which follows the Nakagami-m distribution. Hence, μ_{ij} and σ_{ij}^2 can be defined as

$$\mu_{ij} = \frac{\Gamma(m_g + \frac{1}{2})}{\Gamma(m_g)} \sqrt{\frac{\Omega_{m_g}}{m_g}} \tag{4.85}$$

and

$$\sigma_{ij}^2 = \Omega_{m_g} \left\{ 1 - \frac{1}{m_g} \left(\frac{\Gamma(m_g + \frac{1}{2})}{\Gamma(m_g)} \right)^2 \right\}, \tag{4.86}$$

$\forall\, i$ and j.

Likewise, the CDF of $\mathscr{G}$ can be derived from its PDF as

$$\begin{aligned} \mathrm{F}_{\mathscr{G}}(y) &= \int_{-\infty}^{y} \mathrm{f}_{\mathscr{G}}(y)\mathrm{d}y \\ &= \begin{cases} 1 - \mathrm{Q}\left(\frac{y-\mu_{\mathscr{G}}}{\sigma_{\mathscr{G}}^2}\right), & \text{if } y > 0, \\ 0, & \text{if } y = 0. \end{cases} \end{aligned} \tag{4.87}$$

4.9.2 Spectral Efficiency

. The SE for the DIRS scenario can be defined as

$$SE = \mathrm{E}\left[\log_2 \left(1 + \frac{\mathscr{B}\mathscr{G}^2 \bar{\rho}}{\mathscr{B}\mathscr{G}^2 \left(\kappa_t^2 + \kappa_r^2\right) \bar{\rho} + 1} \right) \right], \tag{4.88}$$

or equivalently,

$$SE = \mathrm{E}\left[\log_2 \left(1 + \vartheta_1 \mathscr{G}^2 \bar{\rho} \right) \right] - \mathrm{E}\left[\log_2 \left(1 + \vartheta_2 \mathscr{G}^2 \bar{\rho} \right) \right], \tag{4.89}$$

where $\vartheta_1 = \mathscr{B}\left(1 + \kappa_t^2 + \kappa_r^2\right)$ and $\vartheta_2 = \mathscr{B}\left(\kappa_t^2 + \kappa_r^2\right)$.

The closed-form expression for the SE of the DIRS scenario can be evaluated by solving the expectation over the distribution of channel gain $\mathscr{G}$

$$SE = \frac{1}{\ln 2\sqrt{2\pi\sigma_{\mathscr{G}}^2}} \int_0^{\infty} \ln\left(1 + \frac{y^2\,\mathscr{B}\bar{\rho}}{y^2\,\mathscr{B}\left(\kappa_t^2+\kappa_r^2\right)\bar{\rho}+1}\right) e^{\frac{-(y-\mu_{\mathscr{G}})^2}{2\sigma_{\mathscr{G}}^2}}\,\mathrm{dy}. \tag{4.90}$$

The exact derivation of the integral (in 4.90) appears mathematically intractable, and thus a closed-form expression may not be formed. Hence, we approximate the SE with tight upper and lower bounds by invoking Jensen's inequality.

4.9.2.1 Upper Bound

We define the upper bound of the SE as SE_u, where $SE \leq SE_u$. Applying Jensen's inequality, SE_u can be evaluated from (4.89) as

$$SE_u = \log_2\left(1+\vartheta_1\,\bar{\rho}\,\mathrm{E}\left[\mathscr{G}^2\right]\right) - \log_2\left(1+\vartheta_2\,\bar{\rho}\,\mathrm{E}\left[\mathscr{G}^2\right]\right). \tag{4.91}$$

Now the expectation of $\mathrm{E}\left[\mathscr{G}^2\right]$ can be evaluated utilizing the relationship $\mathrm{Var}[X] = \mathrm{E}\left[X^2\right] - (\mathrm{E}[X])^2$ as

$$\begin{aligned}\mathrm{E}\left[\mathscr{G}^2\right] =& \mathrm{Var}[\mathscr{G}] + (\mathrm{E}[\mathscr{G}])^2,\\ =& \sigma_{\mathscr{G}}^2 + \mu_{\mathscr{G}}^2.\end{aligned} \tag{4.92}$$

Thus, utilizing (4.92), the upper bound for the SE of the dual IRS scenario can be expressed as

$$\begin{aligned}SE_u = \log_2&\left[1+\left(1+\kappa_t^2+\kappa_r^2\right)\bar{\rho}\,M_1M_2\,\mathscr{B}\,\Omega_{m_g}\left\{1+\frac{(M_1M_2-1)}{m_g}\left(\frac{\Gamma(m_g+\frac{1}{2})}{\Gamma(m_g)}\right)^2\right\}\right]\\ &-\log_2\left[1+\left(\kappa_t^2+\kappa_r^2\right)\bar{\rho}\,M_1M_2\,\mathscr{B}\,\Omega_{m_g}\left\{1+\frac{(M_1M_2-1)}{m_g}\left(\frac{\Gamma(m_g+\frac{1}{2})}{\Gamma(m_g)}\right)^2\right\}\right].\end{aligned} \tag{4.93}$$

4.9.2.2 Lower Bound

Likewise, the lower bound for the SE is defined as SE_l, where $SE \geq SE_l$. Again applying Jensen's inequality, SE_l, can be evaluated from (4.89) as

$$SE_l = \log_2\left(1+\frac{\vartheta_1\bar{\rho}}{\mathrm{E}\left[\frac{1}{\mathscr{G}^2}\right]}\right) - \log_2\left(1+\frac{\vartheta_2\bar{\rho}}{\mathrm{E}\left[\frac{1}{\mathscr{G}^2}\right]}\right). \tag{4.94}$$

Now the expectation $\mathrm{E}\left[\frac{1}{\mathscr{G}^2}\right]$ can be solved utilizing the Taylor series expansion and can be approximated as [91]

$$\mathrm{E}\left[\frac{1}{\mathscr{G}^2}\right] \approx \frac{1}{\mathrm{E}\left[\mathscr{G}^2\right]} + \frac{\mathrm{Var}\left[\mathscr{G}^2\right]}{\left[\mathrm{E}\left[\mathscr{G}^2\right]\right]^3}. \tag{4.95}$$

since the statistical characteristics of $\mathscr{G}$ is already known to be Gaussian distributed (as discussed earlier in subsection A), $\mathscr{G}^2$ will follow a non-central chi-square distribution. Thus the mean and variance of $\mathscr{G}^2$ can be expressed as

$$\mathrm{Var}\left[\mathscr{G}^2\right] = 2\,\sigma_{\mathscr{G}}^2\left(\sigma_{\mathscr{G}}^2 + 2\,\mu_{\mathscr{G}}^2\right), \tag{4.96}$$

and

$$\mathrm{E}\left[\mathscr{G}^2\right] = \sigma_{\mathscr{G}}^2 + \mu_{\mathscr{G}}^2, \tag{4.97}$$

respectively.

Thus, utilizing these expressions, the lower bound for the SE of the dual IRS scenario can be expressed as

$$SE_l = \log_2\left[1+\frac{\left(1+\kappa_t^2+\kappa_r^2\right)\bar{\rho}\,\mathscr{B}M_1M_2\,\Omega_{m_g}\left\{1+\frac{(M_1M_2-1)}{m_g}\left(\frac{\Gamma(m_g+\frac{1}{2})}{\Gamma(m_g)}\right)^2\right\}^3}{2\left\{1+\frac{(2M_1M_2-1)\left(\Gamma(m_g+\frac{1}{2})\right)^2}{m_g\left(\Gamma(m_g)\right)^2}\right\}\left\{1-\frac{\left(\Gamma(m_g+\frac{1}{2})\right)^2}{m_g\left(\Gamma(m_g)\right)^2}\right\}+\left\{1+\frac{(M_1M_2-1)\left(\Gamma(m_g+\frac{1}{2})\right)^2}{m_g\left(\Gamma(m_g)\right)^2}\right\}^2}\right]$$
$$-\log_2\left[1+\frac{\left(\kappa_t^2+\kappa_r^2\right)\bar{\rho}\,\mathscr{B}M_1M_2\,\Omega_{m_g}\left\{1+\frac{(M_1M_2-1)}{m_g}\left(\frac{\Gamma(m_g+\frac{1}{2})}{\Gamma(m_g)}\right)^2\right\}^3}{2\left\{1+\frac{(2M_1M_2-1)\left(\Gamma(m_g+\frac{1}{2})\right)^2}{m_g\left(\Gamma(m_g)\right)^2}\right\}\left\{1-\frac{\left(\Gamma(m_g+\frac{1}{2})\right)^2}{m_g\left(\Gamma(m_g)\right)^2}\right\}+\left\{1+\frac{(M_1M_2-1)\left(\Gamma(m_g+\frac{1}{2})\right)^2}{m_g\left(\Gamma(m_g)\right)^2}\right\}^2}\right]. \tag{4.98}$$

Remark: For the ideal transceiver-based DIRS scenario, the upper and lower bound on the SE can be evaluated by substituting $\kappa_t = \kappa_r = 0$ in (4.93) and (4.98), respectively.

4.9.2.3 Approximation for Large M

Now, with the upper and lower bound of the SE of the DIRS scenario, the exact SE lies in between and can be expressed as

$$SE_l \leq SE \leq SE_u, \tag{4.99}$$

however, for the larger values of M_1 and M_2, i.e., $M_1, M_2 \gg 1$, both SE_u and SE_l converges to SE, and this approximation of SE can be given as

$$\overline{SE} = \log_2\left[1 + \frac{\bar{\rho}\,\vartheta_1\, M_1^2 M_2^2\, \Omega_{m_g}\Gamma(m_g+\frac{1}{2})^2}{m_g\Gamma(m_g)^2}\right] - \log_2\left[1 + \frac{\bar{\rho}\,\vartheta_2\, M_1^2 M_2^2\, \Omega_{m_g}\Gamma(m_g+\frac{1}{2})^2}{m_g\Gamma(m_g)^2}\right]. \tag{4.100}$$

Remark: Likewise, the approximate SE for large M of the ideal transceiver-based DIRS scenario can be evaluated by substituting $\vartheta_1 = \mathscr{B}$ and $\vartheta_2 = 0$ in (4.100).

4.9.3 Outage

The e2e outage for the DIRS scenario, P_{out}, can be defined in terms of a rate threshold, R_{th}, as $P_{out} = \Pr\left[R^{in} < R_{th}\right]$, which can be simplified as

$$\begin{aligned} P_{out} &= \Pr\left[\log_2\left(1 + \frac{\mathscr{B}\mathscr{G}^2\bar{\rho}}{\mathscr{B}\mathscr{G}^2\left(\kappa_t^2+\kappa_r^2\right)\bar{\rho}+1}\right) < R_{th}\right], \\ &= \Pr\left[\mathscr{G}^2 < \frac{\chi}{\mathscr{B}\bar{\rho}\left(1-\left(\kappa_s^2+\kappa_d^2\right)\chi\right)}\right], \end{aligned} \tag{4.101}$$

where $\chi = 2^{R_{th}} - 1$.

Thus, the closed-form expression of the outage probability for the DIRS scenario can be evaluated as

$$\begin{aligned} P_{out} &= \mathrm{F}_{\mathscr{G}}\left(\Upsilon\right), \\ &= 1 - \mathrm{Q}\left(\frac{\Upsilon - \mu_{\mathscr{G}}}{\sigma_{\mathscr{G}}^2}\right), \end{aligned} \tag{4.102}$$

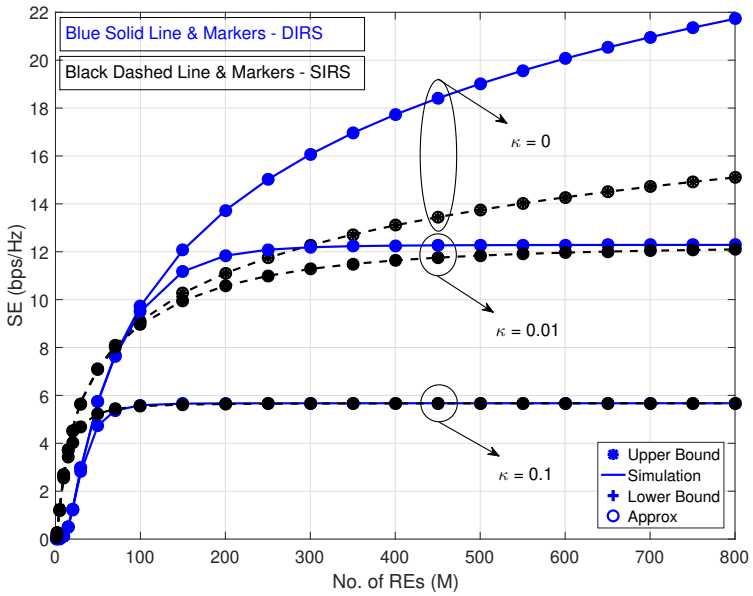

Figure 4.9: SE versus M for both dual and single IRS-assisted communication system, here $P_t = 30\,\text{dBm}$.

where

$$\Upsilon = \sqrt{\frac{\chi}{\mathscr{B}\bar{\rho}\left(1-\left(\kappa_s^2+\kappa_d^2\right)\chi\right)}}. \tag{4.103}$$

Remark: The OP for the ideal transceiver-based DIRS scenario can be evaluated from (4.102) by substituting Υ with $\kappa_t = \kappa_r = 0$ in (4.103).

4.10 Simulation Results

This section discusses and presents the simulation result for the proposed dual- IRS-aided communication system's performance and compares the performance with a single- IRS-aided communication system. For the direct links between IRSs, the Nakagami fading parameter is assumed to be $m_g = 5$ for the DIRS scenario. Likewise, for the IRS-to-UE in the SIRS scenario, it is assumed to be $m_h = 2$. Further, the distances d_{SR}, d_{RR}, d_{RD1} are assumed to be 10, 100 and 10 meters, respectively while d_{SR} and d_{RD} are assumed to be 10 and 100 meters, respectively. Similarly for the simulation purpose, $M_1 = M_2 = M$ and $\kappa_t = \kappa_r = \kappa$.

Fig. 4.9 shows the SE for both the DIRS and SIRS scenarios with an ideal and non-ideal transceiver. The result shows that the derived bounds are pretty tight and near the approximate values derived analytically. Further, it is evident that due to the multiplicative pathloss effect, the SIRS scenario provides better performance than the DIRS for smaller M. Increasing M

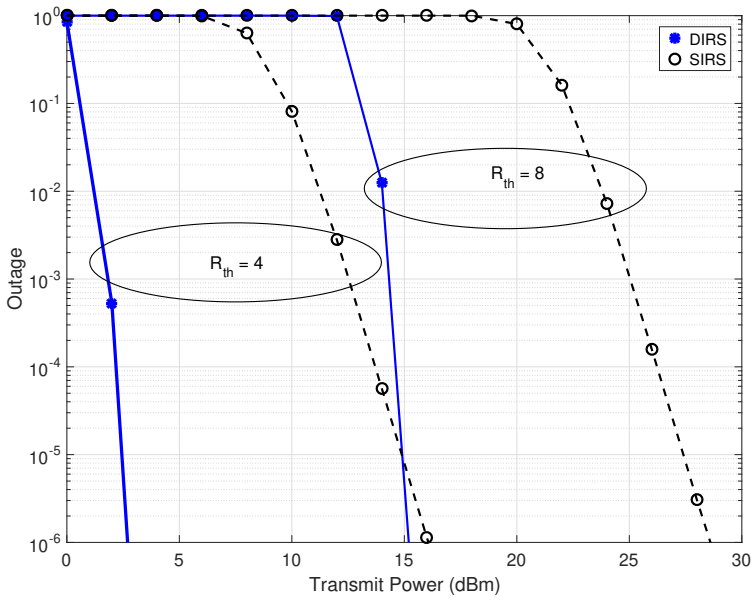

Figure 4.10: OP versus P_t for both dual and single IRS-assisted communication system, here $M = 200$ and $\kappa = 0.01$.

mitigates the impact of the multiplicative pathloss; thus, for large M, DIRS outperforms SIRS. However, for the non-ideal transceiver case, the SE of both DIRS and SIRS saturates to a similar level independent of M.

Likewise, Fig. 4.10 shows the outage performance of both DIRS and SIRS scenarios under a non-ideal transceiver. Specifically, it shows the OP with respect to transmit SNR for two different rate thresholds, viz. $R_th = 4, 8$ bps/Hz. It can easily be observed here that due to the fourth-order gain in SNR (i.e., $M_1^2 M_2^2$), the DIRS scenario outperforms the SIRS scenario where the gain provided by IRS is of second-order (i.e., N^2). The result verifies the superior performance of DIRS over SIRS in terms of OP.

4.11 Conclusion of Part II

In this part, we investigated a dual IRS-aided communication system's performance under a non-ideal transceiver. Specifically, we have evaluated the SE and the OP for the dual IRS-aided communication model. Additionally, the performance is compared with a single IRS-aided communication system under a non-ideal transceiver. The multiplicative pathloss affects the performance of dual IRS. However, it can be mitigated by increasing the number of REs in the ideal transceiver case. From the analytical framework, it has been shown that utilizing distributed IRS by dividing the large IRS into two smaller IRSs provides significant performance gain in terms of SE and OP both. However, for the non-ideal transceiver case, the distortion

noise due to hardware impairments saturates the SE of both DIRS and SIRS scenarios. No further gain can be realized by increasing the number of REs. Hence, these constraints must be considered while designing the practical IRS-aided communication system.

Chapter 5

Performance Comparison of IRS- and FD Relay-Aided Communication Systems

5.1 Introduction

IRS is similar to a relay, where the relay actively processes and re-transmits the amplified signal. However, the critical difference in the IRS is the passive reflection without any amplification but with beamforming. Moreover, in conventional relaying, time-division duplexing or frequency-division duplexing is utilized to provide out-of-band FD operations. However, this results in a significant loss of precious spectral resources. Utilizing the same time-frequency resource for concurrent transmission and reception, i.e., in-band FD transmission, can theoretically double the SE of the HD systems [5].

The performance comparison of the IRS with an ideal AF relay was studied in [7], where the IRS is shown to have a large EE. Further, in [43], the performance of the IRS-assisted system is compared with the ideal AF relay in terms of outage probability, SER and ergodic capacity. Here also, the IRS-assisted system outperforms conventional AF relaying. Likewise, in [60], Bjornson et al. have compared the performance of IRS-assisted systems against DF relaying. The authors have shown that IRS-aided transmission only sometimes outweighs conventional DF relaying. However, for a very large number of REs, the IRS can outperform the DF relay. Moreover, in [61], the authors have considered some novel 5G channel models and revised the results for IRSs, and DF relays, where they have shown that the IRS and DF relay can complement each other's strengths and can both have a place in 5G and beyond 5G architectures. Finally, Renzo et al. have summarized the key differences and similarities between the IRSs and the relays in [62]. As evident from above, the performance comparison for IRS and relaying has been studied in the literature, considering the ideal hardware scenario.

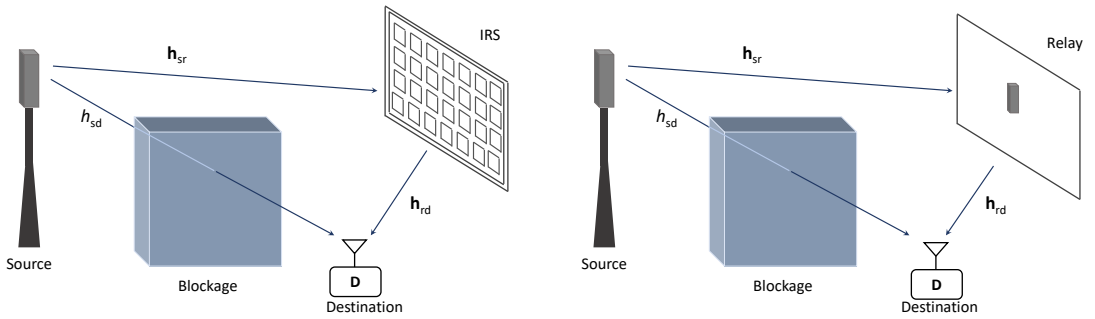

(a) IRS-assisted Wireless System (b) FD Relay-assisted Wireless System

Figure 5.1: Schematic for the considered scenario.

However, as shown in [86, 92], a non-ideal transmitter at the source severely restricts the performance of an IRS-assisted wireless communication system. Motivated by the above, in this article, we investigate and compare the performance of IRS-supported transmission and relaying in the presence of a non-ideal transmitter. Further, in [86, 92], the authors have analyzed the performance of an IRS-assisted system for a fixed set-up; this work also analyzed the impact of the placement of IRS as well as compared it with respect to both HD and FD relaying. Since DF relaying is well-known to have better performance than AF relaying in terms of achievable rates [93], in this work, we consider DF relaying as it will serve as a better performance benchmark. Furthermore, we have considered both half-duplex and FD modes of operation while comparing the performance of the IRS-assisted system.

5.2 System Model

In this work, we have considered a system where a source tries to communicate with the destination. The transmission is aided by an IRS or a DF relay, as shown in Fig. 5.1.

5.2.1 Channel Model

5.2.1.1 IRS-assisted Transmission

As illustrated in Fig. 5.1(a), we have considered the scenario where a source is communicating with the destination via an IRS. The IRS, which consists of N discrete REs, facilitates the information transfer. The channel between the source and the IRS is denoted as $\mathbf{h}_{sr}$, and the one between the IRS and the destination is denoted as $\mathbf{h}_{rd}$. Further, the source-to-IRS distance and the IRS-to-destination distance are denoted as d_{sr} and d_{rd}, respectively, whereas d_{sd} denotes the source-to-destination distance. The sum distance of source-to-destination via relay link is D,

i.e., $D = d_{sr} + d_{rd}$. Further, we considered the scenario where a blockage obstructs the direct link between source and destination and the IRS is deployed to assist the communication[1]. Since there is no direct line of sight link, $D > d_{sd}$, i.e., implies that the IRS relay cannot be placed between the source-to-destination link.

5.2.1.2 Relay-assisted Transmission

For the relay-assisted system, we have considered a relay in place of the IRS, as shown in Fig. 5.1(b). Specifically, we consider a single antenna-based source and destination communicating via a DF relay. In this scenario, the direct link connecting the source and destination is supposed to be obstructed or heavily shadowed, so the relay has been placed to set up a reliable communication link. A FD mode has been considered for the relay, where the relay node is equipped with a pair of antennas, one each for transmitting and receiving. In contrast, the source and destination are presumed to be single-antenna devices[2]. Furthermore, it is assumed that the relay has perfect knowledge of CSI. The transmit data symbols for the source and relay are denoted by x_s and $\mathbf{x}_r$, respectively, and are assumed to be i.i.d. with zero mean and variance as $P_s = \mathrm{E}\left\{s_x s_x^H\right\}$ and $P_r = \mathrm{tr}\left(\mathrm{E}\left\{\mathbf{r}_x \mathbf{r}_x^H\right\}\right)$ respectively. P_s and P_r represent the transmit power constraints at the source and the relay, respectively. The SI channel, h_{si}, is represented mathematically as a frequency non-selective Rayleigh flat fading channel with i.i.d. elements, $h_{si} \sim \mathscr{CN}(0,1)$ [63].

5.2.2 Transceiver Impairments

Conventionally, it has been shown in the literature that the assumption of considering ideal hardware is not practical as the transceiver architecture at the RF front-end is prone to various inevitable additive impairments such as I/Q imbalance, phase noise, and nonlinearity of RF. A generic approach for modeling the joint impact of all these impairments considers that the resultant distortion noises are Gaussian distributed, with their average power proportional to the signal's average transmit power.

As a result, the above imperfections will cause a mismatch between the actual transmitted signal and the desired signal, x, where $x \in \mathscr{CN}(0, \sigma_{in}^2)$. As a result, the actual transmitted

[1]The above-considered scenario is one of the practical applications of the IRS that has been explored in literature [43].

[2]The scenario mentioned above suits cellular networks where the multi-antenna BS works as a relay for end-users. Since the UEs are generally constrained by space and complexity, they are assumed to be single-antenna entities operating in a half-duplex mode. However, the BS has no such restrictions, so it can easily be equipped with multiple antennas and operate in a full-duplex mode.

signal, $\tilde{x}$, can be rewritten as follows:

$$\tilde{x} = x + w, \tag{5.1}$$

where w represents the distortion caused by the aggregated hardware imperfections, and it can be modeled as a zero-mean complex Gaussian process whose variance can be expressed as

$$\sigma_w^2 = \xi^2 \sigma_{in}^2, \tag{5.2}$$

where ξ is a proportionality constant describing the residual impairment at the source.

5.2.3 Received Signal Model

5.2.3.1 IRS-assisted Transmission

The reflected signal from IRS, which is received at the destination, can be denoted as

$$\begin{aligned} y &= \sum_{i=1}^{N} h_{sr} r_i h_{rd} \tilde{x}_t + n_d \\ &= \mathscr{G} r_i \tilde{x}_t + n_d, \end{aligned} \tag{5.3}$$

where n_d denotes the AWGN noise with $\mathscr{CN}(0, \sigma^2)$. Further, with $\mathscr{G} = \sum_{i=1}^{N} [|h_{sr}|]_i [|h_{rd}|]_i$ being the gain provided by the IRS.

Moreover, $r_i = |r_i| \exp(j\varphi_i)$ represents the response of the ith RE where φ_i denotes the phase shift that is applied by the ith RE of the IRS[3]. Without losing any generality, we assume that $|r_i| = 1$[4]. Further, the phase can be optimally set to reflect the incoming signal toward the user. The optimal phase shift that can be adjusted is $\varphi_i = -\left(\varphi_{[h_{sr}]_i} + \varphi_{[h_{rd}]_i}\right)$, and so, with the optimal beamforming at IRS, r_i can be rewritten to as $r_i = \exp\left(-j\left(\varphi_{[h_{sr}]_i} + \varphi_{[h_{rd}]_i}\right)\right)$. Thus, utilizing (5.1), the received signal at the destination can now be expressed as

$$y = \mathscr{G}\tilde{x}_t + n_d = \mathscr{G}x_t + \mathscr{G}w_t + n_d. \tag{5.4}$$

[3]Practically, the phase-shift is discrete and depends on the realization of IRS; however, this does not impact our analysis as it has been shown in the literature that a 3-bit based IRS has nearly the same performance as that of a continuous phase shift IRS.

[4]This is in line with the realistic assumptions taken in literature [43].

5.2.3.2 FD Relay-assisted Transmission

The received signal at the FD relay, y_R, can be expressed as

$$y_r = h_{sr}\tilde{x}_s + h_{si}\tilde{x}_r + n_r, \tag{5.5}$$

where n_r is the AWGN noise with $\mathscr{CN}(0,\sigma^2)$.

The SI can be mitigated at the FD relay by estimating it and subtracting it from the received signal. However, the presence of various imperfections results in some RSI. Thus, after estimating $h_{si}\tilde{x}_r$, it can be subtracted from y_r, the received signal at the relay. Thus, in (5.5), the received signal can now be written as:

$$y_r = h_{sr}\tilde{x}_s + d_r + n_r, \tag{5.6}$$

where d_r denotes the RSI with $d_R \sim \mathscr{CN}(0,\sigma^2_{rsi})$ and $\sigma^2_{rsi} = \alpha P_r^{\nu}$. Further, α and ν $(0 \leq \nu \leq 1)$ are constants depending upon the efficacy of the employed SI cancellation scheme.

Thus, the equivalent received signal in (5.6) can be rewritten by substituting (5.1) as

$$y_r = h_{sr}x_s + h_{sr}w_s + d_r + n_r, \tag{5.7}$$

Likewise, the received signal y_d at the destination can be written as

$$y_d = h_{rd}\tilde{x}_r + n_d. \tag{5.8}$$

or equivalently, using (5.1) it can be re-written as

$$y_d = h_{rd}x_r + h_{rd}w_d + n_d. \tag{5.9}$$

5.3 Channel Capacity and EE Evaluation

This section presents the analytical formulation for the system capacity and EE. The EE can be defined as the ratio of the rate over the total power consumed [94],

$$EE = \frac{Rate}{P_t + P_{cir}}. \tag{5.10}$$

where $P_t = P_s + P_r$ is the total transmitted power at the source and relay, and P_{cir} is the circuit power consumption.

5.3.1 Circuit Power Modeling

The source power consumption comprises the transmit power at the source, P_s, circuit power consumption in HPA, P^S_{hpa}, and other circuitry[5], P^S_c. Now, the HPA power consumption can be modeled as $P^S_{hpa} = \beta P_s$, where $\beta = \frac{1}{\omega}$ and ω is the drain efficiency of HPA. Thus, the total power consumed at the source is $P^S_{tot} = (1+\beta)P_s + P^S_c$.

Likewise, the total power consumption at the FD relay can be denoted as $P^R_{tot} = (1+\beta)P_r + P^R_c$, where P^R_c is the circuit power consumption (excluding the HPA power consumption) at the FD relay. Similarly, the power consumed at the destination is $P^D_{tot} = P^D_c$, where P^D_c is the power consumed in the destination circuitry.

Since the IRS is equipped with multiple REs, for ease of exposition and without losing any generality, we assume that the power consumed by each of the REs is identical [7]. So, the power consumed at the IRS is $P^{IRS} = NP_{RE}$, where P_{RE} is the circuit power consumption at each RE in the IRS.

5.3.2 IRS-assisted Transmission

In this subsection, we will formulate the channel capacity expression for IRS-assisted transmission and then evaluate the EE of the system. The SDNR can be obtained from (5.2) and (5.4) as

$$\begin{aligned}\Gamma_{IRS} &= \frac{\mathscr{G}^2 P_t}{\mathscr{G}^2 \xi_t^2 P_t + \sigma^2} \\ &= \frac{\mathscr{G}^2}{\xi_t^2 \mathscr{G}^2 + \frac{1}{\Gamma_t}},\end{aligned} \tag{5.11}$$

where, $\Gamma_t = \frac{P_t}{\sigma^2}$, denotes the transmit SNR. So, the channel capacity of the IRS-assisted network can be expressed as follows:

$$R_{IRS} = \log_2(1+\Gamma_{IRS}). \tag{5.12}$$

After taking into account the circuit power consumption as discussed above, the EE in (5.10) and (5.12) can be expressed as

$$EE = \frac{R_{IRS}}{(1+\beta)P_t + P^S_c + NP_{RE} + P^D_c} \tag{5.13}$$

[5]This accounts for the power consumed in other blocks apart from HPA, such as mixers, digital-to-analog converters, and frequency synthesizers.

From (5.13), it can be observed that increasing N increases the power consumption linearly, whereas the SE increases logarithmically with respect to N. Thus, the overall impact will be a compound effect of both, where the EE increases initially with increasing N, but later, the EE decreases. This has also been verified through simulation results in the next section.

5.3.3 FD Relay-assisted Transmission

In this subsection, we formulate the channel capacity relay-assisted transmission and then evaluate the EE of the system. The SDNR for the source-to-relay link can be obtained from (5.2) and (5.7) and is represented as

$$\begin{aligned}\Gamma_{SR} &= \frac{|h_{sr}|^2 P_s}{|h_{sr}|^2 \xi_s^2 P_s + \sigma_{rsi}^2 + \sigma^2} \\ &= \frac{\Gamma_s}{\xi_s^2 \Gamma_s + \Gamma_{rsi} + 1},\end{aligned} \tag{5.14}$$

where $\Gamma_s = P_s |h_{sr}|^2 / \sigma^2$ and $\Gamma_{rsi} = \sigma_{rsi}^2 / \sigma^2$. Likewise, the SDNR for the relay-to-destination link can be obtained from (5.2) and (5.9) as:

$$\begin{aligned}\Gamma_{RD} &= \frac{|h_{rd}|^2 P_r}{|h_{rd}|^2 \xi_r^2 P_r + \sigma^2} \\ &= \frac{\Gamma_r}{\xi_r^2 \Gamma_r + 1},\end{aligned} \tag{5.15}$$

where $\Gamma_r = P_r |h_{rd}|^2 / \sigma^2$. Thus the end-to-end SDNR of the source-to-destination via relay link can be expressed from (5.14) and (5.15) as

$$\Gamma_{FD} = \min\{\Gamma_{SR}, \Gamma_{RD}\}. \tag{5.16}$$

Therefore, the channel capacity for the relay-assisted system can be expressed as follows:

$$\begin{aligned}R_{FD} &= \log_2(1 + \Gamma_{FD}) \\ &= \log_2(1 + \min\{\Gamma_{SR}, \Gamma_{RD}\})\end{aligned} \tag{5.17}$$

The EE for FD relay-assisted transmission can be evaluated from (5.10) and (5.17) as

$$EE = \frac{R_{FD}}{(1+\beta)P_t + P_c^R + P_c^S + + P_{SIC} + P_c^D} \tag{5.18}$$

Table 5.1: Simulation Parameters for IRS/FD-assisted Communication

Parameter	Simulation Values
σ^2	0 dB
ν	1
α	80 dB
ξ_t, ξ_s, ξ_r	0.1
β	0.8
P_c^S, P_c^R, P_c^D	10 dBm [7]
P_{RE}	10 dBm [7]
G_t, G_r	0 dBi

Special Case (Half-Duplex): For the HD mode of operation at the relay, each of the source and the relay would transmit for half of the time interval. Additionally, the SI term would no longer be valid. So, the channel capacity would be as below:

$$R_{HD} = \frac{1}{2}\log_2(1+\Gamma_{HD}), \tag{5.19}$$

where, Γ_{HD} can be defined from (5.14) and (5.15) as

$$\Gamma_{HD} = \min\left\{\frac{\Gamma_s}{\xi_s^2\Gamma_s+1}, \frac{\Gamma_r}{\xi_r^2\Gamma_r+1}\right\}. \tag{5.20}$$

Therefore, the corresponding EE can be expressed as

$$EE = \frac{R_{HD}}{(1/2)(1+\beta)P_t + P_c^S + P_c^R + P_c^D} \tag{5.21}$$

The factor (1/2) indicates that the source and relay transmit only during half of the time slot, which makes the EE of the half-duplex system better than its FD counterpart.

5.4 Simulation Results

This section presents the simulation results for the performance of both IRS-assisted and relay-assisted transmission systems. The major simulation parameters are listed in Table 5.1. Further, we specify the placement parameter as ρ, which defines the IRS/relay localization as $d_{sr} = \rho D$ and $d_{rd} = (1-\rho)D$. Also, to have a better performance benchmark, the total transmit power is kept constant for both IRS and relay-assisted systems such that $P_s + P_r = P_t$ and for ease of exposition $P_s = P_r$.

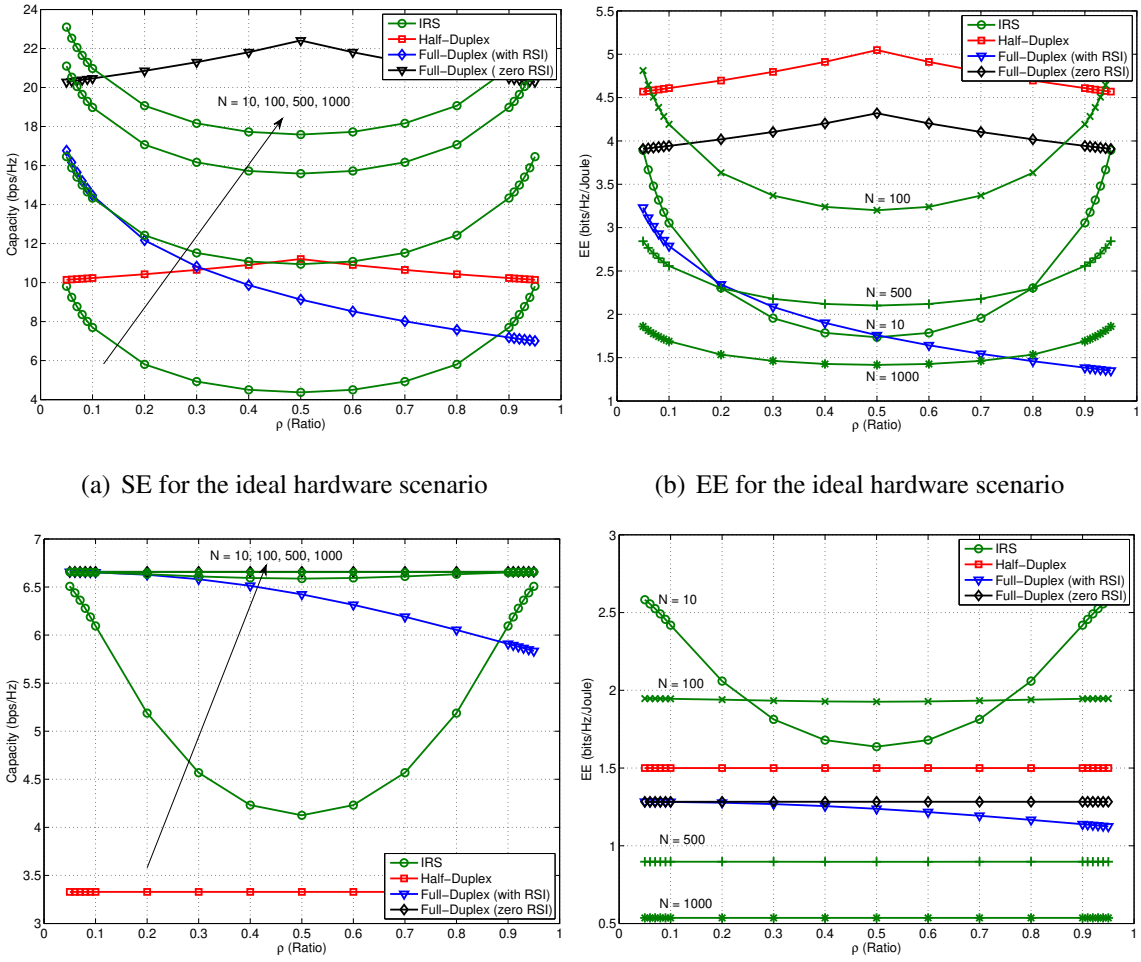

(a) SE for the ideal hardware scenario

(b) EE for the ideal hardware scenario

(c) SE for the non-ideal hardware scenario

(d) EE for the non-ideal hardware scenario

Figure 5.2: SE and EE with respect to placement parameter for both the ideal and non-ideal hardware transmitter case for $D = 110$ m.

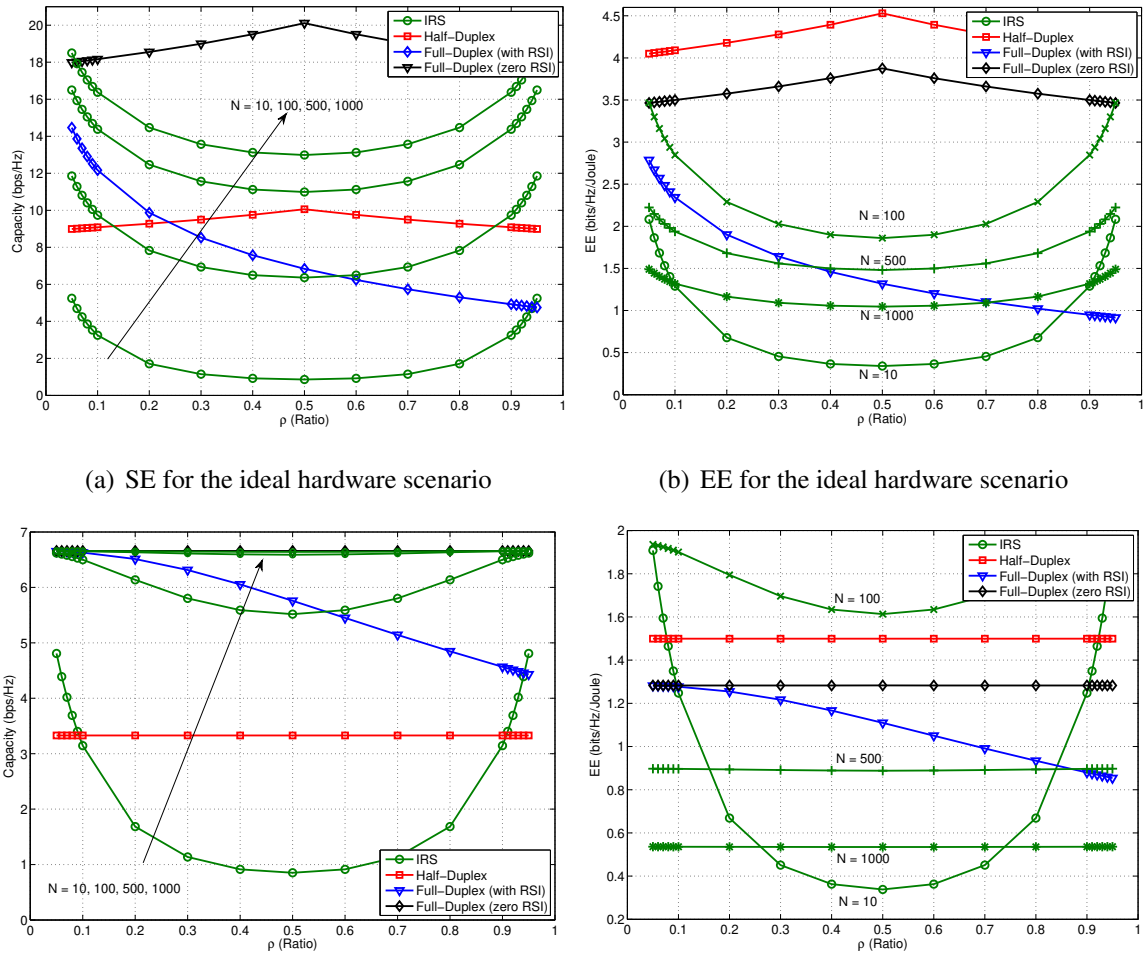

(a) SE for the ideal hardware scenario

(b) EE for the ideal hardware scenario

(c) SE for the non-ideal hardware scenario

(d) EE for the non-ideal hardware scenario

Figure 5.3: SE and EE with respect to placement parameter considering both ideal and non-ideal transmitter for $D = 220$ m.

The channel gain is modeled using the 3GPP Urban Micro (UMi) as described and discussed in [60]. Similar to [60, 61], we neglected the shadow fading to have a deterministic channel gain, $\beta(d)$ (i.e., $h_i = \sqrt{\beta(d)}, i \in sr, rd$). At the carrier frequency of 3 GHz, $\beta(d)$ can be expressed as:

$$\beta(d)\ [\text{dB}] = G_{\text{t}}\ [\text{dBi}] + G_{\text{r}}\ [\text{dBi}] + \begin{cases} -37.5 - 22\log_{10}(d/1\,\text{m}) & \text{if LOS}, \\ -35.1 - 36.7\log_{10}(d/1\,\text{m}) & \text{if NLOS}, \end{cases} \tag{5.22}$$

where G_{t} and G_{r} denote the transmit and receive antenna gain at the source/relay and relay/destination, respectively.

Fig. 5.2 shows the SE and the EE for both ideal and non-ideal transmitters considering the total distance to be $D = 110$ m. Specifically, Figs. 5.2(a) and 5.2(c) show the capacity for both IRS-assisted and relay-assisted transmission systems for the ideal and non-ideal transmitter, respectively. The following observations can be made from Fig. 5.2(a): a) the performance of IRS improves when the number of REs are increased, b) while increasing the number of REs, the IRS-assisted system is able to outperform DF relaying for very large M, c) the performance IRS-assisted system is significantly improved when the IRS is in close proximity of the source or when the destination is very close to IRS, d) ideal FD relay-assisted system provides the exact double capacity, however, the practical performance is affected by the RSI, and e) practical FD-DF-relaying is significantly impacted by RSI when the relay is far away from the source, this is because of the fact that when the relay is moving farther from source, the received signal strength falls off and so the RSI's impact dominates the overall performance[6].

In addition, the following insights can be gained from Fig. 5.2(c): f) The non-ideal hardware transmitter-based IRS-assisted system can never outperform the ideal FD-DF relaying in terms of capacity. g) As the number of REs increases, the capacity saturates. h) After $N = 100$, there is hardly any measurable gain in capacity, even by changing the location of the IRS. i) The location also influences the capacity of relay-assisted transmission as the distortion noise dominates the capacity, so by altering the location of the relay, the capacity can be increased. In the ideal hardware transmitter case, the capacity is maximized when the relay is placed at rho = 0.5.

Figs. 5.2(b) and 5.2(d) show the EE of the ideal and non-ideal transmitter, respectively. Also, Fig. 5.2(b) shows the EE for different M, i.e., the number of REs in the IRS, where it is evident that the EE initially increases with increasing M; later on, it decreases. Further, Fig. 5.2(d) shows that for the non-ideal hardware transmitter case, the EE decreases considerably with increasing M. This is because the capacity saturates with increasing M; however, the energy consumption increases linearly. Consequently, it results in an overall reduction in the EE of the IRS-assisted transmission system. This can also be verified from (5.13). Further, it can also be verified that the half-duplex relay-assisted system is the most energy-efficient. This is because, in contrast to FD relaying, the source and the relay transmit only for half the interval. This can also be viewed from (5.21). Further, in the FD-relaying, there is additional power consumption in the SI cancellation circuitry, as can be viewed in (5.18).

Fig. 5.3 shows another set of capacity and EE results for the non-ideal transmitter case when the total distance is increased to $D = 220$ m. The following points are worth noting while comparing Fig. 5.2 and Fig. 5.3. a) For large N, the impact of distortion noise is more

[6]The performance of practical FD-DF-relaying can be improved further through optimal power allocation, which is out of scope for the current work, however, it can be considered for the future extension of this work.

severe, the capacity is saturated and not impacted by the placement of IRS, however, when N is small, the placement of IRS impacts the capacity. Further, the capacity decreases when the total distance is increased. This is due to the fact that the path-loss increases with increasing distance. b) The EE of the IRS-assisted system is impacted more severely when the distance is increased. Even FD relaying is more energy-efficient than the IRS-assisted transmission system.

It can be inferred here that the IRS-assisted system can only outperform the capacity of the relay-assisted system for shorter distances and ideal hardware transmitter cases. Moreover, the capacity of ideal-hardware-based IRS-assisted can be further enhanced by placing it near the source or destination. Furthermore, for non-ideal hardware systems, FD-relaying consistently outperforms the IRS-assisted system, regardless of IRS placement and size, i.e., M. A similar argument can be provided for the EE of the IRS-assisted system and the FD-based DF-relaying.

5.5 Conclusion

In this chapter, the performance of a IRS-assisted wireless system is investigated and compared with that of a FD relay-assisted wireless system in the presence of non-ideal transceivers. Specifically, the performance is compared in terms of channel capacity and EE. The main observation is that the IRS-assisted system can never outperform the capacity achieved by ideal full-duplex relaying for the non-ideal hardware scenario. Further, by increasing the number of REs, the capacity of the IRS-assisted system saturates to the capacity achieved by the ideal FD relay-assisted system. However, this also results in the reduction of the EE of the IRS-assisted system. Thus, there is a trade-off with respect to increasing the number of REs that can be observed in the capacity and EE of the IRS-assisted system. Apart from this, several other insights have also been provided while discussing the results.

Chapter 6

Conclusion and Future Work

6.1 Summary of the Contributions

Due to seamless wireless connectivity, the amount of data traffic on a wireless network has been growing steadily. This means that available resources need to be used as effectively as possible. For the sake of sustainable development, wireless communication systems must be energy-efficient so that they can handle all of this data traffic. In this dissertation, we have primarily focused on the FD communication technique, which theoretically doubles the spectrum utilization efficiency. However, in practice, it is limited by the residual SI. Further, this SI can also be harnessed for improving the EE of a FD system through S-ER.

Further, we analyze the impact of S-ER on the performance of FD-based systems under RSI. The inherently present SI in the FD systems is utilized opportunistically to harvest energy, thereby enhancing the EE of the system. However, this comes at the cost of slightly degrading the system's SE due to reduced array gain. The allocation of antennas for S-ER and information transmission can be done based on the desired QoS requirement. Analytical expressions are derived for the SE, OP and EE. The obtained results show that S-ER improves the EE of the systems by recycling a portion of the transmitted energy at the expense of a slight degradation in the SE. As long as this degradation in SE satisfies the desired QoS, S-ER can be utilized to improve the EE of the FD system. Further, an adaptive S-ER scheme is proposed that compensates for the degradation in SE and enhances the EE simultaneously.

Further, with the advent of metamaterials, IRS, a passive realization of FD with zero SI, can achieve ultra-high SE and EE. This thesis investigates the performance of IRS-assisted communication systems under practical, non-ideal hardware scenarios. Further, we also characterized the joint impact of the transceiver's HIs and IRS phase errors on the performance of an IRS-aided communication system with and without a direct link. Specifically, we have

derived the closed-form expressions of the SE, EE and OP. Although both transceiver HIs and IRS phase errors degrade performance, the impact of transceiver HI is far more severe and damaging. In particular, the transceiver HI saturates the SE. This saturation level is independent of the number of REs in the IRS and the transmit power. Likewise, for the particular case of a high transmit SNR and a large number of reflecting elements, the SE saturates to the same level independent of the transmit SNR, the number of reflecting elements, and the availability of a direct link. Likewise, the multiplicative pathloss affects the performance of a dual IRS-aided communication system. However, it can be mitigated by increasing the number of REs in the ideal transceiver case. From the analytical framework, it has been shown that utilizing a distributed IRS by dividing the large IRS into two smaller IRSs provides significant performance gains in terms of SE and OP. However, for the non-ideal transceiver case, the distortion noise due to hardware impairments saturates the SE of both DIRS and SIRS scenarios. No further gain can be realized by increasing the number of REs.Consequently, the impact of non-ideal hardware cannot be neglected in a practical IRS-enabled system design.

Later, we compared the relative performances of the FD relay and the IRS-assisted communication system under practical, non-ideal transceiver scenarios. The main observation is that the IRS-assisted system can never outperform the capacity achieved by ideal full-duplex relaying in the non-ideal hardware scenario. Thus, transceivers are far more crucial to the performance of IRS-assisted communication systems. Further, by increasing the number of REs, the capacity of the IRS-assisted system saturates at the capacity achieved by the ideal FD relay-assisted system. However, this also results in the reduction of the EE of the IRS-assisted system. Thus, there is a trade-off with respect to increasing the number of REs that can be observed in the capacity and EE of the IRS-assisted system. Hence, these constraints must be considered while designing a practical IRS-aided communication system.

A communication engineer can efficiently utilize the proposed analytical framework to design the link budget for FD/IRS-based communication systems without performing extensive simulations or tedious experiments.

6.2 Mitigation Techniques and Future Work

As discussed in the literature, the HPA is the primary source in the radio architecture that contributes most to nonlinear distortion. In order to reduce the distortion, the HPA can be forced into operating with a high IBO. However, increasing IBO results in poorer energy efficiency because HPAs are designed to provide maximum efficiency in the nonlinear region. Another method to reduce the effects of nonlinear distortion is to use digital pre-distortion. This method does not have an adverse effect on the energy efficiency of the transmitter. Likewise,

post-distortion is carried out on the receiver side in order to compensate for the distortions. However, it increases the complexity of the circuitry in both the transmitter and the receiver.

There are numerous ways in which this dissertation's work can be expanded. The following are some potential future research directions:

- Apart from residual SI, several other impairments are present in the FD relay-based communication systems, such as cross-talk and channel correlation. The FD relay-based communication system's performance suffers due to these impairments. As a result, when analyzing the performance of an FD relay system, it is critical to consider the influence of these limitations.

- Likewise, in this dissertation, the impact of a correlated channel is not considered for the performance analysis of IRS-assisted communication systems. This can also be a potential research idea to evaluate the performance degradation due to the correlated channels. Furthermore, near-field-based IRS beamforming is also an exciting research idea for further extension of this work.

- In addition to the above, the combination of FD relay with IRS is yet to be explored. Thus, the performance of a combination of active and passive FD relaying would be interesting to explore.

Appendix A

Author's Publications

Journals

1. **M. H. N. Shaikh**, V. A. Bohara, A. Srivastava and G. Ghatak, "An Energy Efficient Dual IRS-aided Outdoor-to-Indoor Communication System," submitted in *IEEE Systems Journal*.

2. **M. H. N. Shaikh**, V. A. Bohara and A. Srivastava, "On the Performance of Dual RIS-Aided Communication System under Non-Ideal Transceiver over Nakagami-*m* Fading Channels," *Internet Technology Letters*, vol. 5, no. 6, 2022.

3. **M. H. N. Shaikh**, V. A. Bohara, A. Srivastava and G. Ghatak, "A Downlink RIS-aided NOMA System with Hardware Impairments: Performance Characterization and Analysis," *IEEE Open Journal of Signal Processing*, vol. 3, pp. 288-305, 2022.

4. K. Joshi, **M. H. N. Shaikh**, S. A. Naqvi, and V. A. Bohara, "On the performance of IRS-assisted OFDM system with non-ideal oscillator and amplifier," *Internet Technology Letters*, vol. 5, no. 4, 2022.

5. **M. H. N. Shaikh**, V. A. Bohara, A. Srivastava and G. Ghatak, "Performance Analysis of Intelligent Reflecting Surface-Assisted Wireless System with Non-Ideal Transceiver," *IEEE Open Journal of the Communications Society*, vol. 2, pp. 671-686, 2021.

6. **M. H. N. Shaikh**, V. A. Bohara and A. Srivastava, "Performance Analysis of a Full-Duplex MIMO Decode-and-Forward Relay System With Self-Energy Recycling," *IEEE Access*, vol. 8, pp. 226248-226266, 2020.

7. **M. H. N. Shaikh**, V. A. Bohara, P. Aggarwal and A. Srivastava, "Energy Efficiency Evaluation for Downlink Full-Duplex Nonlinear MU-MIMO-OFDM System With Self-Energy Recycling," *IEEE Systems Journal*, vol. 14, no. 3, pp. 3313-3324, 2020.

Conferences

1. **M. H. N. Shaikh**, V. A. Bohara and A. Srivastava, "IRS-Aided Communication System with Phase Noise and Hardware Impairments: Performance Analysis and Characterization," accepted in *COMSNETS 2023*.

2. K. Lata, V. A. Bohara, A. Srivastava and **M. H. N. Shaikh**, "Intelligent Reflecting Surfaces Versus Optical Mirrors: Performance Comparison for Indoor Physical Layer Security Environments," *IEEE International Conference on Advanced Networks and Telecommunications Systems (ANTS)*, IIT-Gandhinagar, India, 2022, pp. 1-6.

3. **M. H. N. Shaikh**, V. A. Bohara, A. Srivastava and G. Ghatak, "On the Performance of RIS-Aided NOMA System with Non-ideal Transceiver over Nakagami-m Fading," *IEEE Wireless Communications and Networking Conference (WCNC)*, 2022, pp. 1737-1742.

4. **M. H. N. Shaikh**, V. A. Bohara, A. Srivastava and G. Ghatak, "Intelligent Reflecting Surfaces Versus Full-Duplex Relaying: Performance Comparison for Non-Ideal Transmitter Case," *IEEE 32nd Annual International Symposium on Personal, Indoor and Mobile Radio Communications (PIMRC)*, Helsinki, Finland, 2021, pp. 513-518.

5. **M. H. N. Shaikh**, V. A. Bohara and A. Srivastava, "Performance Enhancement in Full-Duplex AF Relay System through Smart Antenna Allocation," *IEEE 3rd 5G World Forum (5GWF)*, Bangalore, India, 2020, pp. 303-308.

6. **M. H. N. Shaikh**, V. A. Bohara, A. Srivastava and G. Ghatak, "EE Enhancement in FD MIMO Relay System through Adaptive Antenna Allocation and Self-Energy Recycling," *IEEE International Conference on Communications Workshops (ICC Workshops)*, Dublin, Ireland, 2020, pp. 1-6.

7. **M. H. N. Shaikh**, V. A. Bohara, and A. Srivastava, "Spectral Analysis of WOLA-OFDM in the Presence of DPD and HPA," *Twenty-sixth National Conference on Communications (NCC)*, Kharagpur, India, 2020, pp. 1-6.

8. **M. H. N. Shaikh**, V. A. Bohara, and A. Srivastava, "Energy Efficiency Enhancement in Full-Duplex Relay System through Adaptive Antenna Allocation," *2019 IEEE International Conference on Advanced Networks and Telecommunications Systems (ANTS)*, BITS-Goa, India, 2019, pp. 1-5.

9. **M. H. N. Shaikh**, V. A. Bohara, P. Aggarwal and A. Srivastava, "On EE-SE Trade-Off for Downlink Full Duplex MISO Systems with Self-Energy Recycling," *IEEE 89th Vehicular Technology Conference (VTC2019-Spring)*, Kuala Lumpur, Malaysia, 2019, pp. 1-5.

10. **M. H. N. Shaikh**, A. Agarwal, P. Aggarwal and V. A. Bohara, "On the Spectral Content of Nonlinear Carrier Aggregated Windowed OFDM Systems," *IEEE International Conference on Advanced Networks and Telecommunications Systems (ANTS)*, Indore, India, 2018, pp. 1-5.

References

[1] M. A. Habibi, M. Nasimi, B. Han, and H. D. Schotten, "A comprehensive survey of RAN architectures toward 5G mobile communication system," *IEEE Access*, vol. 7, pp. 70 371–70 421, May 2019.

[2] V. N. I. Cisco, "The zettabyte era: Trends and analysis."

[3] M. Xiao, S. Mumtaz, Y. Huang, L. Dai, Y. Li, M. Matthaiou, G. K. Karagiannidis, E. Björnson, K. Yang, C. I, and A. Ghosh, "Millimeter wave communications for future mobile networks," *IEEE Journal on Selected Areas in Communications*, vol. 35, no. 9, pp. 1909–1935, 2017.

[4] L. Lu, G. Y. Li, A. L. Swindlehurst, A. Ashikhmin, and R. Zhang, "An overview of massive MIMO: Benefits and challenges," *IEEE Journal of Selected Topics in Signal Processing*, vol. 8, no. 5, pp. 742–758, 2014.

[5] G. Liu, F. R. Yu, H. Ji, V. C. M. Leung, and X. Li, "In-band full-duplex relaying: A survey, research issues and challenges," *IEEE Communications Surveys Tutorials*, vol. 17, no. 2, pp. 500–524, Secondquarter 2015.

[6] E. Basar, M. Di Renzo, J. De Rosny, M. Debbah, M.-S. Alouini, and R. Zhang, "Wireless communications through reconfigurable intelligent surfaces," *IEEE Access*, vol. 7, pp. 116 753–116 773, 2019.

[7] C. Huang, A. Zappone, G. C. Alexandropoulos, M. Debbah, and C. Yuen, "Reconfigurable intelligent surfaces for energy efficiency in wireless communication," *IEEE Transactions on Wireless Communications*, vol. 18, no. 8, pp. 4157–4170, 2019.

[8] K. E. Kolodziej, B. T. Perry, and J. S. Herd, "In-band full-duplex technology: Techniques and systems survey," *IEEE Transactions on Microwave Theory and Techniques*, vol. 67, no. 7, pp. 3025–3041, 2019.

[9] A. Sabharwal, P. Schniter, D. Guo, D. W. Bliss, S. Rangarajan, and R. Wichman, "In-band full-duplex wireless: Challenges and opportunities," *IEEE Journal on Selected Areas in Communications*, vol. 32, no. 9, pp. 1637–1652, 2014.

[10] T. Gansler and G. Salomonsson, "Nonintrusive measurements of the telephone channel," *IEEE Transactions on Communications*, vol. 47, no. 1, pp. 158–167, 1999.

[11] Z. Zhang, X. Chai, K. Long, A. V. Vasilakos, and L. Hanzo, "Full duplex techniques for 5G networks: self-interference cancellation, protocol design, and relay selection," *IEEE Communications Magazine*, vol. 53, no. 5, pp. 128–137, May 2015.

[12] M. Heino, D. Korpi, T. Huusari, E. Antonio-Rodriguez, S. Venkatasubramanian, T. Riihonen, L. Anttila, C. Icheln, K. Haneda, R. Wichman, and M. Valkama, "Recent advances in antenna design and interference cancellation algorithms for in-band full duplex relays," *IEEE Communications Magazine*, vol. 53, no. 5, pp. 91–101, May 2015.

[13] E. Ahmed, A. M. Eltawil, and A. Sabharwal, "Self-interference cancellation with nonlinear distortion suppression for full-duplex systems," in *2013 Asilomar Conference on Signals, Systems and Computers*, Nov. 2013, pp. 1199–1203.

[14] A. Masmoudi, "Self-interference cancellation for full-duplex wireless communications systems," Ph.D. dissertation, McGill University, 2016.

[15] C. Li, Z. Chen, Y. Wang, Y. Yao, and B. Xia, "Outage analysis of the full-duplex decode-and-forward two-way relay system," *IEEE Transactions on Vehicular Technology*, vol. 66, no. 5, pp. 4073–4086, May 2016.

[16] T. K. Baranwal, D. S. Michalopoulos, and R. Schober, "Outage analysis of multihop full duplex relaying," *IEEE Communications Letters*, vol. 17, no. 1, pp. 63–66, Jan. 2013.

[17] T. Riihonen, S. Werner, and R. Wichman, "Mitigation of loopback self-interference in full-duplex MIMO relays," *IEEE Transactions on Signal Processing*, vol. 59, no. 12, pp. 5983–5993, Dec. 2011.

[18] H. Cui, M. Ma, L. Song, and B. Jiao, "Relay selection for two-way full duplex relay networks with amplify-and-forward protocol," *IEEE Transactions on Wireless Communications*, vol. 13, no. 7, pp. 3768–3777, Jul. 2014.

[19] L. Jiménez Rodríguez, N. H. Tran, and T. Le-Ngoc, "Performance of full-duplex AF relaying in the presence of residual self-interference," *IEEE Journal on Selected Areas in Communications*, vol. 32, no. 9, pp. 1752–1764, Sep. 2014.

[20] L. J. Rodriguez, N. H. Tran, and T. Le-Ngoc, "Optimal power allocation and capacity of full-duplex AF relaying under residual self-interference," *IEEE Wireless Communications Letters*, vol. 3, no. 2, pp. 233–236, Apr. 2014.

[21] L. J. Rodriguez, N. H. Tran, and T. Le-Ngoc, "Performance of full-duplex AF relaying in the presence of residual self-interference," *IEEE Journal on Selected Areas in Communications*, vol. 32, no. 9, pp. 1752–1764, Jun. 2014.

[22] S. Li, K. Yang, M. Zhou, J. Wu, L. Song, Y. Li, and H. Li, "Full-duplex amplify-and-forward relaying: Power and location optimization," *IEEE Transactions on Vehicular Technology*, vol. 66, no. 9, pp. 8458–8468, Sep. 2017.

[23] B. Yu, L. Yang, X. Cheng, and R. Cao, "Power and location optimization for full-duplex decode-and-forward relaying," *IEEE Transactions on Communications*, vol. 63, no. 12, pp. 4743–4753, Dec. 2015.

[24] Z. Zhang, Z. Ma, M. Xiao, G. K. Karagiannidis, Z. Ding, and P. Fan, "Two-timeslot two-way full-duplex relaying for 5G wireless communication networks," *IEEE Transactions on Communications*, vol. 64, no. 7, pp. 2873–2887, Jul. 2016.

[25] P. Grover and A. Sahai, "Shannon meets tesla: Wireless information and power transfer," in *2010 IEEE International Symposium on Information Theory*, Jun. 2010, pp. 2363–2367.

[26] Z. Ding, C. Zhong, D. Wing Kwan Ng, M. Peng, H. A. Suraweera, R. Schober, and H. V. Poor, "Application of smart antenna technologies in simultaneous wireless information and power transfer," *IEEE Communications Magazine*, vol. 53, no. 4, pp. 86–93, Apr. 2015.

[27] M. Mohammadi, B. K. Chalise, H. A. Suraweera, C. Zhong, G. Zheng, and I. Krikidis, "Throughput analysis and optimization of wireless-powered multiple antenna full-duplex relay systems," *IEEE Transactions on Communications*, vol. 64, no. 4, pp. 1769–1785, Apr. 2016.

[28] H. Liang, C. Zhong, X. Chen, H. A. Suraweera, and Z. Zhang, "Wireless powered dual-hop multi-antenna relaying systems: Impact of CSI and antenna correlation," *IEEE Transactions on Wireless Communications*, vol. 16, no. 4, pp. 2505–2519, Apr. 2017.

[29] C. Zhong, H. A. Suraweera, G. Zheng, I. Krikidis, and Z. Zhang, "Wireless information and power transfer with full duplex relaying," *IEEE Transactions on Communications*, vol. 62, no. 10, pp. 3447–3461, Oct. 2014.

[30] Y. Zeng and R. Zhang, "Full-duplex wireless-powered relay with self-energy recycling," *IEEE Wireless Communications Letters*, vol. 4, no. 2, pp. 201–204, Apr. 2015.

[31] D. Hwang, K. C. Hwang, D. I. Kim, and T.-J. Lee, "Self-energy recycling for RF powered multi-antenna relay channels," *IEEE Transactions on Wireless Communications*, vol. 16, no. 2, pp. 812–824, Feb. 2017.

[32] A. Yadav, O. Dobre, and H. V. Poor, "Is self-interference in full-duplex communications a foe or a friend?" *IEEE Signal Processing Letters*, vol. 25, no. 7, pp. 951–955, Jul. 2018.

[33] O. T. Demir and T. E. Tuncer, "Optimum QoS-aware beamformer design for full-duplex relay with self-energy recycling," *IEEE Wireless Communications Letters*, vol. 7, no. 1, pp. 122–125, Feb. 2018.

[34] W. Long, R. Chen, M. Moretti, W. Zhang, and J. Li, "A promising technology for 6G wireless networks: Intelligent reflecting surface," *Journal of Communications and Information Networks*, vol. 6, no. 1, pp. 1–16, 2021.

[35] B. Zong, C. Fan, X. Wang, X. Duan, B. Wang, and J. Wang, "6G technologies: Key drivers, core requirements, system architectures, and enabling technologies," *IEEE Vehicular Technology Magazine*, vol. 14, no. 3, pp. 18–27, 2019.

[36] Z. Zhang, Y. Xiao, Z. Ma, M. Xiao, Z. Ding, X. Lei, G. K. Karagiannidis, and P. Fan, "6G wireless networks: Vision, requirements, architecture, and key technologies," *IEEE Vehicular Technology Magazine*, vol. 14, no. 3, pp. 28–41, 2019.

[37] M. Di Renzo, M. Debbah, D.-T. Phan-Huy, A. Zappone, M.-S. Alouini, C. Yuen, V. Sciancalepore, G. C. Alexandropoulos, J. Hoydis, and H. Gacanin, "Smart radio environments empowered by reconfigurable ai meta-surfaces: An idea whose time has come," *EURASIP Journal on Wireless Communications and Networking*, vol. 2019, no. 1, pp. 1–20, 2019.

[38] G. Gui, M. Liu, F. Tang, N. Kato, and F. Adachi, "6G: Opening new horizons for integration of comfort, security, and intelligence," *IEEE Wireless Communications*, vol. 27, no. 5, pp. 126–132, Oct. 2020.

[39] S. Dang, O. Amin, B. Shihada, and M.-S. Alouini, "What should 6G be?" *Nature Electronics*, vol. 3, no. 1, pp. 20–29, 2020.

[40] C. Huang, G. C. Alexandropoulos, A. Zappone, M. Debbah, and C. Yuen, "Energy efficient multi-user MISO communication using low resolution large intelligent surfaces," in *Proc. IEEE Global Communications Conference Workshops (GC Workshops)*, 2018, pp. 1–6.

[41] J. Lyu and R. Zhang, "Hybrid active/passive wireless network aided by intelligent reflecting surface: System modeling and performance analysis," *IEEE Transactions on Wireless Communications*, vol. 20, no. 11, pp. 7196–7212, 2021.

[42] Y. Yang, B. Zheng, S. Zhang, and R. Zhang, "Intelligent reflecting surface meets OFDM: Protocol design and rate maximization," *IEEE Transactions on Communications*, vol. 68, no. 7, pp. 4522–4535, 2020.

[43] A. A. Boulogeorgos and A. Alexiou, "Performance analysis of reconfigurable intelligent surface-assisted wireless systems and comparison with relaying," *IEEE Access*, vol. 8, pp. 94 463–94 483, 2020.

[44] S. Hu, F. Rusek, and O. Edfors, "The potential of using large antenna arrays on intelligent surfaces," in *Proc. IEEE 85th Vehicular Technology Conference (VTC Spring)*, 2017, pp. 1–6.

[45] S. Hu, F. Rusek, and O. Edfors, "Beyond massive MIMO: The potential of data transmission with large intelligent surfaces," *IEEE Transactions on Signal Processing*, vol. 66, no. 10, pp. 2746–2758, May 2018.

[46] S. Hu, F. Rusek, and O. Edfors, "Beyond massive MIMO: The potential of positioning with large intelligent surfaces," *IEEE Transactions on Signal Processing*, vol. 66, no. 7, pp. 1761–1774, 2018.

[47] H. Zhang, B. Di, L. Song, and Z. Han, "Reconfigurable intelligent surfaces assisted communications with limited phase shifts: How many phase shifts are enough?" *IEEE Transactions on Vehicular Technology*, vol. 69, no. 4, pp. 4498–4502, 2020.

[48] M. Jung, W. Saad, Y. Jang, G. Kong, and S. Choi, "Reliability analysis of large intelligent surfaces (LISs): Rate distribution and outage probability," *IEEE Wireless Communications Letters*, vol. 8, no. 6, pp. 1662–1666, Dec. 2019.

[49] E. Basar, "Transmission through large intelligent surfaces: A new frontier in wireless communications," in *2019 European Conference on Networks and Communications (EuCNC)*, 2019, pp. 112–117.

[50] V. C. Thirumavalavan and T. S. Jayaraman, "BER analysis of reconfigurable intelligent surface assisted downlink power domain NOMA system," in *Proc. IEEE COMSNETS*, 2020, pp. 519–522.

[51] C. Pan, H. Ren, K. Wang, M. Elkashlan, A. Nallanathan, J. Wang, and L. Hanzo, "Intelligent reflecting surface aided MIMO broadcasting for simultaneous wireless information and power transfer," *IEEE Journal on Selected Areas in Communications*, vol. 38, no. 8, pp. 1719–1734, Aug. 2020.

[52] B. Lyu, P. Ramezani, D. T. Hoang, S. Gong, Z. Yang, and A. Jamalipour, "Optimized energy and information relaying in self-sustainable IRS-empowered WPCN," *IEEE Transactions on Communications*, vol. 69, no. 1, pp. 619–633, Jan. 2021.

[53] E. Basar, "Reconfigurable intelligent surface-based index modulation: A new beyond MIMO paradigm for 6G," *IEEE Transactions on Communications*, vol. 68, no. 5, pp. 3187–3196, 2020.

[54] Q. Wu and R. Zhang, "Beamforming optimization for intelligent reflecting surface with discrete phase shifts," in *Proc. IEEE ICASSP*, 2019, pp. 7830–7833.

[55] X. Yu, D. Xu, and R. Schober, "Enabling secure wireless communications via intelligent reflecting surfaces," in *Proc. IEEE Global Communications Conference (GLOBECOM)*, 2019, pp. 1–6.

[56] Y. Chen, Y. Wang, J. Zhang, and Z. Li, "Resource allocation for intelligent reflecting surface aided vehicular communications," *IEEE Transactions on Vehicular Technology*, vol. 69, no. 10, pp. 12 321–12 326, Oct. 2020.

[57] M. Di Renzo, A. Zappone, M. Debbah, M. S. Alouini, C. Yuen, J. de Rosny, and S. Tretyakov, "Smart radio environments empowered by reconfigurable intelligent surfaces: How it works, state of research, and the road ahead," *IEEE Journal on Selected Areas in Communications*, vol. 38, no. 11, pp. 2450–2525, Nov. 2020.

[58] Q. Wu and R. Zhang, "Towards smart and reconfigurable environment: Intelligent reflecting surface aided wireless network," *IEEE Communications Magazine*, vol. 58, no. 1, pp. 106–112, 2020.

[59] C. Liaskos, S. Nie, A. Tsioliaridou, A. Pitsillides, S. Ioannidis, and I. Akyildiz, "A new wireless communication paradigm through software-controlled metasurfaces," *IEEE Communications Magazine*, vol. 56, no. 9, pp. 162–169, Sep. 2018.

[60] E. Bjornson, O. Ozdogan, and E. G. Larsson, "Intelligent reflecting surface versus decode-and-forward: How large surfaces are needed to beat relaying?" *IEEE Wireless Communications Letters*, vol. 9, no. 2, pp. 244–248, Feb. 2020.

[61] I. Chatzigeorgiou, "The impact of 5G channel models on the performance of intelligent reflecting surfaces and decode-and-forward relaying," in *Proc. IEEE PIMRC*, 2020, pp. 1–4.

[62] M. Di Renzo, K. Ntontin, J. Song, F. H. Danufane, X. Qian, F. Lazarakis, J. De Rosny, D. Phan-Huy, O. Simeone, R. Zhang, M. Debbah, G. Lerosey, M. Fink, S. Tretyakov, and S. Shamai, "Reconfigurable intelligent surfaces vs. relaying: Differences, similarities, and performance comparison," *IEEE Open Journal of the Communications Society*, vol. 1, pp. 798–807, 2020.

[63] H. Chen, G. Li, and J. Cai, "Spectral-energy efficiency tradeoff in full-duplex two-way relay networks," *IEEE Systems Journal*, vol. 12, no. 1, pp. 583–592, Mar. 2018.

[64] A. Almradi and K. A. Hamdi, "MIMO full-duplex relaying in the presence of co-channel interference," *IEEE Transactions on Vehicular Technology*, vol. 66, no. 6, pp. 4874–4885, Jun. 2017.

[65] H. Li, L. Song, and M. Debbah, "Energy efficiency of large-scale multiple antenna systems with transmit antenna selection," *IEEE Transactions on Communications*, vol. 62, no. 2, pp. 638–647, Jan. 2014.

[66] J. Ma and C. Huang, "Energy efficiency of decode-and-forward full- duplex relay channels," in *2018 IEEE Global Communications Conference (GLOBECOM)*, Dec. 2018, pp. 1–6.

[67] J. Qiao, H. Zhang, F. Zhao, and D. Yuan, "Secure transmission and self-energy recycling with partial eavesdropper CSI," *IEEE Journal on Selected Areas in Communications*, vol. 36, no. 7, pp. 1531–1543, Jul. 2018.

[68] M. R. A. Khandaker and K. Wong, "Robust secrecy beamforming with energy-harvesting eavesdroppers," *IEEE Wireless Communications Letters*, vol. 4, no. 1, pp. 10–13, Feb. 2015.

[69] H.-C. Yang and M.-S. Alouini, *Order statistics in wireless communications: diversity, adaptation, and scheduling in MIMO and OFDM systems*. Cambridge: Cambridge University Press, 2011.

[70] H. Shin and J. H. Lee, "Capacity of multiple-antenna fading channels: spatial fading correlation, double scattering, and keyhole," *IEEE Transactions on Information Theory*, vol. 49, no. 10, pp. 2636–2647, Oct. 2003.

[71] I. S. Gradshteyn and I. M. Ryzhik, *Table of Integrals, Series, and Products*, 7th ed. Boston: Elsevier, 2014.

[72] M. K. Simon and M.-S. Alouini, *Digital communication over fading channels*. New York: John Wiley & Sons, 2005.

[73] P. Aggarwal and V. A. Bohara, "Analytical characterization of dual-band multi-user MIMO-OFDM system with nonlinear transmitter constraints," *IEEE Transactions on Communications*, vol. 66, no. 10, pp. 4536–4549, Oct. 2018.

[74] H. Chen, G. Li, and J. Cai, "Spectral–energy efficiency tradeoff in full-duplex two-way relay networks," *IEEE Systems Journal*, vol. 12, no. 1, pp. 583–592, Mar. 2018.

[75] L.-U. Choi and R. D. Murch, "A transmit preprocessing technique for multiuser MIMO systems using a decomposition approach," *IEEE Transactions on Wireless Communications*, vol. 3, no. 1, pp. 20–24, Jan. 2004.

[76] P. Aggarwal and V. A. Bohara, "Characterization of HPA using two dimensional general memory polynomial for dual band carrier aggregated MIMO-OFDM systems," in *2016 IEEE International Conference on Communications (ICC)*. IEEE, May 2016, pp. 1–7.

[77] V. A. Bohara and S. H. Ting, "Analytical performance of orthogonal frequency division multiplexing systems impaired by a non-linear high-power amplifier with memory," *IET Communications*, vol. 3, no. 10, pp. 1659–1666, Oct. 2009.

[78] P. Gandotra, R. K. Jha, and S. Jain, "Green communication in next generation cellular networks: A survey," *IEEE Access*, vol. 5, pp. 11 727–11 758, Jul. 2017.

[79] M.-S. Alouini and A. J. Goldsmith, "Capacity of rayleigh fading channels under different adaptive transmission and diversity-combining techniques," *IEEE Transactions on Vehicular Technology*, vol. 48, no. 4, pp. 1165–1181, Jul. 1999.

[80] A. M. Salhab and M. H. Samuh, "Accurate performance analysis of reconfigurable intelligent surfaces over rician fading channels," *IEEE Wireless Communications Letters*, vol. 10, no. 5, pp. 1051–1055, May 2021.

[81] X. Yang, M. Matthaiou, J. Yang, C.-K. Wen, F. Gao, and S. Jin, "Hardware-constrained millimeter-wave systems for 5G: Challenges, opportunities, and solutions," *IEEE Communication Magazine*, vol. 57, no. 1, pp. 44–50, Jan. 2019.

[82] M.-A. Badiu and J. P. Coon, "Communication through a large reflecting surface with phase errors," *IEEE Wireless Communications Letters*, vol. 9, no. 2, pp. 184–188, Feb. 2020.

[83] Q. Tao, J. Wang, and C. Zhong, "Performance analysis of intelligent reflecting surface aided communication systems," *IEEE Communications Letters*, vol. 24, no. 11, pp. 2464–2468, Nov. 2020.

[84] M. Al-Jarrah, E. Alsusa, A. Al-Dweik, and D. K. C. So, "Capacity analysis of IRS-based UAV communications with imperfect phase compensation," *IEEE Wireless Communications Letters*, vol. 10, no. 7, pp. 1479–1483, Jul. 2021.

[85] M. H. N. Shaikh, V. A. Bohara, P. Aggarwal, and A. Srivastava, "Energy efficiency evaluation for downlink full-duplex nonlinear MU-MIMO-OFDM system with self-energy recycling," *IEEE Systems Journal*, vol. 14, no. 3, pp. 3313–3324, 2020.

[86] M. H. N. Shaikh, V. A. Bohara, A. Srivastava, and G. Ghatak, "Performance analysis of intelligent reflecting surface-assisted wireless system with non-ideal transceiver," *IEEE Open Journal of the Communications Society*, vol. 2, pp. 671–686, 2021.

[87] D. Selimis, K. P. Peppas, G. C. Alexandropoulos, and F. I. Lazarakis, "On the performance analysis of RIS-empowered communications over nakagami-m fading," *IEEE Communications Letters*, vol. 25, no. 7, pp. 2191–2195, 2021.

[88] R. C. Ferreira, M. S. P. Facina, F. A. P. De Figueiredo, G. Fraidenraich, and E. R. De Lima, "Bit error probability for large intelligent surfaces under double-nakagami fading channels," *IEEE Open Journal of the Communications Society*, vol. 1, pp. 750–759, 2020.

[89] L. Yang, Y. Yang, M. O. Hasna, and M.-S. Alouini, "Coverage, probability of SNR gain, and DOR analysis of RIS-aided communication systems," *IEEE Wireless Communications Letters*, vol. 9, no. 8, pp. 1268–1272, 2020.

[90] L. Yang, F. Meng, Q. Wu, D. B. da Costa, and M.-S. Alouini, "Accurate closed-form approximations to channel distributions of RIS-aided wireless systems," *IEEE Wireless Communications Letters*, vol. 9, no. 11, pp. 1985–1989, 2020.

[91] D. Kudathanthirige, D. Gunasinghe, and G. Amarasuriya, "Performance analysis of intelligent reflective surfaces for wireless communication," in *Proc. IEEE International Conference on Communications (ICC)*, 2020, pp. 1–6.

[92] A. A. Boulogeorgos and A. Alexiou, "How much do hardware imperfections affect the performance of reconfigurable intelligent surface-assisted systems?" *IEEE Open Journal of the Communications Society*, vol. 1, pp. 1185–1195, 2020.

[93] G. Farhadi and N. C. Beaulieu, "On the ergodic capacity of multi-hop wireless relaying systems," *IEEE Transactions on Wireless Communications*, vol. 8, no. 5, pp. 2286–2291, 2009.

[94] M. H. N. Shaikh, V. A. Bohara, and A. Srivastava, "Performance analysis of a full-duplex MIMO decode-and-forward relay system with self-energy recycling," *IEEE Access*, vol. 8, pp. 226 248–226 266, 2020.